Alma Mater Studiorum - Università di Bologna

DOTTORATO DI RICERCA IN

SCIENZE BIOMEDICHE E NEUROMOTORIE

Ciclo 35

Settore Concorsuale: 06/D6 - NEUROLOGIA

Settore Scientifico Disciplinare: MED/26 - NEUROLOGIA

NEURO-OPHTHALMOLOGICAL AND ELECTROPHYSIOLOGICAL CHARACTERIZATION OF MITOCHONDRIAL DISEASES

Presentata da: Dott.ssa Giulia Amore

Coordinatore Dottorato

Prof.ssa Matilde Yung Follo

Supervisore

Prof. Valerio Carelli

Co-supervisore
Dott.ssa Chiara La Morgia

Esame finale anno 2023

ABSTRACT

Introduction and aims: Neuro-ophthalmological findings in mitochondrial diseases are very common and may manifest in form of optic atrophy, pigmentary retinopathy, chronic progressive external ophthalmoplegia and retrochiasmal visual loss. The aims of this project were a deep characterization of the neuro-ophthalmological and electrophysiological phenotypes of patients with genetically confirmed mitochondrial diseases, either due to nuclear or mitochondrial DNA mutations. Identification of specific phenotype-genotype correlations and of clinical-instrumental measures of progression/response to therapy were secondary aims.

Methods: The project is articulated into 3 parts: 1) characterization of patients with Dominant Optic Atrophy (DOA) phenotype associated with mutations in two nuclear genes (*AFG3L2* and *ACO2*), rare cause of disease, in comparison with classical *OPA1*-associated DOA; 2) characterization of patients with mtDNA mutations affecting tRNA-encoding genes, causing respectively MELAS and MERRF syndromes, and correlation with heteroplasmy; 3) longitudinal evaluation of acute Leber's Hereditary Optic Neuropathy (LHON) patients with m.11778G>A/MTND4 mutation treated with rAAV2/2-ND4 gene therapy. We performed a comprehensive neuro-ophthalmological assessment including Optic Coherence Tomography (OCT), visual fields and autofluorescence, coupled with electrophysiological examination, variably combining pattern electroretinogram (P-ERG), visual evoked potential (VEP), full-field ERG, and Photopic negative response (PhNR).

Results: In the first part, we described and compared 23 *ACO2* and 13 *AFG3L2* patients with 72 age- and gender-matched *OPA1* patients. All patients presented optic atrophy predominant in the temporal quadrant with various degrees of visual impairment. Comparison between *AFG3L2* and *OPA1* failed to reveal any significant difference. *ACO2* patients presented overall higher values of nasal retinal nerve fiber layer (RNFL) thickness and average and sectorial ganglion cell layer (GCL) thickness compared to both *AFG3L2* and *OPA1*, reflecting also in a less severe functional impairment at P-ERG and VEP. These results were confirmed also comparing separately affected and visually asymptomatic patients.

In the second part, we compared 33 MELAS and 8 MERRF patients. Retinopathy was the most common neuro-ophthalmological manifestation in 17/33 MELAS patients, displaying a large variability of clinical expression and severity amongst patients, confirmed at autofluorescence and electrophysiology. Conversely, optic atrophy was the most common finding in 7/8 MERRF patients, reflecting also in significantly lower values of RNFL thickness at OCT compared to MELAS despite an overall preserved visual function. A significant negative correlation of heteroplasmic mutant loads with age was confirmed both in blood and urinary cells in MELAS, but not in muscle nor in MERRF. Correlation of heteroplasmic mutant loads with neuro-ophthalmological parameters failed to disclose

any significance in MELAS, while mutational load negatively correlated with both RNFL and GCL thickness in MERRF.

In the third part, we prospectively investigated modifications in visual acuity, OCT parameters, Flash VEP and PhNR of 9 acute LHON patients co-treated for the first time with gene therapy and idebenone at 900mg/die. We compared the results at 3 timepoints (before intravitreal injection, after 6 and 12 months). We observed a significant progressive decrease overtime of RNFL thickness, reduction of N2 component at Flash VEP and of PhNR amplitude with increased PhNR latency. Interestingly, visual acuity significantly improved overall at last evaluation of about -0.37 LogMAR, and it correlated significantly with time from onset and from injection, but not with idebenone therapy duration.

Discussion: clinically DOA remains a fairly homogeneous entity despite growing genetic heterogeneity. *ACO2* seems associated overall to better preservation of retinal ganglion cells (RGCs), probably depending on a different pathogenic mechanism involving mtDNA maintenance, as opposed to *AFG3L2*, which is involved in *OPA1* processing, and it resulted virtually indistinguishable from classic *OPA1*-DOA. MELAS and MERRF patients presented with a clearly distinct ocular phenotype, respectively retinopathy in MELAS and optic atrophy in MERRF, possibly reflecting a selective susceptibility of different retinal cell types, respectively photoreceptors in MELAS and RGCs in MERRF, to a prevalent and global energy defect or to a prevalent oxidative stress insult. Longitudinal follow up of subacute LHON patients treated with gene therapy confirmed the reduction in RNFL thickness expected by natural history disease progression, describing for the first time the progressive deterioration in electrophysiological parameters, especially PhNR amplitude, which provides a direct measure of RGCs function. The amount of visual acuity improvement (-0,37 LogMAR) is remarkably similar to the one observed in recent clinical trials with rAAV2/2-ND4 gene therapy, nevertheless the effect of co-administration of idebenone therapy cannot be completely ruled out.

INDEX

1. GENERAL INTRODUCTION

Mitochondria are double-membrane cytoplasmic organelles, present in virtually all eukaryote cell, that host a number of metabolic pathways, including amino acid metabolism and fatty acid oxidation, and are involved in the apoptotic signalling for cell death; nevertheless, their major function is to produce energy in form of adenosine triphosphate (ATP) for the cell through the biochemical process of oxidative phosphorylation (OXPHOS). This is carried out by the mitochondrial respiratory chain, which consists in a series of redox reactions taking place at the inner mitochondrial membrane. Four embedded respiratory enzymatic complexes shuttle electrons one to the other and conserve the released energy by transferring protons across the membrane, thus building an electrochemical gradient charging the membrane potential, which is eventually used by a fifth enzyme to catalyse the ATP synthesis, the final reaction of OXPHOS (DiMauro et al., 2013).

Mitochondria carry multiple copies of their own circular mitochondrial DNA (mtDNA). This small genome contains 13 genes encoding subunits of the OXPHOS complexes, and other 24 genes necessary to the local protein synthesis: two mitochondrial specific ribosomal RNAs (rRNAs) and 22 transfer RNAs (tRNAs). This is also needed because the genetic code of mtDNA differs from the nuclear DNA (nDNA), making the two genomes reciprocally untranslatable. The mtDNA polypeptides are all subunits of four OXPHOS complexes, namely I, III, IV and V, and they interact with over 70 protein subunits encoded by nuclear genes and several non-protein prosthetic groups. Additional nucleus-encoded factors are essential for mtDNA maintenance and expression, as well as for formation and activity of the mitochondrial respiratory chain (Zeviani and Carelli, 2021). Consequently, genetic defects affecting mtDNA or OXPHOS-related nDNA genes can impair ATP synthesis and determine a mitochondrial dysfunction, ultimately causing human disease that may affect either paediatric or adult patients. To fully understand the pathogenic mechanisms of mitochondrial diseases, it is necessary to remind the key differences between the nDNA and mtDNA genetics. First, mutations affecting the mtDNA do not follow the traditional Mendelian rules since all mitochondria are inherited exclusively through the female germline, i.e. the oocytes, hence mtDNA mutations are only transmitted through the maternal lineage. Second, the concept of homoplasmy/heteroplasmy that depends on the presence of a homogenous mtDNA sequence or the coexistence of mutant and wild type mtDNA, which may segregate differently in somatic tissues and in the germline. Third, the threshold effect implicating that a certain amount of mutant load is necessary to cause mitochondrial dysfunction and this may vary from tissue to tissue. Forth, the high mutational rate and selection of different sequence variants, which ultimately shapes the population-specific mtDNA haplogroups (La Morgia et al 2020). These paradigms and the double genetic

contribution account for the extreme complexity of genotype–phenotype correlations in mitochondrial diseases, in terms of variable penetrance and clinical expressivity, which is also due to selective cellular susceptibility to a specific genetic and biochemical defect. Tissue and organs with high energy demand, such as brain, skeletal and cardiac muscles and eyes, are more susceptible to inadequate ATP supply caused by mitochondrial dysfunction. This explains why primary mitochondrial disorders usually cause neurodegeneration and/or myopathy as main symptoms both in children and adults (DiMauro et al., 2013). However, specific mitochondrial syndromes may involve any other organ, either individually or in combination. Although individually rare, when taken together as a group, primary mitochondrial disorders affect 1 individual in 4300 live births in Europe. However, the number of individuals carrying a mtDNA mutation, even in a percentage below the clinical threshold, is probably much higher, around 1 in 500 live births (McFarland et al., 2010).

1.1 NEURO-OPHTHALMOLOGIC FINDINGS IN MITOCHONDRIAL DISEASES

Ophthalmological findings in mitochondrial disease are very common, although their frequency is still unclear. The four most common neuro-ophthalmic manifestations are: optic neuropathy, pigmentary retinopathy, muscular involvement in form of isolated ptosis or chronic progressive external ophthalmoplegia (CPEO), and retrochiasmal visual loss (Fraser et al., 2010).

A retrospective study of 59 pediatric patients with genetically confirmed mitochondrial disease found that 81% had ophthalmologic manifestations. A total of 28% of patients had abnormal macular and/or peripheral retinal pigmentation, while retinal dystrophy was present in 27%. Other common findings included: reduced eye motility, partial or total optic atrophy and refractive errors (Gronlund et al., 2010). Another pediatric study showed ocular involvement in 40/75 (53%) of patients. However, genetic diagnosis was not available for all patients (Skladal et al., 2003). A more recent retrospective study (Zhu et al., 2017) including 74 patients with confirmed mitochondrial syndrome or mutation, showed a lower prevalence of ophthalmological abnormalities, present in 35% of patients. Retinal pigmentary changes were the most common finding, present in 16% of patients, while optic atrophy was noted in 10%. Decreased extra-ocular movements were present in 8% of patients.

We briefly describe the state of the art of the most common ophthalmological manifestations and the related mitochondrial disease, including available electrophysiological studies.

1.1.1 Optic atrophy (OA)

In the presence of mitochondrial mutations, bilateral OA may occur as part of systemic disease or as isolated manifestation, as in the two most common Hereditary Optic Neuropathies, i.e. Leber's Hereditary Optic Neuropathy (LHON) and Dominant Optic Atrophy (DOA). These two diseases,

even if different in genetic transmission, have in common the selective vulnerability of the retinal ganglion cells (RGCs) and their axons forming the optic nerve. Histochemical studies have shown an uneven distribution of mitochondria in RGC axons with clustering in unmyelinated retinal and prelaminar portions and an abrupt decrease in number posteriorly to the lamina cribrosa where myelination begins. This suggests increased energy requirement and a special vulnerability of the prelaminar RGC axons to bioenergetic failure, in particular of the smaller-diameter P-type RGCs and their fibers in the papillomacular bundle, explaining the typical loss of central vision in both LHON and DOA (Carelli et al., 2004).

LHON

LHON is a maternally inherited disease, associated with mtDNA point mutations in genes encoding subunits of complex I of the respiratory chain. The three most common mtDNA mutations, accounting for about 90% of cases, are: m.11778G>A/MT-ND4 (69%), m.14484T>C/MT-ND6 (14%), and m.3460G>A/MT-ND1 (13%). The classical presentation of LHON is a rapid, painless loss of central and color vision in one eye, followed by the fellow eye within days to months. Males are more affected than females with a 4:1 ratio (Newman, 2004). The prognosis is usually severe, with most patients progressing to very poor visual acuities associated with a dense central or cecocentral scotoma on visual fields (VF) testing. Fundus findings in the acute stages, and possibly in the asymptomatic mutation carriers, include circumpapillary telangiectatic microangiopathy and swelling of the retinal nerve fiber layer (RNFL) without leakage (pseudoedema). As the disease progresses a rapid axonal loss in the papillomacular bundle leads to temporal and eventually diffuse atrophy of the optic nerve head. Optical coherence tomography (OCT) allows quantifying the characteristic RNFL and RGC changes (Barboni et al., 2010; Balducci et al., 2016). Electrophysiological studies in LHON variably demonstrated a retinal dysfunction at pattern electroretinogram (P-ERG) and multifocal ERG and impaired neural conduction at Visual Evoked Potentials (VEP) (Salomao et al., 2004; Kurtenbach et al., 2004; Ziccardi et al., 2013; Guy et al., 2014; Jarc-Vidmar et al., 2016). Recently, it was discovered that RGCs generate a slow negative wave response following the b-wave of the cone response on photopic electroretinogram and is referred to as the photopic negative response (PhNR). Studies on LHON families, reported that PhNR amplitudes were severely reduced in patients affected by LHON compared to carriers and mildly reduced in carriers, suggesting a potential subclinical RGC dysfunction also in asymptomatic patients (Karanjia et al., 2017; Majander et al., 2017; Botelho et al., 2021).

Pupillary light reflex is typically spared in LHON even in advanced stages. A subset of RGCs expressing melanopsin (mRGCs) is responsible for the afferent pupillary reflex and is relatively

preserved in mitochondrial optic neuropathies (La Morgia et al., 2012). Their function in LHON patients has been studied using chromatic pupillometry and PLR was maintained despite the severity of optic atrophy. (Moura et al., 2013)

DOA

DOA is the most common autosomal hereditary optic neuropathy due, in the majority of cases (60–70%), to mutations in the *OPA1* gene on chromosome 3q28-29, encoding a dynamin-related GTPase anchored to the inner mitochondrial membrane and implicated in several subcellular functions including mitochondrial fusion, cristae morphology, mtDNA maintenance, apoptosis and OXPHOS efficiency (Lanaers et al., 2020).

DOA patients typically present with slowly progressive, painless, bilateral, symmetric visual loss, beginning insidiously in the first two decades of life. Compared to LHON, vision loss is usually milder and VF shows the typical central or cecocentral scotoma. As for LHON, the optic disc atrophy in DOA is secondary to RGC loss; it may be present as a subtle temporal pallor or more diffuse and can be confirmed by OCT scans (Asanad et al., 2019).

Electrophysiological studies showed abnormality at P-ERG, VEP and multifocal ERG (Holder et al., 1998; Granse et al., 2003; Reis et al., 2013), a reduction in PhNR has also recently been described (Morny et al., 2015).

Other mitochondrial optic neuropathies

Clinically indistinguishable phenocopies of LHON or DOA have been described in association with mutations in other nuclear genes, such as *ACO2, AFG3L2, SPG7, TMEM126A, DRP1* (Maresca and Carelli, 2021). Variable degrees of OA may be present along with other neurological and extra-neurological symptoms in syndromic mitochondrial diseases like Myoclonic Epilepsy with Ragged Red Fibers (MERRF), Mitochondrial Encephalopathy with Lactic Acidosis and Stroke-like episodes (MELAS) and Leigh syndrome (Zhu et al., 2017), or in other genetic disorders causing modification in mitochondrial-related proteins (Freidreich Ataxia, Wolfram Syndrome, Charcot-Marie-Tooth disease, Hereditary Spastic Paraplegia) (Yu-Wai-Man et al., 2021).

1.1.2 Pigmentary retinopathy (PR)

PR is a non-specific manifestation of numerous mitochondrial disorders, associated with a variety of nDNA and mtDNA mutations. The retinal pigment epithelium (RPE) is particularly vulnerable to compromised mitochondrial function, presumably because of the high degree of oxidative stress during the phagocytosis of photoreceptor outer segments. The changes in RPE can range from the

classical salt and pepper retinopathy to severe bone spicule formations (typical of retinitis pigmentosa) or choriocapillaris atrophy (Zeviani and Carelli, 2021). PR is a prominent feature in Neuropathy Ataxia and Retinitis Pigmentosa (NARP), Maternally Inherited Leigh Syndrome (MILS) and Kearns-Sayre Syndrome (KSS), in the latter usually associated with CPEO. Mild pigmentary changes may also be seen in patients with MELAS and MERRF. Variable combination with other ophthalmological manifestations and ERG abnormalities have been demonstrated in a few studies, in particular in KSS (Gronlund et al., 2010) and Leigh syndrome (Han et al., 2015, Akebrand et al., 2016).

1.1.3 Ptosis/CPEO

Mitochondria represent approximately 60% of the cell volume in eye muscles, indicating high-energy requirements and consequently an increased sensitivity to faulty mtDNA replication. CPEO is a frequent manifestation of mitochondrial myopathies, characterized by insidious and painless bilateral upper eyelid ptosis with mostly symmetrical limitation of eye movements, evolving slowly and progressively usually without diplopia (Kisilevsky et al., 2020). Isolated ptosis without ophthalmoplegia may be present in early phases, posing a diagnostic challenge with other neurological disorders. Visual acuity and pupillary response are typically spared.

CPEO syndromes may be variably inherited or develop sporadically. Most frequently, a large-scale rearrangement of the mtDNA (single deletion) is responsible for sporadic CPEO, whereas mtDNA point mutations may account for maternal inherited CPEO or recessive/dominant mutations in nuclear genes (*TWINKLE, POLG1, POLG2, ANT1, TP*) are associated with secondary multiple large-scale rearrangements (multiple deletions), as all these genes are implicated in mtDNA replication and maintenance (Orsucci et al., 2021, Arena et al., 2022).

Only a few studies investigated electrophysiological responses in CPEO patients and showed in the majority of patients some ERG and/or VEP alterations (Berdjis et al., 1985, Ambrosio et al., 1995, Sanderson et al., 2021).

1.1.4 Retrochiasmal visual loss

Visual impairment in patients with mitochondrial disorders may also occur due to disruption of the retrochiasmal visual pathways, usually due to metabolic strokes, resulting in homonymous hemianopic defects or cortical blindness.

The most common mitochondrial disease with stroke-like episode is MELAS, which is caused, in approximately 80% of patients, by the mtDNA m.3243A > G mutation in the *MT-TL1* gene encoding for mitochondrial tRNALeu(UUR). Patients may present different combinations of neuro-

ophthalmological manifestations, in particular PR or OA (Latlava et al., 2002, de Laat et al., 2013), along with retrochiasmal lesions due to stroke like episodes.

1.2 THERAPEUTIC OPTIONS IN HEREDITARY OPTIC NEUROPATHIES

A definitive treatment for Hereditary Optic Neuropathies, such are LHON and DOA, is missing, nevertheless some options are currently available and under continuous evolution: ranging from molecules acting to overcome the metabolic defect or compensate the mitochondrial disfunction, to gene therapies and stem cells application. A comprehensive review of the available options was carried out during the first year of this project and published (Amore et al., 2021).

At present, the only approved drug for LHON is idebenone (https://www.ema.europa.eu/en/medicines/human/EPAR/raxone). Idebenone is a synthetic short-chain analogue of Coenzyme Q10 with antioxidant properties, which has shown partial effectiveness in increasing visual recovery in LHON patients especially in the acute stage in a randomised, double-blinded, placebo-controlled study (RHODOS) (Klopstok et al., 2011). The use of idebenone in *OPA1*-related DOA is still under investigations but preliminary data indicate a possible beneficial effect of this therapy (Romagnoli et al., 2020). Other pharmaceutical agents, such as EPI-74, elamipretide (mtp-131), oestrogens-related compounds, rapamycin, and microRNA (miRNA) based, by targeting different pathways, have been or are currently under investigation in LHON at clinical and pre-clinical stages (Amore et al., 2021). The ultimate goal for the treatment of Hereditary Optic Neuropathies is the correction of the genetic defect, or the prevention of its transmission to the progeny. In LHON, a significant step forward is expected from gene therapy, consisting in an adeno-associated-viral vectors (AAV2) engineered to deliver the wild-type copy of ND4 complex I subunit and intended to be allotopically expressed from the nucleus and imported within mitochondria for functional complementation (Guy et al., 2002). Multiple trials, targeting acute LHON patients harboring the m.11778G>A/MTND4 mutation, are concluded or currently ongoing in Europe, US and China. In details, RESCUE and REVERSE trials evaluated the effects of the rAAV2/2-ND4 (GS010 LUMEVOQ) delivered by unilateral intravitreal injections, reporting a bilateral improvement of visual acuity at 96 weeks, sustained also 3 years after treatment (Newman et al., 2021, Yu-Wai-Man et al., 2020). The most recent REFLECT trial, comparing bilateral with unilateral intravitreal injections, confirmed a significant improvement of vision in the bilateral group (Yu-Wai-Man et al., 2022). LUMEVOQ is currently under review by the EMA for approval. As far it concerns gene therapy in *OPA1*-related DOA, there are ongoing preclinical studies on mouse models (Sarzi et al., 2018, Juschke et al., 2021), with multiple approaches being considered, but there is no active clinical trial in humans yet.

2. GENERAL METHODS

2.1 AIMS OF THE PROJECT

Primary aims:

- deep characterization of the neuro-ophthalmological phenotype of patients with confirmed mitochondrial diseases, presenting with one of the following ocular manifestations: optic atrophy or pigmentary retinopathy.
- refine the knowledge of neuro-ophthalmological manifestations in mitochondrial diseases adding electrophysiological procedures to the standard neuro-ophthalmological evaluation

Secondary aims: correlation among genetic, clinical and electrophysiological results in order to:

- identify specific genotype-phenotype correlations, including patients harbouring rare mutations.
- evaluate the role of different genetic, clinical and functional factors in determining the ocular phenotype.
- identify potential anatomical or functional measures biomarking involvement or progression that can be used for early diagnosis, follow-up or therapeutic trials.
- achieve a better understanding of the pathogenic mechanisms underlying different ocular manifestations in mitochondrial diseases.

The project is articulated into 3 main parts:

- PART 1: neuro-ophthalmological and electrophysiological characterization of patients presenting with a DOA phenotype associated with mutations in two rare nuclear genes (*AFG3L2* and *ACO2*), in comparison with the classical *OPA1*-associated DOA.
- PART 2: deep neuro-ophthalmological and electrophysiological characterization of patients harbouring mtDNA mutations affecting tRNA-encoding genes, causing respectively MELAS and MERRF syndromes. Comparison between ophthalmological phenotypes and correlation with heteroplasmic mutant loads.
- PART 3: neuro-ophthalmological and electrophysiological longitudinal evaluation of acute LHON patients with the m.11778G>A/MTND4 mutation treated with rAAV2/2-ND4 gene therapy as compassionate use, for which co-administration of idebenone represents a significant difference from the previous clinical trials.

2.2 RECRUITMENT

We recruited patients with genetically confirmed mitochondrial disease, either due to nuclear or mitochondrial DNA mutations, on the basis of the ocular phenotype at the IRCCS Istituto delle

Scienze Neurologiche di Bologna (ISNB), UOC Clinica Neurologica, Bellaria Hospital (Bologna). Participation to the study was proposed during follow-up visits or by phone calls performed on regular basis to check for health conditions. Informed consent for all patients was obtained during ambulatory visits.

The main groups of mitochondrial diseases under investigation were: hereditary optic neuropathies (DOA and LHON) and mitochondrial encephalo-myopathies associated with pigmentary retinopathy (MELAS and MERRF).

We retrieved previously collected clinical data and genetic testing (retrospective phase); neuro-ophthalmological and electrophysiological evaluation were subsequently performed, in case of evolving conditions, such as LHON in acute stage, evaluation was repeated at 6 and 12 months (prospective phase).

Retrospective data were collected using a previously approved protocol on natural history of Hereditary Optic Neuropathies: 121-2019-OSS-AUSLBO-19012.

We also obtained approval from local Ethical Committee for the electrophysiology study protocol: MITOEYE20 812-2020-SPER-AUSLBO – 20140.

All genetic testing was performed at the Laboratory of Neurogenetics of the IRCCS ISNB. Genetic testing, depending on the clinical suspicion, included the screening for classical mtDNA mutations with quantitative heteroplasmy measurements on available tissues and/or sequencing of the major mitochondrial-associated nuclear genes. For negative cases, the complete mtDNA sequence was performed, followed eventually by Next Generation Sequencing (NGS) target panel. NGS panel including 35 genes associated with genetic forms of optic atrophy. The amplicon-based NGS library (TruSeq Custom Amplicon; Illumina, San Diego, CA) was sequenced on Illumina MiSeq. For bioinformatic analysis, reads were aligned to the human genome (hg19) and the identified variants were annotated (ANNOVAR) and filtered, focusing on rare variants (≤0.5% in public databases) causing potentially damaging changes (Combined Annotation Dependent Depletion, PolyPhen-2, DANN). Variant confirmation and segregation analysis were performed by Sanger sequencing. Exome sequencing was performed in selected cases. The NGS and exome analysis were performed in the frame of the GR project: GR-2016-02361449 “Italian Project on Hereditary Optic Neuropathies (IPHON): from genetic basis to therapy” (PI: Dr. L Caporali).

Inclusion criteria

-Patients with genetically confirmed diagnosis of mitochondrial disease presenting one of the following ocular phenotypes: optic atrophy or pigmentary retinopathy.

-Age from 11 to 80 years

-Signature of the informed consent

Exclusion criteria

-Spherical or cylindrical refractive errors more than 3 or 2 diopters respectively

-Presence of posterior pole pathology (i.e. macular degeneration, retinal detachment, vascular retinal pathology) except for hereditary optic neuropathy and pigmentary retinopathy.

-Ocular pressure more than 20 mmHg

-Severe lens opacity

-Contraindication to intermittent light stimulation (like photosensitive epilepsy) or severe photophobia

We created dedicated databases to collect genetic, clinical and electrophysiological data for each group of mitochondrial disease under investigation. Statistical analyses were carried out using R software (version 4.0.0) and IBM SPSS Statistics for Windows, version 20.0 (IBM Corp., Armonk, N.Y., USA) software. Specific comparison and correlation tests will be specified for each part of the protocol.

2.3 NEURO-OPHTHALMOLOGIC EVALUATION

All patients included were examined at the Neuro-ophthalmology Clinic, UOC Clinica Neurologica, IRCCS ISNB, Ospedale Bellaria and the following parameters were recorded:

- best corrected visual acuity (BCVA) assessed using Snellen Charts
- color vision assessed using Ishihara tables
- slit lamp examination of the anterior segment
- fundus oculi examination
- applanation tonometry
- ocular motility
- computerized visual fields protocol 30-2 (Humprey Field Analyzer, Zeiss)
- optical coherence tomography (OCT Triton, Topcon) to assess RNFL and GCL thickness
- autofluorescence (Spectralis, Heidelberg)

2.4 ELECTROPHYSIOLOGIC EVALUATION

In subgroups of patients, a disease-specific electrophysiological protocol was applied and included more of the following tests:

-pattern electroretinogram (P-ERG) to differentiate retinal from optic nerve dysfunction and monitor ganglion cells dysfunction.

-visual evoked potential (VEP), either pattern or flash (FVEP), to assess integrity of central vision pathways.

-scotopic and photopic full field electroretinogramm (ff-ERG) to assess cone and rod function.

-photopic negative response (PhNR) to assess RCG function.

Details of the selected electrophysiological examinations will be specified for each part of the protocol. Description of the technical protocols is shown in appendix 1.

3. PART 1: NEURO-OPHTHALMOLOGICAL AND ELECTROPHYSIOLOGICAL CHARACTERIZATION OF NOT-OPA1 DOMINANT OPTIC ATROPHY

3.1 Introduction

Dominant Optic Atrophy (DOA) is an inherited condition due to loss of retinal ganglion cell (RGCs) characterized by autosomal dominant inheritance. Insidious central visual loss or inability to reach full vision at ophthalmic evaluations is usually recognized in the first two decades of life, frequently with a positive family history for low vision even if disease penetrance and severity may vary considerably among relatives (Lenaers et al., 2020). Although optic atrophy is usually the only clinical feature, DOA may be associated with other neurological signs such as hearing loss, chronic progressive external ophthalmoplegia (CPEO) and myopathy, peripheral neuropathy and other rare manifestations such as parkinsonism, dementia or multiple sclerosis, a condition referred to as DOA-*plus* (Yu-Wai-Man et al., 2010; Carelli et al., 2015)

Around 60% of cases are due to heterozygous pathogenic variants in the *OPA1* gene (Delettre et al., 2000; Alexander et al., 2000), which encodes for an inner mitochondrial membrane (IMM) protein processed in multiple isoforms fulfilling several functions within the cell, such as fusion of IMM and shaping of cristae morphology, but also OXHOS efficiency and energy metabolism, apoptosis control, calcium handling and maintenance of the mitochondrial genome integrity (Del Dotto et al., 2019). Interestingly, at the opposite end of mitochondrial dynamics, also defective fission as due to mutations in the *DNM1L*/*DRP1* gene may lead to DOA in a minority of cases (OPA5) (Gerber et al., 2017), pointing to balance between fusion and fission as a key mechanism for RGCs survival and optic nerve physiology (Maresca et al., 2021).

Another gene (*OPA3*) and three further loci (OPA4, OPA5, OPA8) are known to be associated with DOA, while additional loci and genes (OPA2, OPA6 and OPA7/*TMEM126A*) are responsible for X-linked or recessive forms of optic atrophy (Newman et al.,2023). Currently, the list of genes associated with DOA is facing a rapid growth thanks to the systematic use of Next Generation Sequencing (NGS) and it was recently enriched by the relatively frequent identification of pathogenic variants in *AFG3L2* (MIM# 604581) (Charif et al., 2015; Colavito et al., 2017; Caporali et al., 2020; Charif et al., 2020) and *ACO2* genes (Charif et al., 2021). Other rare genetic causes of DOA are mutations in *SSBP1* (Jurkute et al., 2019; Piro-Megy et al, 2020, Del Dotto et al., 2020) and *SDHA* (Courage et al, 2017).

The *AFG3L2* gene encodes for a mitochondrial protease, which in combination with paraplegin in turn encoded by the *SPG7* gene, forms a mitochondrial matrix AAA metalloprotease (m-AAA), a proteolytic complex located in the IMM responsible for quality control and processing of several mitochondrial proteins, reflecting also in OPA1 processing (Gerdes et al., 2012). Mutations in

AFG3L2 were originally described to cause a dominant form of spinocerebellar ataxia (SCA28, MIM# 610246) (Di Bella et al., 2010), whereas homozygous mutations have been associated with a recessive spastic ataxia syndrome (SPAX5, MIM# 614487) (Pierson et al., 2011). In recent years, heterozygous mutations in this gene have been increasingly recognized to cause non-syndromic DOA (Charif et al., 2015; Colavito et al., 2017; Caporali et al., 2020; Charif et al., 2020). Remarkably, the SCA28-associated mutations are located in the proteolytic domain, whereas all DOA-associated *AFG3L2* mutations cluster in the ATPase domain (Caporali et al., 2020). The pathogenic role of DOA-associated *AFG3L2* mutations was confirmed in yeast and in patients' fibroblasts, leading to the interesting observation of abnormal accumulation of short isoforms of OPA1, skewing mitochondrial dynamics towards fission of mitochondria, with consequent fragmentation of the mitochondrial network (Caporali et al., 2020; Baderna et al., 2020). Interestingly, recessive pathogenic mutations in the *SPG7* gene were associated with spastic paraparesis, pure or associated with optic atrophy (Casari et al., 1998), and not surprisingly also for this gene dominant mutations associated with DOA have been reported (Klebe et al., 2012, Charif et al., 2020)

Dominant mutations in another mitochondrial gene, *ACO2* encoding for the tricarboxylic-acid-cycle enzyme aconitase, have been very recently described to be a frequent cause of dominantly inherited isolated optic atrophy (Metodiev et al., 2014; Charif et al., 2021). Recessive mutations in *ACO2* have been previously associated with two distinct and severe infantile disorders: infantile cerebellar-retinal degeneration (ICRD; OMIM #614599) and optic atrophy 9 (OPA9; OMIM #616289) (Spiegel et al., 2012). Monoallelic mutation in *ACO2*-mutant fibroblasts have been demonstrated to be sufficient to cause mitochondrial respiration dysfunction and mtDNA depletion, leading to an increase in susceptibility to oxidative stress and cell death (Neumann et al., 2020).

In this part of the project, we aimed at characterizing the neuro-ophthalmological phenotype of patients with *AFG3L2* and *ACO2*-associated DOA, in comparison with the classical *OPA1*-DOA patients, highlighting, if any, the different genotype-phenotype correlations.

3.2 Cohort study and clinical assessment

We investigated a cohort of patients with non-syndromic optic atrophy obeying the diagnostic criteria for DOA harboring heterozygous mutations in *AFG3L2* or *ACO2 g*enes (Appendix 2).

Information about family history, disease onset and other symptoms were recorded. Given the insidious presentation of DOA, age at first evidence of optic atrophy was categorized into 3 groups: preschool (<6 years), childhood-adolescence (6-18 years) and adulthood (>18 years). Neuro-ophthalmological examination included: best corrected visual acuity (BCVA) in LogMAR, color vision (Ishihara test), optic nerve appearance at slit lamp examination/fundus picture assessed by at

least two different ophthalmologists or two subsequent visits, computerized visual fields (VF) (Humphrey Field Analyzer, protocol Sita Standard 30-2, Zeiss, San Leandro, CA, USA), and Optical Coherence Tomography (OCT) to assess optic nerve head (ONH) size, retinal nerve fibre layer (RNFL) thickness and ganglion cell layer (GCL) segmentation analysis of the macula (DRI Triton, Topcon, Tokyo, Japan) (Barboni et al., 2005).

OCT protocols images were obtained using a 3-dimensional wide scan protocol with a size of 12×9 mm consisting of 256 B-scans, each comprising 512 A-scans. Peripapillary RNFL thickness were measured using a 360° 3.4-mm diameter circle scan with thicknesses measured across the superior, nasal, inferior, and temporal sectors and segmentation analysis of the macula measured across six sectors of the 6-mm diameter circular annulus centered on the foveal included GCL.

We included patients with vision loss defined as LogMAR>0 from now on referred as affected/symptomatic, as well as patients with normal visual acuity defined as LogMAR<0 but displaying fundoscopic or instrumental signs of disease (temporal pallor or reduced RNFL thickness at OCT or both), from now on referred as subclinical. Patients with myopia higher than 3 diopters or astigmatism higher than 2 diopters were excluded. Relatives harboring a pathogenic mutation without any sign of visual involvement, clinical or instrumental, were excluded.

Neuro-ophthalmological data were compared with a group of classic *OPA1*-related DOA patients followed regularly at our Neuro-ophthalmology Clinic. We retrospectively retrieved neuro-ophthalmological data of the last available visit from patients carrying a heterozygous mutation in the *OPA1* gene (Appendix 2), we included patients followed since 2018 who had comparable OCT measures, both affected and subclinical patients displaying instrumental sign of disease were included. Patients with myopia higher than 3 diopters or astigmatism higher than 2 diopters were excluded. Patients with mutations in *OPA1* were matched by age and gender with a 2:1 ratio with patients carrying mutation in *AFG3L2* or *ACO2* genes to reduce the confounding effect of age and gender in group comparisons.

Patients in the three groups were further classified according to type of mutation they carried, namely missense or causing haploinsufficiency.

In subgroups of patients, we also performed a complete electrophysiological assessment including: visual evoked potential (VEP) to assess integrity of central vision pathways, pattern electroretinogram (P-ERG) to differentiate retinal from optic nerve dysfunction and monitor ganglion cells dysfunction, scotopic and photopic full field electroretinogramm (ff-ERG) to assess cone and rod function and photopic negative response (PhNR) to assess RCG function (Appendix 1).

3.3 Statistical analysis

The three groups (from now on referred as AFG3L2, ACO2 and OPA1) were analyzed to compare gender, age, mutation distribution and visual function outcomes.

For each group, continuous variables were summarized with statistics including the number of patients (n), mean, standard deviation (SD), median, interquartile range (IQR). Shapiro-Wilk and Kolmogorov-Smirnov normality tests were used to assess the normal distribution of data. Demographic data were compared using univariate ANOVA with Least Significant Difference (LSD) post-hoc test if normally distributed, contrariwise Kruskal-Wallis test was used, followed by Dunn Bonferroni post-hoc test.

The following visual endpoints were analyzed: BCVA, mean deviation (MD) and fovea at VF, Ishihara color vision testing, ONH size, RNFL (average, temporal, superior, nasal, and inferior quadrants), and GCL (average and 6 individual macular sectors: superotemporal, superior, superonasal, inferonasal, inferior, and inferotemporal) thickness.

Primary statistical analysis was conducted for the aforementioned visual endpoints to compare the three-patient groups by applying Clustered Wilcoxon rank sum test (Rosner-Glynn-Lee method) and Benjamini & Hochberg method was applied to adjust p-values for multiple comparisons. In particular, comparison among the three groups was conducted first on all patients, then only on subjects with clear visual dysfunction (reduced visual acuity defined as LOGMAR >0). Separately, subjects with normal visual acuity but fundoscopic or instrumental signs of disease were also compared.

Secondary statistical analysis was performed in the same manner as the primary one with Clustered Wilcoxon rank sum test on the afore mentioned visual endpoints by stratifying each group of patients (AFG3L2/ACO2/OPA1) by gender (male VS female) and mutation type (missense VS haploinsufficiency) to identify any specific mutation type genotype-phenotype correlation. Given the exploratory character for these secondary sub-group analyses, no adjustments for multiplicity were applied.

Electrophysiological results were compared using Mann-Whitney U non-parametric test.

Two-sided p-values will be presented. Statistical analyses were carried out using R software (version 4.0.0) and IBM SPSS Statistics for Windows, version 20.0 (IBM Corp., Armonk, N.Y., USA) software.

3.4 Results

Demographic and general clinical/genetic features of the cohort are shown in Table 1.

A total of 13 AFG3L2 patients (9 males) belonging to 6 pedigrees (reported in Caporali et al., 2020) and 23 ACO2 patients (17 males) from 15 families, were recruited. Mean age was respectively 36,5±20,2 for AFG3L2, and 34,7±16,9 years for ACO2 patients. Neuro-ophthalmological data of 72 matched OPA1 patients (mean age 36,21±17,4 years, 50 males) were retrieved and compared. As results of the matching procedure, age and gender were similarly distributed among the three groups: the p-values were respectively 0.93 and 0.76 (Table 1).

A total of 91 affected patients (respectively 63 OPA1, 17 ACO2 and 11 AFG3L2) and 17 subclinical patients (respectively 9 OPA1, 6 ACO2 and 2 AFG3L2) were included.

Among affected, we found a similar distribution of age at onset in the 3 groups (p=0.39), with a higher prevalence of onset in childhood/adolescence in all 3 groups (Table 1). The number of affected relatives was not statistically different among groups (p=0.16) (Table 1). Apart from optic atrophy, other mild neurological symptoms, isolated or combined, were present in 23 patients (16 OPA1, 3 ACO2 and 4 AFG3L2 respectively, p=0.40) (Table 1).

All AFG3L2 patients presented missense mutations affecting the ATP-ase domain, as previously reported (Caporali et al., 2020), whereas the ACO2 patients harbored a missense mutation in 56% (n=13) of cases and other genetic defects predicted to causing haploinsufficiency (deletions, frameshift or splice defects) in the remaining 44% (n=10) of cases. Patients with *OPA1* mutations were classified according to mutation type causing haploinsufficiency (n=57, 79%) or a missense variant (n=15, 21%). All mutations are listed in Appendix 2.

Neuro-ophthalmological features of ACO2, AFG3L2 and OPA1 groups are summarized in Table 2.

In the ACO2 group, 2 eyes were excluded from analysis because of severe amblyopia and retinal venous occlusion respectively. Comparable OCT results (DRI Triton, Topcon) were available for 34 out of 44 eyes in the ACO2 group, 14 out of 26 eyes in the AFG3L2 group and all 144 OPA1 eyes. VF were available or comparable (Humphrey, protocol 30-2) for 35 eyes in the ACO2 group, 24 eyes in the AFG3L2 group and 104 eyes in the OPA1 group.

	ACO2	AFG3L2	OPA1	p
Subjects [N]	23	13	72	
Eyes [N]	44	26	144	
Age [years, mean±SD]	34,7±16,9	36,5±20.2	36,2±17,4	[a] 0.93
Sex [male, N(%)]	17 (73%)	9 (70%)	50 (70%)	[b] 0.76
Mutation - missense [N(%)]	13 (56%)	13 (100%)	15 (21%)	
- haploinsufficiency [N(%)]	10 (44%)	0	57 (79%)	
Status - affected [N(%)]	17 (74%)	11 (85%)	63 (87%)	[b] 0.25
- asymtomatic [N(%)]	6 (26%)	2 (15%)	9 (13%)	[b] 0.25
Onset [N (%)]	17	8 (3 missing)	63	[b] 0.39
- Preschool	4 (23%)	2 (25%)	18 (29%)	
- Childhood-adolescence	11 (65%)	4 (50%)	31 (49%)	
- adulthood	2 (12%)	2 (25%)	14 (22%)	
N° affected relatives [mean±SD]	1,1±0,9	2±1,3	2,26±2,4	[a] 0.16
Other neurological symptoms [N(%)]	3 (13%)	4 (30%)	16 (25%)	[b] 0.40
- hearing loss	0	2	5	
- movement disorder	1	1	2	
- cognitive/psychiatric	1	2	4	
- migraine	1	0	3	
- myopathy/ptosis	0	0	2	

Table 1. Cohort description

[a] p-value referred to Kruskal Wallis test.

[b] p-value referred to Chi-squared test.

Abbreviations: N: absolute frequency, %: relative frequency, SD: standard deviation.

	ACO2	AFG3L2	OPA1
Eyes [N]	44	26	144
Fundus [N(%)]			
- Normal	6 (14%)	2 (8%)	2 (1%)
- Temporal pallor	25 (57%)	24 (92%)	120 (83%)
- Diffuse pallor	13 (29%)	0	22 (15%)
BCVA [LogMAR, mean±SD]	0,39±0,71	0,48±0,34	0,41±0,52
Colors [median±IQR]	1 (0 - 12)	1 (0.25 - 3)	2 (0 - 11)
VF [eyes, N]	35	24	104
MD [dB, mean±SD]	-5,71±4,09	-8,71±7,25	-6,69±4,91
Fovea [dB mean±SD]	26,84±6,24	26,5±12,26	27,32±9,47
OCT [eyes, N]	34	14	143
OHN size [mean±SD]	2,02±0,43	1,69±0,28	1,86±0,38
RNFL AVG [µm, mean±SD]	69,28±18,8	56,57±14,91	63,62±14,66
RNFL T [µm, mean±SD]	35,83±13,56	29,86±6,84	32,76±9,64
RNFL S [µm, mean±SD]	91,86±22,6	76,29±25,13	88,09±23,45
RNFL N [µm, mean±SD]	69,41±17,8	51,5±12,33	58,15±13,78
RNFL I [µm, mean±SD]	79,80±26,03	69,21±23,1	75,56±21,28
GCL AVG [µm, mean±SD]	49,07±8,98	39,12±8,32	41,84±6,44
GCL SN [µm, mean±SD]	49,03±10,78	35,86±9,82	42,54±8,38
GCL S [µm, mean±SD]	51,72±9,2	39,5±8,13	44,01±7,88
GCL ST [µm, mean±SD]	48,91±9,04	42,00±9,41	41,70±7,45
GCL IT [µm, mean±SD]	48,03±8,67	42,00±9,21	40,40±6,45
GCL I [µm, mean±SD]	48,49±7,71	39,07±8,05	41,39±5,26
GCL IN [µm, mean±SD]	48,23±10	36,29±8,82	40,91±7,75

Table 2. Neuro-ophthalmological results in ACO2, AFG3L2 and OPA1 groups.

Continuous variables are presented as mean ± standard deviation, while categorical variables as absolute and relative frequencies.

Abbreviations: N: absolute frequency, SD: standard deviation, VA: visual acuity, VF: visual fields, MD: mean deviation, OCT: optic coherence tomography, ONH: optic nerve head, RNFL: retinal nerve fiber layer, GCL: ganglion cell layer, AVG: average, T: temporal, S: superior, N: nasal, I: inferior, SN: supero-nasal, ST: supero-temporal, IT: inferotemporal, IN: inferonasal

At fundus examination the majority of ACO2, AFG3L2 and OPA1 patients presented temporal optic disc pallor (57%, 83% and 92% respectively) (Table 2). Mean visual acuity in LogMAR was 0,41±0,52 in OPA1, 0,39±0,71, in ACO2 and 0,48±0,34 in AFG3L2 group without significant differences among groups (p=0.84). VF showed a variable degree and pattern of bilateral central scotoma in all patients, however both MD and fovea sensitivity values did not differ among groups (p=0.41 and p=0.12 respectively). The average RNFL thickness at OCT was 63,62±14,66 in OPA1, 69,28±18,8 in ACO2 and 56,57±14,91 in AFG3L2 without significant differences among groups (p=0.066) (Fig 1). ACO2 patients compared to AFG3L2 resulted having higher values in OHN size (p=0.020), nasal RNFL thickness (p=0.029) (Fig 1) and average (p=0.012), supero-nasal (p=0.013), superior (p=0.003), inferior (p=0.012) and infero-nasal (p=0.010) GCL thickness (Fig 2); after adjusting p-values for multiple comparisons, significance was confirmed only for the superior sector of the GCL (p-adj=0.026). Comparing ACO2 and OPA1, ACO2 had significant higher RNFL thickness in the nasal sector (p=0.023) (Fig 1) and higher GCL thickness (Fig 2), both average (p=0.0007) and sectorial (supero-nasal p=0.027, superior p=0.001, supero-temporal p=0.003, infero-temporal p=0.0005, inferior p=0.0001, infero-nasal p= 0.004). After adjustment, significance was lost for nasal RNFL, while it remained for GCL thickness in average (p-adj=0.011) and all sectors except the supero-nasal (superior p-adj=0.015, superotemporal p-adj=0.026, inferotemporal p-adj= 0.011, inferior p-adj=0.007, inferonasal p-adj=0.026) (Fig 2). Between the AFG3L2 and OPA1 groups, we found no significant difference in visual and OCT parameters.

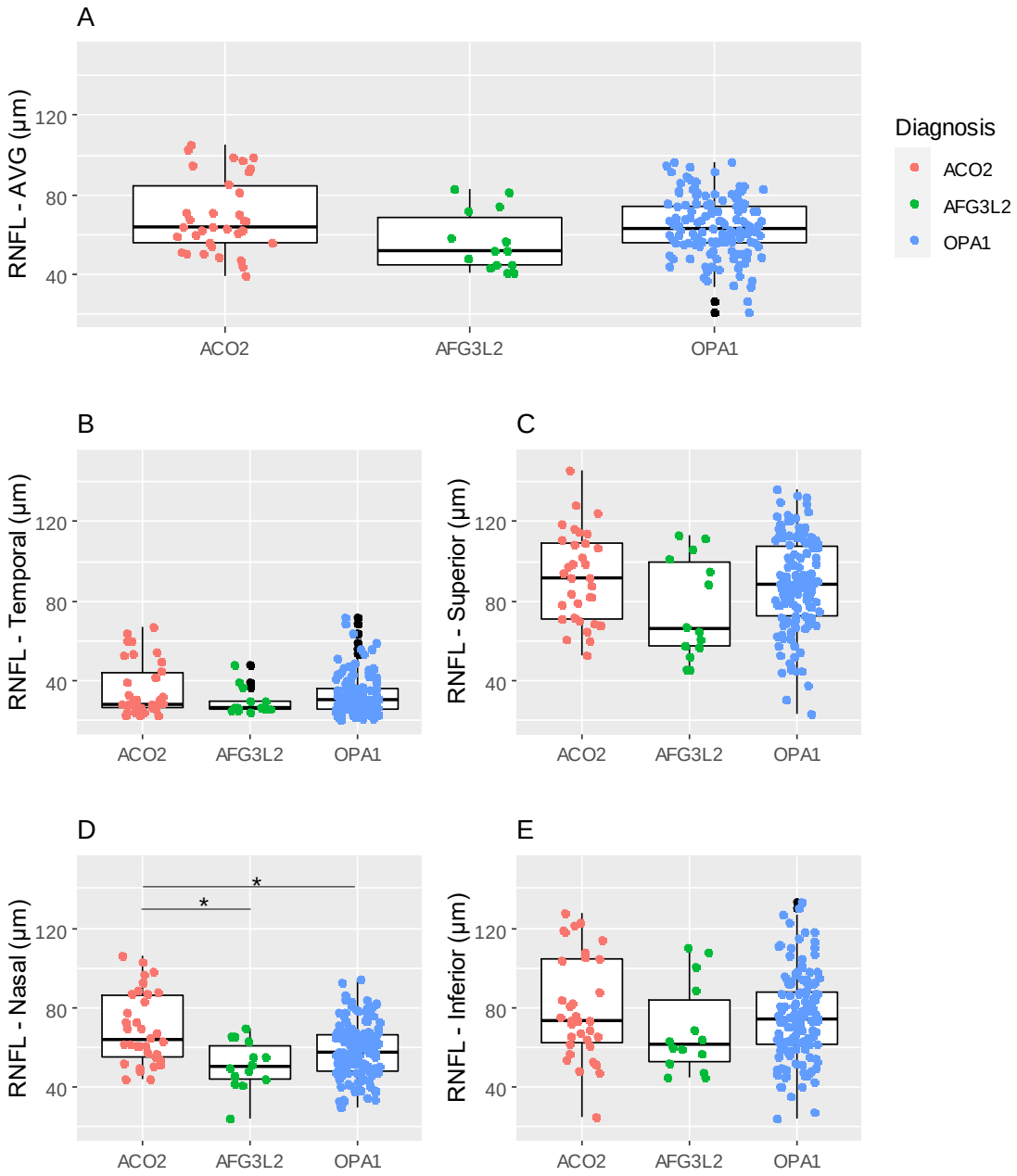

Figure 1. Average and sectorial RNFL thickness in ACO2, AFG3L2 and OPA1 groups.

*p<0.05

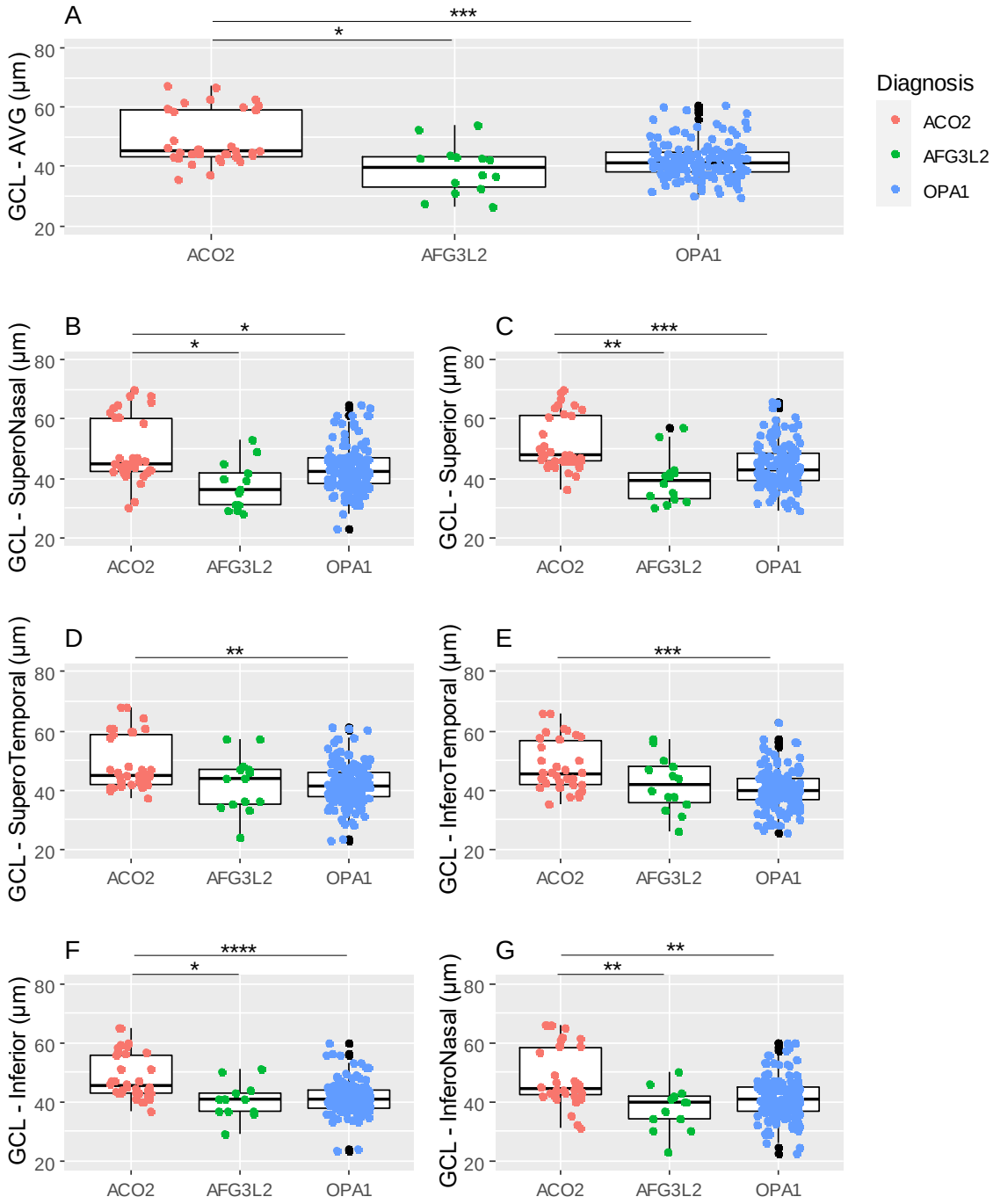

Figure 2. Average and sectorial GCL thickness in ACO2, AFG3L2 and OPA1 groups.

*p<0.05, **p<0.01, ***p<0.001, ****p<0.0001

Then, we focused on patients with clear reduced visual acuity (affected/symptomatic). Data from 17 ACO2, 11 AFG3L2 and 63 OPA1 were compared. ACO2 patients compared to AFG3L2 resulted having higher values in OHN size (p=0.044), average (p=0.048), superior (p=0.012), and infero-nasal (p=0.041) CGL thickness; while compared to OPA1, ACO2 patients had significant higher GCL thickness on average (p=0.009), superior (p=0.014), supero-temporal (p=0.037), infero-temporal (p=0.006) and inferior (p=0.002) sectors (Fig 3 and 4). Nevertheless, after adjusting p-values for multiple comparisons, significance was lost in all parameters. Comparing AFG3L2 and OPA1 groups, we found no difference in any visual and OCT parameters (Fig 3 and 4).

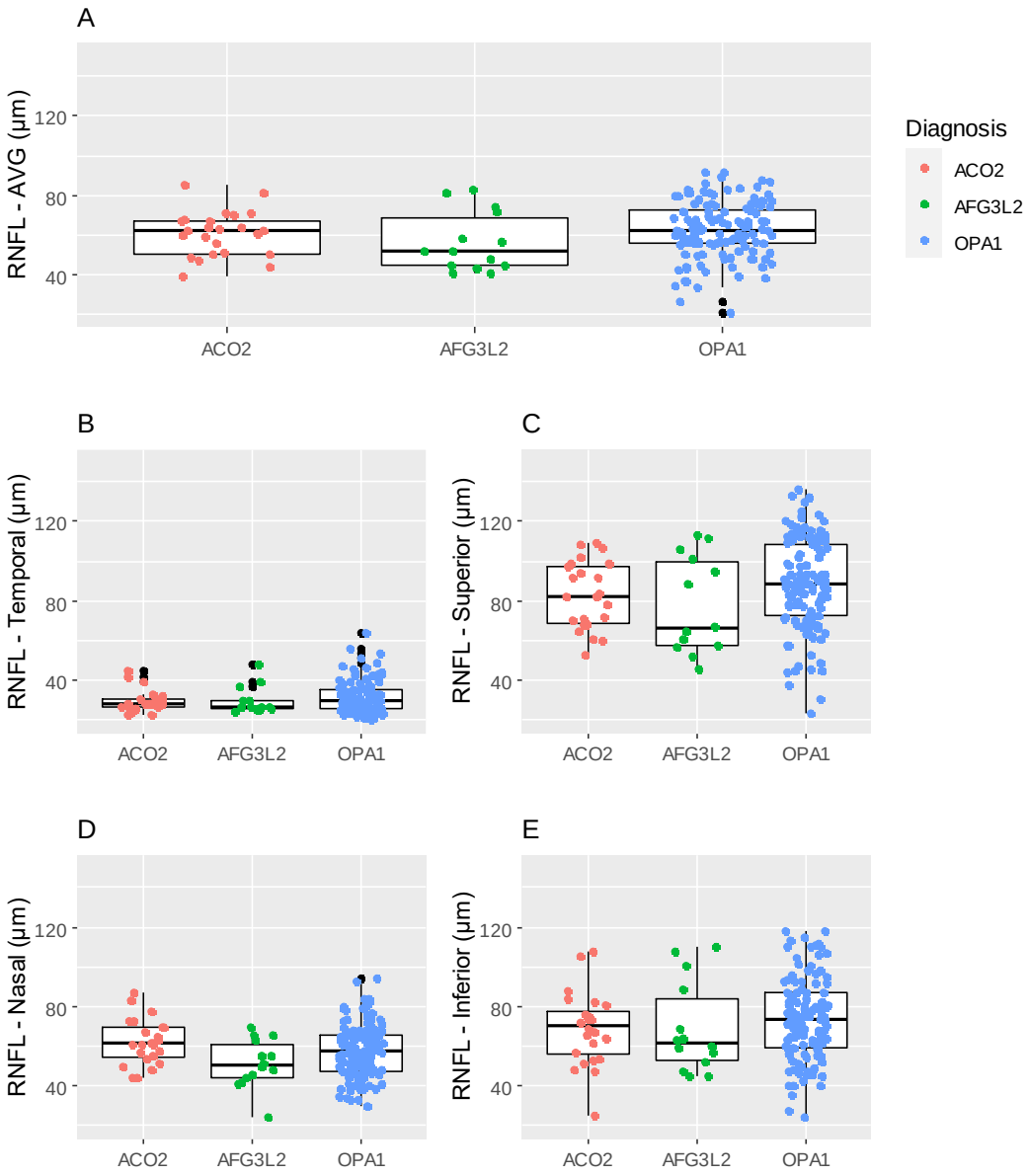

Figure 3. Average and sectorial RNFL thickness in ACO2, AFG3L2 and OPA1 symptomatic patients.

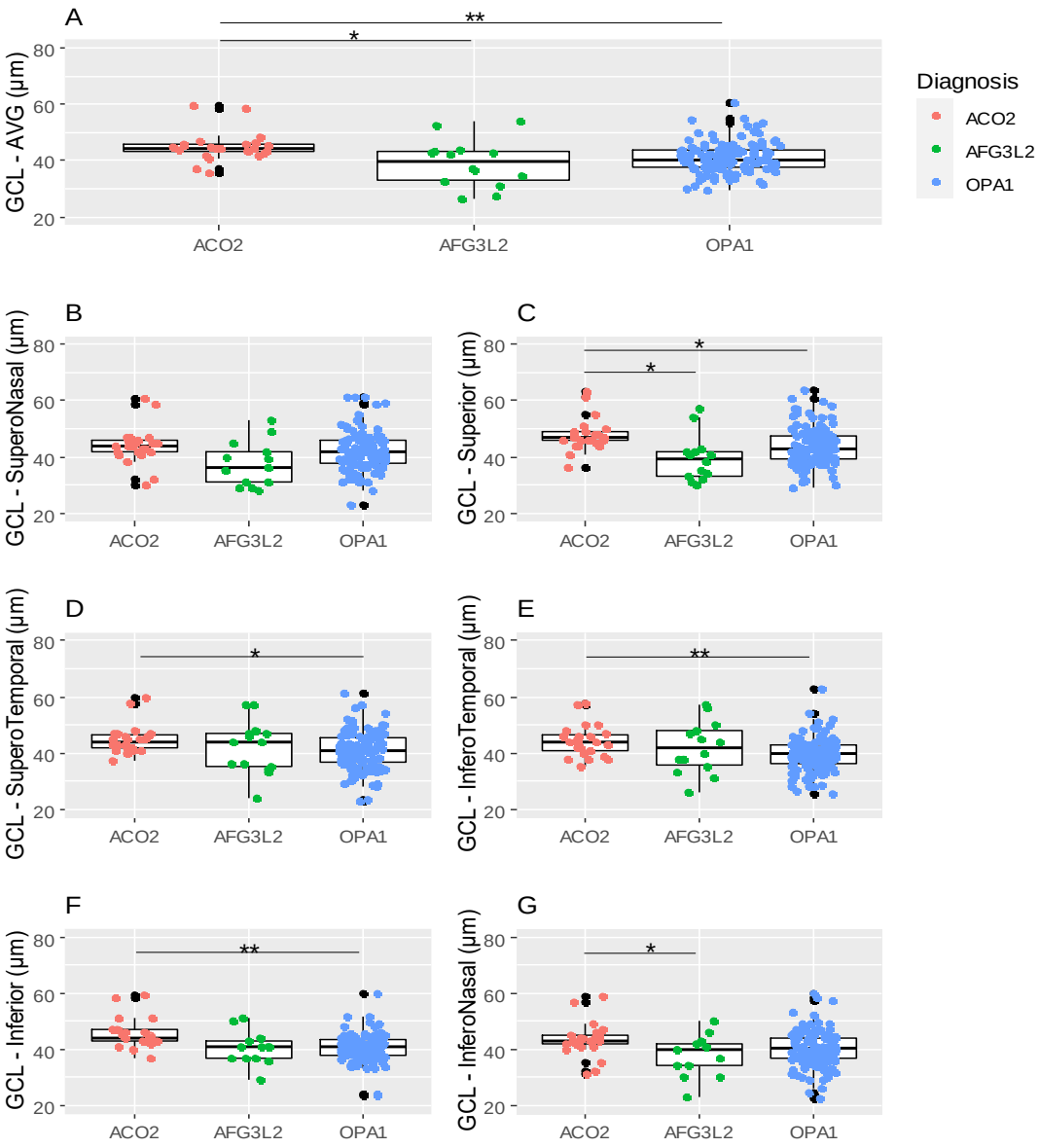

Figure 4. Average and sectorial GCL thickness in ACO2, AFG3L2 and OPA1 symptomatic patients.

*p<0.05, **p<0.01.

We then focused on the subclinical subjects defined as those maintaining normal vision (subclinical); we were able to compare the OCT data (RNFL and GCL thickness) only from 5 ACO2 and 9 OPA1, since unfortunately 1 ACO2 and 2 AFG3L2 asymptomatic patients did not have comparable OCT data. ACO2 patients compared to OPA1 showed higher values in nasal RNFL thickness (p=0.038), average (p=0.036) and all sectors GCL thickness except for the superior (supero-nasal p=0.047, supero-temporal p=0.036, infero-temporal p=0.039 inferior p=0.042 and infero-nasal p=0.02); after adjusting p-values for multiple comparisons, significance was not confirmed (Fig 5).

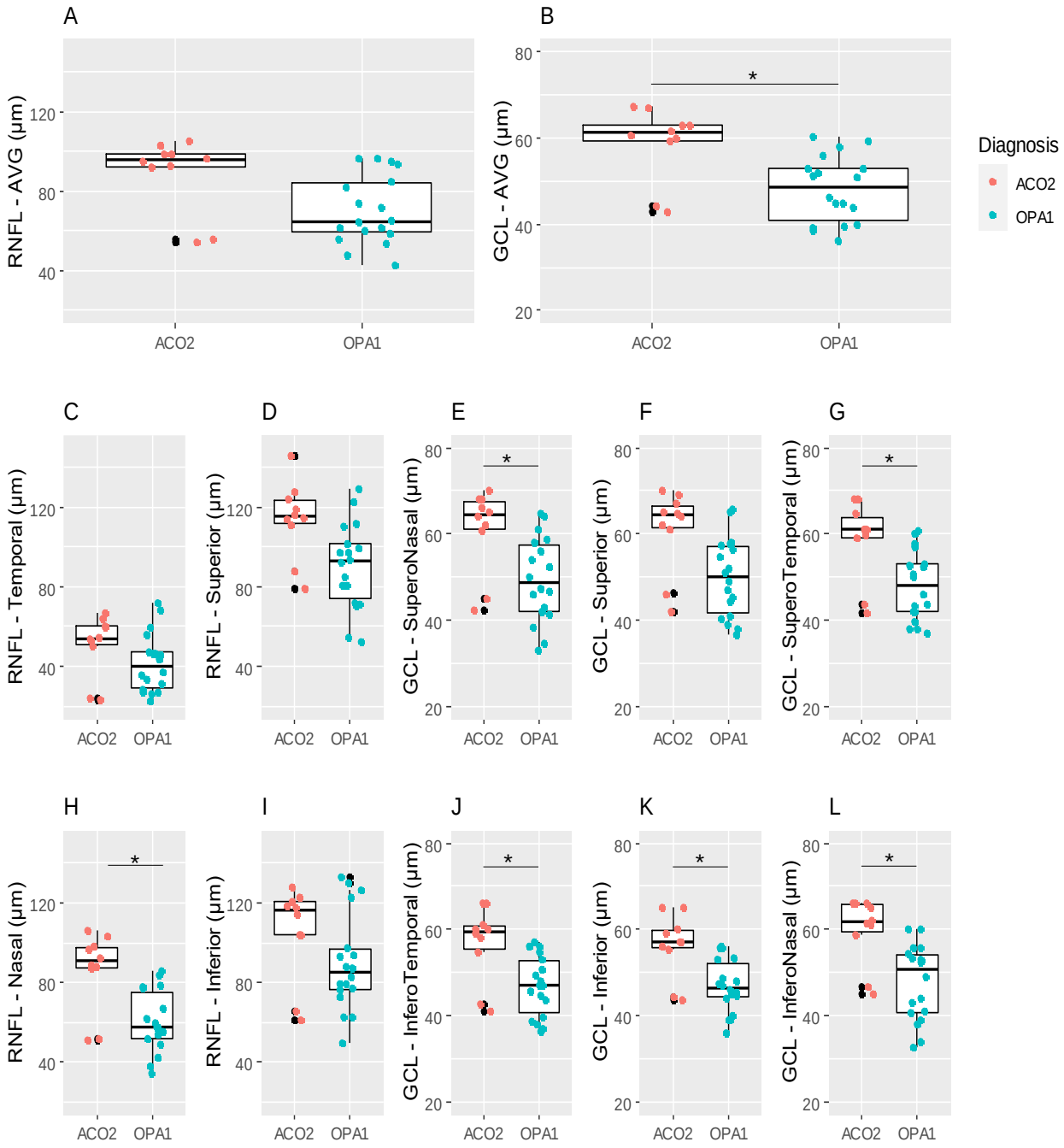

Figure 5. Average and sectorial GCL thickness in ACO2 and OPA1 asymptomatic patients. *p<0.05

We also looked at gender difference within each group (ACO2, OPA1 and AFG3L2), and we found no statistically significant difference between males and females in the neuro-ophthalmological parameters.

We then stratified neuro-ophthalmological results according to the type of mutation (missense or causing haploinsufficiency) in the ACO2 and OPA1 groups in order to find any specific genotype-phenotype correlation. In the ACO2 group, we compared 13 patients with missense mutation (referred as ACO2-m) with 10 haploinsufficiency mutation carriers (referred as ACO2-h). We failed to disclose any significant difference in the explored parameters between the 2 groups (data not shown). Nevertheless, we observed that ACO-m group showed lower values of GCL thickness close the significance threshold in the average (p=0.059), supero-nasal (p=0.055) and superior (p=0.054) sectors (Fig 6).

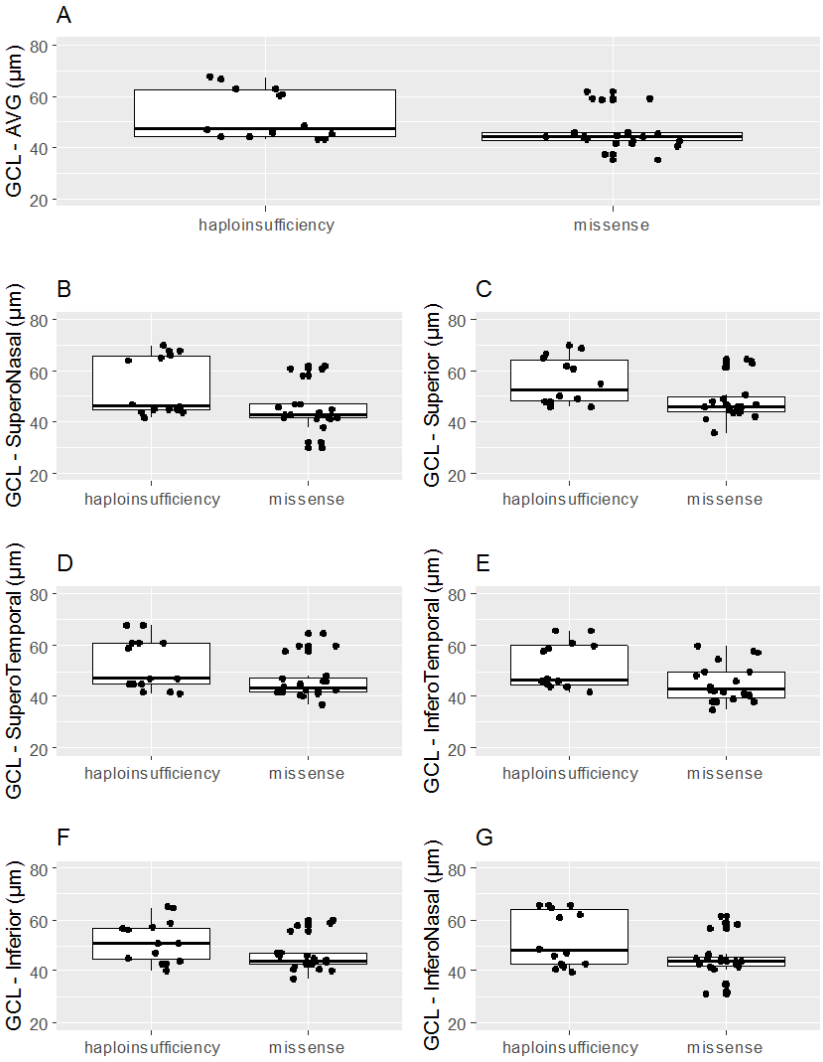

Figure 6. Average and sectorial GCL thickness within the ACO2 group, stratified by missense or haploinsufficiency mutation.

Within the OPA1 group, we compared results of 15 missense carriers (OPA1-m) and 57 patients with haploinsufficiency (OPA1-h). As already described in literature (Barboni et al., 2014), the OPA1-m group presented a more severe manifestation of disease, showing lower values of BCVA (p=0.01), colours (p=0.008), MD at VF (p=0.048), ONH size (p=0.039), average (p=0.036) and superior (p=0.011) RNFL thickness (data not shown).

We were able to collect electrophysiological data in a subgroup of patients: 6 ACO2, 2 AFG3L2 patients and 9 OPA1 patients. We compared the results of ACO2 patients with OPA1 and AFG3L2 patients combined since no difference was evident at the neuro-ophthalmological analysis. Mean age was 39,82±17,95 years in OPA1+AFG3L2 group and 39±20,64 years for ACO2 group. In the ACO2 group, except for two asymptomatic subjects, patients showed a reduced amplitude of the N95 component at P-ERG and of P100 at VEP. ff-ERG and PhNR were overall within normal limits. In the OPA1+AFG3L2 group, all tested patients showed amplitude reduction of N95 at P-ERG and of P100 at VEP, as well as a reduced PhNR amplitude, while ff-ERG resulted normal. (Fig 7).

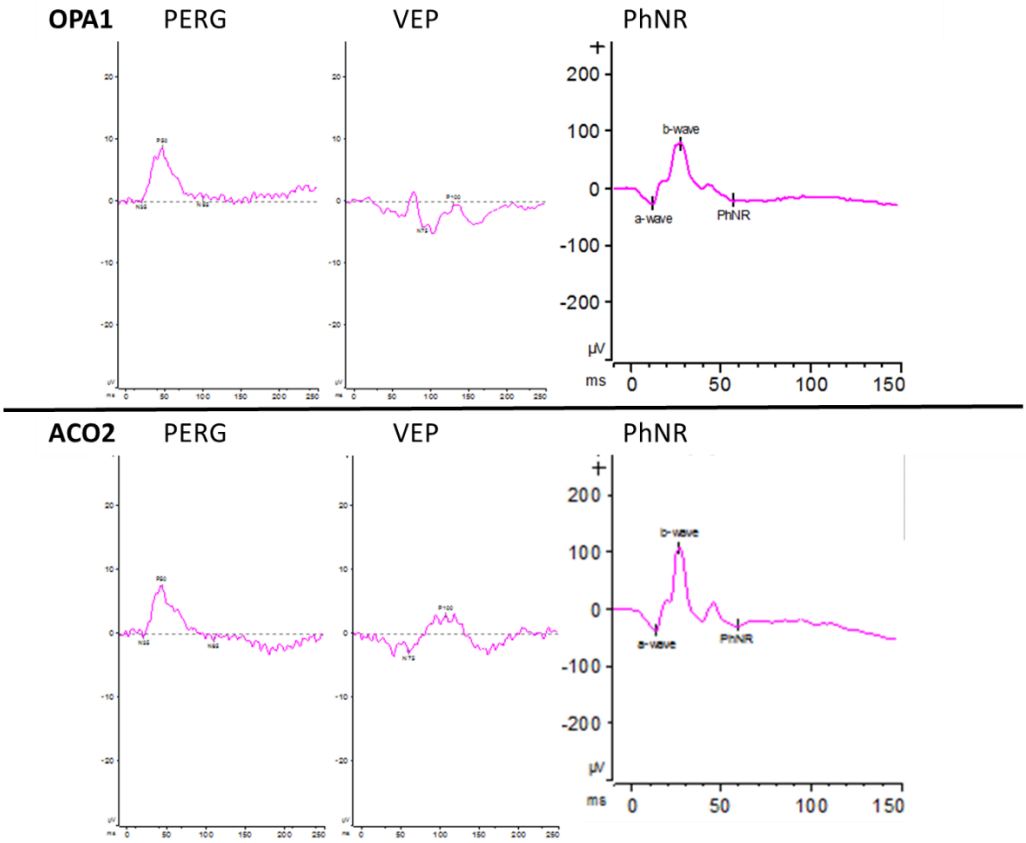

Figure 7. P-ERG, VEP and PhNR waveforms in a patient with OPA1 mutation (upper panels) and in a patient with mutation in ACO2 gene (lower panels)

At comparison between groups, P-ERG registrations showed significant lower N95 amplitude in the OPA1+AFG3L2 group compared to ACO2 (-4,29±1,93 vs -7,32±1,13 µV, p=0.001), while N95 latency was significantly delayed in ACO2 (95,64±3,81 vs 104,75±5,6 ms, p=0.000). VEP showed lower P100 amplitude in OPA1+AFG3L2 compared to ACO2, despite not reaching statistical significance (3,621±1,71 vs 7,83 ±5.54 µV, p=0.511), and significant prolonged latencies in OPA1+AFG3L2 (111±11,31 vs 97,75±5,70 ms, p=0.010). No difference in scotopic and photopic ERG was observed between groups. PhNR amplitudes did not differ between groups while PhNR latency was delayed in ACO2 compared to OPA1+AFG3L2 (63,409±9,18 vs 69,25±6 ms, p=0.024). (Fig 8). These results were confirmed also after excluding from the analysis the two asymptomatic ACO2 patients.

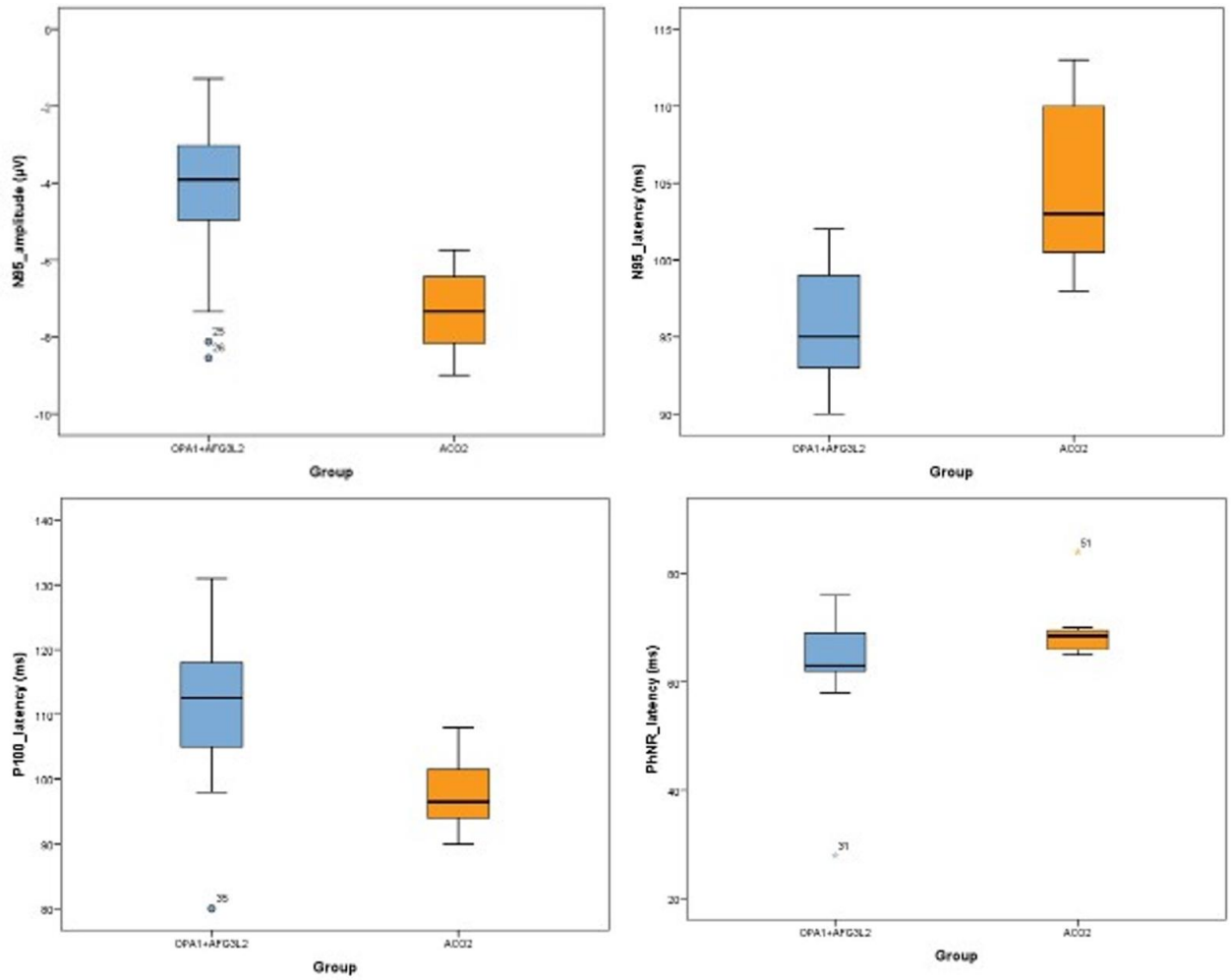

Figure 8. Significant differences in electrophysiological parameters between the OPA1+AFG3L2 group and the ACO2 group.

3.5 Discussion

We compared the ophthalmological phenotype of patients carrying two recently defined frequent genetic causes of DOA, i.e. *ACO2* and *AFG3L2* heterozygous mutations (Rocatcher et al., 2022), with a matched group of classical *OPA1*-related DOA patients. We found that, while *AFG3L2*-mutant patients were virtually identical to *OPA1*-related DOA, those carrying monoallelic *ACO2* variants had in general better RGC preservation, as assessed by RNFL/GCL thickness at OCT, even if visual acuities and visual fields were comparable. This was true for symptomatic patients, but the same pattern was also reflected in the subclinical mutation carriers, where only an OCT abnormality could be detected without visual defects. Electrophysiological assessment confirmed in a way a less severe damage of the optic nerve in ACO2 compared to OPA1 and AFG3L2 patients (Morny et al., 2015). Nevertheless, we observed slight prolonged retinal responses concerning N95 and PhNR, probably reflecting an early RGCs dysfunction in ACO2 patients (Berezovsky et al., 2021).

The limited case series hampered significance once cases were stratified by mutation category, i.e. missense vs haploinsufficiency mutations, but as for the well-established greater severity of missense mutations in *OPA1* (Barboni et al., 2014), a similar tendency was recognized for *ACO2*. In general, optic atrophy in ACO2 and AFG3L2 patients was congruent with the canonical phenotypic characteristics of *OPA1*-DOA, with a prevalent childhood onset, temporal pallor, and an insidious, stable or slowly progressive clinical course.

The fact that *AFG3L2*-DOA cases, all carrying missense mutations affecting the ATPase domain, resulted to be a phenocopy of *OPA1*-DOA, may be explained by an indirect effect of *AFG3L2* mutations on OPA1 processing. In fact, *AFG3L2* encodes a subunit of a proteolytic complex located in the IMM, involved in mitochondrial protein quality control. Mutations affecting the ATPase domain impair both the proteolytic and the dislocase activity of AFG3L2, which is essential for the processing of proteins. The impairment in m-AAA function has been proposed to cause an excess of proteins in the IMM, determining a reduction in mitochondrial membrane potential and activation of the stress-related protease OMA1 that directly processes the long OPA1 isoforms into shorter ones (Baderna et al., 2020). We recently demonstrated in patient-derived fibroblasts that AFG3L2 dysfunction results in an accumulation of short forms of OPA1 reflecting into an augmented fragmentation of the mitochondrial network, which is a well-known pathogenic paradigm for mitochondrial optic neuropathies (Caporali et al., 2020). Hence, the mechanism by which *AFG3L2* mutations lead to optic atrophy is assumed to be the unbalanced processing of OPA1, ultimately causing a phenotype that is indistinguishable from *OPA1*-related DOA. The same mechanism is proposed for DOA associated to dominant mutations in *SPG7* gene, whose protein product combines with AFG3L2 to form the m-AAA protease and whose recessive mutations cause Hereditary Spastic

Paraplegia type 7 (HSP7) (Casari et al., 1998). Notably, contrarywise to *AFG3L2* DOA-associated mutations, the *SPG7* variants leading to DOA seem to be dispersed amongst the recessive variants that cause HSP7. Moreover, mutations leading to frameshift suggest that SPG7 haploinsufficiency might be the primary pathophysiologic mechanism determining DOA (Charif et al., 2020).

On the other hand, *ACO2*-DOA, despite being not different in terms of functional measures such as BCVA and VF parameters, consistently showed higher values of nasal RNFL and GCL thickness at OCT compared to both AFG3L2 and OPA1. The reason for this anatomical difference, which was confirmed also in subclinical patients, can be explained in a different pathogenic mechanism not involving OPA1. ACO2 seems to play a role, regardless its enzymatic activity in the Krebs' cycle, also in mtDNA maintenance. In fact, studies on fibroblasts with *ACO2* mutations have shown, in conjunction with reduced levels of the protein, a reduction of mtDNA copy number up to 50%, which caused impaired mitochondrial respiration and augmented susceptibility to stress-induced and metabolically demanding conditions (Neumann et al., 2020). This could eventually be the cause of the optic nerve atrophy observed in heterozygous *ACO2* mutations. Interestingly, a similar mechanism has been described in fibroblasts derived from patients with mutations, either dominant or recessive, in another nuclear gene, the single stranded binding protein 1 (*SSBP1*). This gene encodes for a key factor of the mtDNA replisome (Jiang et al., 2021). *SSBP1* mutations, like for *ACO2,* can be transmitted as autosomal dominant or recessive traits and lead to either isolated optic atrophy or a complex syndromic form including retinal macular dystrophy, sensorineural deafness, myopathy and kidney dysfunction. The mechanism by which *SSBP1* mutations cause pathology is now established to depend on impaired mtDNA replication, which in turn leads to mtDNA depletion without accumulation of multiple deletions (Jurkute et al., 2019; Piro-Megy et al., 2020; Del Dotto et al., 2020). As final note, both *ACO2* and *SSBP1* genes, in the severe clinical expression may also affect the retinal pigmented epithelium and photoreceptors, besides the RGCs and optic nerve, as mtDNA partial depletion in the retina possibly affects all energy dependent cell types (Zeviani and Carelli, 2021).

Concerning the genotype-phenotype correlations, we confirmed once again that *OPA1* missense mutations displayed a more severe phenotype compared to mutations causing haploinsuffiency, both in terms of functional and anatomical parameters. (Yu-Wai-Man et al., 2010, Barboni et al., 2014). In the current study, a similar tendency, although not statistically significant given the small cohort, was observed with *ACO2*-DOA patients. Subjects harbouring a missense mutation showed overall lower values of BCVA, VF and OCT parameter, especially in the GCL, compared to those having a mutation predicted to cause haploinsufficiency. We can postulate a similar dominant negative mechanism for missense mutation in *ACO2*, as described for *OPA1*. In conclusion, DOA remains a

fairly homogeneous entity on the clinical ground despite the growing genetic heterogeneity underlying the disease. However, *ACO2* seems to stick out for being an overall milder phenotype, in terms of better preservation of RGCs, and we propose that this might depend on a different pathogenic mechanism involving mtDNA maintenance as opposed to *AFG3L2*, which obeys the *OPA1* dysfunction paradigm. These differences may reflect in the future in terms of better prognosis for *ACO2* once therapeutic approaches will be available.

4. PART 2: NEURO-OPHTHALMOLOGICAL AND ELECTROPHYSIOLOGICAL CHARACTERIZATION OF MELAS AND MERRF-ASSOCIATED mtDNA MUTATIONS

4.1 Introduction

Mitochondria are intracellular organelles carrying multiple copies of their own circular mitochondrial DNA (mtDNA). This genome contains a limited set of 13 genes all encoding subunits of the oxidative phosphorylation (OXPHOS) complexes, as well as 22 transfer RNAs (tRNAs) and 2 mitochondrial specific ribosomal RNAs (rRNAs) in order to carry on local protein translation given the slight differences in genetic coding as compared with the nuclear genome (Carelli et al., 2014; DiMauro et al., 2013). Mutations in tRNA genes commonly cause generalized decrease in protein translation, which in turn affects OXPHOS complexes leading to global deficit in cellular energy production affecting in a variable measure several metabolically active tissues (Shaukat et al., 2021). These mutations are usually heteroplasmic, a condition where mutant and wild type mtDNA co-exist within cells and tissues (Stewart et al., 2021). Clinical manifestations mainly depend on two factors: heteroplasmic loads of mutant mtDNA and tissue sensitivity to a specific mutation. Heteroplasmy can vary significantly among different tissues: post-mitotic tissues, like muscle, usually present with higher loads of mutant mtDNA heteroplasmy, whereas in tissues with high turnover rates, like blood cells, mutant mtDNA is negatively counter-selected. This over time decreases the mutant loads in blood cells, frequently resulting in its consistent reduction or even disappearance with age. In contrast, mutant heteroplasmy levels may undergo clonal expansion in single cells within post-mitotic tissues with aging, which in addition promotes somatic accumulation of mtDNA mutations and deletions (Frederiksen et al., 2006). Clinically, symptoms manifest when the mutant heteroplasmic load reaches a certain threshold overtaking the cellular energetic reserve. Usually, but not always, higher levels of heteroplasmy correlate with the severity of the phenotype (Gorman et al., 2016). Despite mitochondria are present in virtually every cell of every tissue, the organs most prone to be affected are usually those most susceptible to energetic failure, such as brain, skeletal and cardiac muscles and eyes. Neuro-ophthalmological findings in mitochondrial disease are very common, although their frequency and combination are still unclear, with the classical phenotypes being: optic atrophy, pigmentary retinopathy, chronic progressive external ophthalmoplegia (CPEO) and cortical visual loss like in stroke-like episodes. (Zhu et al., 2017; La Morgia et al., 2020; Zeviani and Carelli, 2021). In this part of the project, we aimed at defining the neuro-ophthalmological features of the two most common phenotypes due to mtDNA mutations affecting tRNA-encoding genes, known respectively as Mitochondrial myopathy, Encephalopathy, Lactic Acidosis and Stroke-like episodes (MELAS) (Pavlakis et al., 1984) and Myoclonic Epilepsy with Ragged-Red Fibers (MERRF) (Tsairis et al.,

1973). Even if both diseases are most commonly related to tRNA mutations, respectively leucine for MELAS and lysine for MERRF, there are also profound differences.

MELAS is a proteomorphic syndrome due in the majority of cases to the m.3243A > G mtDNA mutation responsible for the adenine to guanine transition in the *MT-TL1* gene encoding the leucine-tRNA (Goto et al., 1990; Kobayashi et al., 1990). Other rarer mutations in *MT-TL1* are also reported (Salsano et al., 2010; Lin et al., 2013; Keilland et al., 2016), as well as mutations in genes encoding for ND subunits of complex I have been described in association with overlap syndromes bridging MELAS with Leber's hereditary optic neuropathy (LHON) and Leigh syndrome (Carelli et al., 2009; La Morgia et al., 2014; Vacchiano et al., 2021). The classical MELAS syndrome presents with three cardinal features: 1) encephalopathy with seizures and/or dementia, 2) myopathy with lactic acidosis at rest and/or ragged red fibers 3) stroke-like episodes causing transient focal symptoms before age 40. Other manifestations include cardiac, endocrine, renal and psychiatric symptoms (Carelli and La Morgia, 2018). Ophthalmological findings, whether present, usually affect the outer retina and particularly the retinal pigmented epithelium (RPE) (Latlava et al., 2002), since photoreceptors in the RPE are particularly sensitive to OXPHOS impairment due to mtDNA mutations, requiring large amounts of energy to maintain their resting potentials (Zeviani and Carelli, 2021). MELAS-associated retinopathy can present in variable degrees of severity even within the same family, ranging from mild pigmentary changes in the outer retinal layers of the macula to a profound chorioretinal atrophy in the macula, nevertheless the fovea is usually relatively spared until late in the disease, resulting in a prolonged preservation of visual acuity (De Laat et al., 2013, Rath et al., 2008). Despite retinopathy is the most common ocular finding in patients with MELAS, some may present a phenotype with greater neuro-ophthalmologic involvement including myopathy with ptosis or CPEO and retrochiasmal visual loss due to stroke like-lesions affecting the visual cortex and occasionally optic atrophy (Hwang et al., 1997).

MERRF is a much rarer multisystemic mitochondrial syndrome, characterized by variable onset of generalized seizures, myoclonus, and ataxia, associated most frequently (80%) with the m.8344A>G mtDNA point mutation causing adenine to guanine transition in the *MT-TK* gene encoding lysine tRNA (Miyaue et al., 2019). Ocular phenotype in MERRF mostly includes CPEO associated with ptosis and optic atrophy (DiMauro et al., 2002; Mancuso et al., 2013). Optic atrophy results from degeneration of retinal ganglion cells (RGCs), which are highly dependent on mitochondrial proficiency for transmitting the action potential along their unmyelinated axons (Carelli et al., 2017). The small axons of the papillomacular bundle, which serves the central vision, are the most sensitive to energy depletion, their selective degeneration presents usually with prevalent temporal optic pallor and decrease in visual acuity, even if asymptomatic patients with only instrumental sign of

neuroretinal involvement have been described (Najjar et al., 2019). However, both MELAS and MERRF share high variability of clinical expression and penetrance even within the same family, partially attributed to mitochondrial copy number differences and heteroplasmy (Chinnery et al., 1997). For this reason, whenever possible we correlated the neuro-ophthalmological phenotype with heteroplasmy of mutant mtDNA.

4.2 Methods

We prospectively recruited subjects harboring a mtDNA mutation known to cause respectively the MELAS or MERRF phenotype. Both patients with complete and incomplete MELAS syndrome, according to Hirano's criteria (Hirano et al. 1992), were included. Information about family history, onset of disease, ocular and extraocular symptoms was recorded or retrieved from previous visits. A modified Newcastle Mitochondrial Disease Scale (NMDAS), excluding the item n°10 on cognition, was retrospectively calculated from last available neurological assessment. Neuro-ophthalmological examination included: best corrected visual acuity (BCVA) in LogMAR, color vision (Ishihara test), ocular motility assessment, slit lamp examination with fundus picture, visual field (VF) (Humphrey Field Analyzer, protocol Sita Standard 30-2, Zeiss, San Leandro, CA, USA) and Optical Coherence Tomography (OCT) to assess retinal nerve fibre layer (RNFL) thickness and ganglion cell layer (GCL) segmentation analysis of the macula (DRI Triton, Topcon, Tokyo, Japan) (Barboni et al., 2005). In patients displaying retinopathy autofluorescence was performed. We also evaluated lactic acid at baseline and when possible after standardized exercise, as previously reported (Montagna et al., 1995).

In subgroups of patients, we also performed a complete electrophysiological assessment including: visual evoked potential (VEP) to assess integrity of central vision pathways, pattern electroretinogram (P-ERG) to differentiate retinal from optic nerve dysfunction and monitor RGCs dysfunction, scotopic and photopic full field electroretinogramm (ff-ERG) to assess cone and rod function and photopic negative response (PhNR) to assess RGCs function (appendix 1).

4.3 Genetic analysis

The level of heteroplasmic mutant load was assessed on available biological samples using the SnapShot method. DNA samples derived from peripheral blood, urinary flake cells and skeletal muscle of patients, previously collected for molecular diagnosis, were analysed. For each sample, the DNA region containing the mutation was amplified and purified, followed by SnapShot procedure to assess the amount of mutated and wild-type DNA. Since the heteroplasmy of mtDNA mutation can vary from tissue to tissue, whenever possible, all available samples from each patient were analysed.

Patients were further classified into three distinct groups depending on the mutation: patients with MELAS syndrome and the classic m.3243A>G/MT-TL1 mutation (MELAS-c); patients with MELAS syndrome with rarer mutations other than m.3243A>G/MT-TL1 (MELAS-r); patients with MERRF syndrome, with m.8344A>G/MT-TK mutation (MERRF).

4.4 Statistical analysis

The two main groups (from now on referred as MELAS and MERRF) were analyzed to compare gender, age, mutation distribution and visual function outcomes. For each group, continuous variables were summarized with statistics including the number of patients (n), mean, standard deviation (SD), median, minimum and maximum (range). Shapiro-Wilk and Kolmogorov-Smirnov normality tests were used to assess the normal distribution of data. Demographic data, heteroplasmy levels in the three different available tissues and lactic acid values were compared between MELAS and MERRF using univariate t-test if normally distributed, contrariwise Mann-Whitney U test was used. The following visual endpoints were analyzed: BCVA, mean deviation (MD) and fovea at VF, Ishihara color vision testing, RNFL (average, temporal, superior, nasal, and inferior quadrants), and GCL (average and 6 individual macular sectors: superotemporal, superior, superonasal, inferonasal, inferior, and inferotemporal) thickness. We applied the Clustered Wilcoxon rank sum test using Rosner-Glynn-Lee method and the Benjamini & Hochberg method to adjust p-values for multiple comparisons. Pearson's correlation was used to relate the heteroplasmic mutant load to age, modified NMDAS score, lactic acid levels and neuro-ophthalmologic data. Statistical significance was established at $p<0.05$. Statistical analyses were carried out using R software (version 4.0.0) and IBM SPSS Statistics for Windows, version 20.0 (IBM Corp., Armonk, N.Y., USA) software.

4.5 Results

Demographic and general clinical/genetic features of the cohort are shown in Table 3.

We evaluated a total of 41 patients, 33 with MELAS (16 males and 17 females) and 8 with MERRF (4 males and 4 females). Mean age was 49,42±14,3 for MELAS patients and 48±16,36 for MERRF. The majority of MELAS patients (26 patients, 79%) harboured the classic m.3243A>G/MT-TL1 mtDNA mutation, while the remaining 7 subjects presented a rarer mutation. In details, 3 had rarer mutations in the same gene (m.3279C>T/MT-TL1, m.3258T>C/MT-TL1, m.3271T>C/MT-TL1), 3 had a mutation in a different mtDNA gene (m.13094T>C/MT-ND5, m.10191T>C/MT-ND3, m.7896G>A/MT-CO2) and one presented a double mutation (m.10009G>A in glycine tRNA encoding gene and 15961G>A in proline tRNA encoding gene). All 8 MERRF patients invariably harboured the classic m.8344A>G/MT-TK mtDNA mutation.

Heteroplasmy levels in the three different tissues analyzed are shown in table 3. As expected, heteroplasmy levels from muscle showed higher mutant loads compared to urinary sediment and blood samples in both groups. Comparing heteroplasmy levels in the two groups it is interesting to note that the percentage of mutant mtDNA heteroplasmy in MERRF patients was significantly higher than in MELAS patients in blood cells (p=0.000) and in muscle (p=0.049), while was not different in urinary sediment (p=0.31).

Clinical core symptoms are described in Table 3. Mean age at onset of disease was 33,15±12,8 for MELAS and 27,13±17 for MERRF. Almost all MELAS patients presented more than one symptom, except for 2 completely asymptomatic carriers and 2 subjects presenting isolated diabetes and optic atrophy respectively. Hearing loss and diabetes were the most common findings respectively in 22 and 21 patients. Moreover, 18 patients had myopathy, 11 experienced at least one stroke-like episode, 10 suffered from epilepsy and 10 presented ataxia. All 8 MERRF patients had signs of myopathy, presenting as isolated symptom in 3 subjects. Two patients also had sensorineural deafness, 5 epilepsy/myoclonus and 3 ataxia. Mean modified NMDAS score was 29,1±16,02 for MELAS and 22±15,97 for MERRF and was not significantly different between the two groups (p=0.28).

Basal lactic acid value was assessed in all patients. Lactic acid at rest was abnormal in 9 MELAS patients (27%) and 1 MERRF patients (12%). Mean lactic acid levels at rest were 21,36±12,98 mg/dL in MELAS and 14,26 ±8,40 mg/dL in MERRF (normal range 5-22 mg/dL, p=0.18). Lactic acid values after exercise were increased and remained abnormally elevated after the recovery time in 25/29 (86%) MELAS and 5/6 (83%) MERRF, without significant differences between groups (p=0.51 and p=0.79 respectively).

	MELAS	MERRF	P
Subjects [N]	33	8	
Age [years, mean±SD]	49,42±14,3	48±16,36	[a] 0.74
Sex [male, N(%)]	16 (48%)	4 (50%)	[b] 0.93
mtDNA Mutation - Classic [N(%)]	26 (79%)	8 (100%)	
- Rarer [N(%)]	7 (21%)	0	
Heteroplasmy levels			
Blood [N]	27	8	
- **Percentage [mean ±SD]**	22,74±15,93	66,8±17,13	[a] 0.000
Urine [N]	24	4	
- **Percentage [mean ±SD]**	57±23,12	69,5±19	[a] 0.31
Muscle [N]	24	3	
- **Percentage [mean ±SD]**	71,17±13,88	88,3±8,95	[a] 0.049
Status - affected [N(%)]	31 (94%)	8 (100%)	[b] 0.47
- asymtomatic [N(%)]	2 (6%)	0	
Mean age at onset [mean ±SD]	33,15±12,8	27,13±17	[a] 0.27
Core symptoms [N (%)]	30 (90%)	8 (100%)	[b] 0.36
- **Stroke-like**	11	0	
- **Epilepsy/myoclonus**	10	5	
- **Hearing loss**	22	3	
- **Myopathy**	18	8	
- **Ataxia**	10	3	
- **Diabetes**	21	0	
NMDAS score [mean ±SD]	29,10±16,02	22±15,97	[a] 0.28

Table 3. Demographic and general clinical/genetic features of MELAS and MERRF patients

[a] p-value referred to t-test test.

[b] p-value referred to Chi-squared test.

Abbreviations: N: absolute frequency, %: relative frequency, SD: standard deviation.

Neuro-ophthalmological symptoms were present in 23 (69%) of MELAS patients, either in combination (56%) or isolated (34%), with retinopathy being the most common manifestation (17/23 patients), followed by optic atrophy in 11/23 patients. Isolated ptosis was evident in 3/23, while CPEO in 6/23 patients and retrochiasmal visual defect was present in 4/23 patients. This latter presenting as homonymous hemianopsia or quadrantopsia due to posterior stroke-like lesions. The severity of retinopathy was very variable among patients even within the same family, ranging from mild salt and pepper irregularity to severe chorioretinal atrophy (Fig 9 and Fig 10 showing examples of retinopathy at fundus picture and autofluorescence respectively). Autofluorescence was performed in 15/17 MELAS patients presenting retinopathy and was graded according to a recent classification of mitochondrial retinopathies (Birtel et al., 2021). In our cohort, 7/15 patients presented type 1

retinopathy characterized by increased and decreased retinal autofluorescence, 4/15 patients presented type 2 retinopathy showing hyperautofluorescent dot or fleck-like lesions and, where present, sharply demarcated dark areas of chorioretinal atrophy, 4/15 patients presented a type 3 retinopathy with peripapillary atrophy and a widespread granular autofluorescent pattern with areas of chorioretinal atrophy.

Among MERRF patients, 7/8 subjects (87%) presented optic atrophy (Fig 11), in association with ptosis in 1 patient and CPEO in 2 patients. None presented retinopathy nor retrochiasmal visual loss.

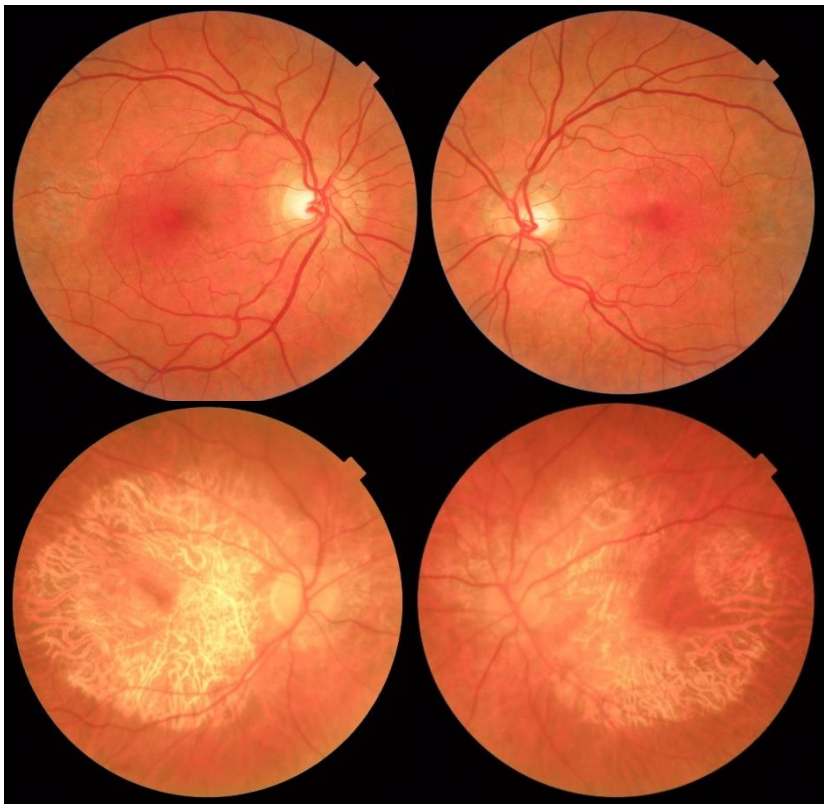

Figure 9. Mild (upper panels) and severe (lower panels) retinopathy at fundus pictures in MELAS patients.

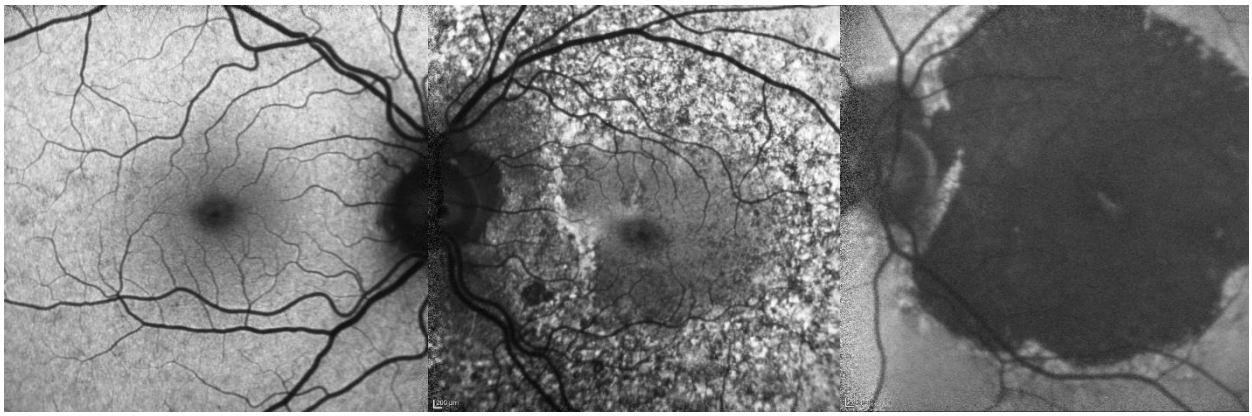

Figure 10. From left to right: worsening degrees of retinopathy at autofluorescence in MELAS patients.

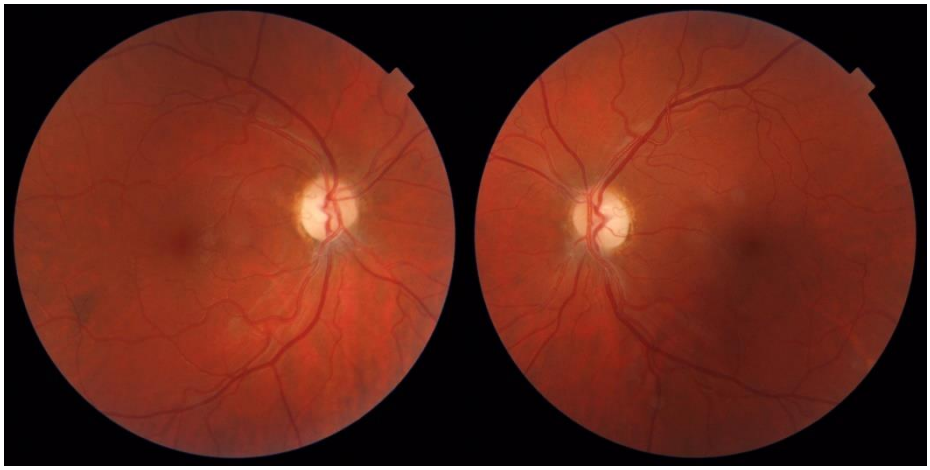

Figure 11. Optic atrophy in a MERRF patient.

Mean visual acuity was -0,04±0,67 LogMAR for MELAS patients and -0,36±0,72 LogMAR for MERRF. VA was clearly reduced (LogMAR>0) in 11/23 (47%) MELAS patients and only 1/7 (14%) MERRF patient. Average RNFL thickness was 87,72±22,32 µm in MELAS and 74,12 ±13,73 µm in MERRF. Overall, quadrant RNFL thinning was consistent with the predominant temporal optic atrophy at fundus examination with the temporal sectors being the thinnest (62,10±14,94 in MELAS and 50,69±15 in MERRF). Average GCL thickness was 54,12±14,10 in MELAS and 55,70±6,57 µm in MERRF.

Neuro-ophthalmological findings are summarized in Table 4. Comparison between the two groups failed to disclose any difference in BCVA, colors and VF parameters. At OCT analysis, MERRF patients compared to MELAS showed significantly lower values of RNFL thickness, both in average (p=0.021), temporal (p=0.044) and nasal sector (p=0.010) (Fig 12). No difference was found in GCL thickness.

	MELAS	MERRF	p
Neuro-ophthalmological symptoms [N(%)]	23 (69%)	7(87%)	[b] 0.30
-Isolated	10 (43%)	4 (57%)	
-Combined	13 (56%)	3 (43%)	
- **Optic atrophy**	11/23 (47%)	7/7 (100%)	[b] 0.009
- **Retinopathy**	17/23 (73%)	0/7 (0%)	[b] 0.008
- **Ptosis**	3/23 (13%)	1/7(13%)	[b] 0.93
- **CPEO**	6/23 (26%)	2/7 (28%)	[b] 0.89
- **Retrochiasmal defects**	4/23 (17%)	0/7 (0%)	[b] 0.30
Eyes [N]	64	16	
BCVA [LogMAR, mean±SD]	-0,04±0,67	-0,36±0,72	[a] 0.30
Colors [mean±SD]	8,44±4,92	8,55±5,05	[a] 0.58
VF [eyes, N]	23	4	
MD [dB, mean±SD]	-14,93±9,75	-10,47±8,65	[a] 0.51
Fovea [dB mean±SD]	30,91±5,41	22,75±16,28	[a] 0.63
OCT [eyes, N]	64	16	
RNFL AVG [µm, mean±SD]	87,72±22,32	74,12±13,73	[a] 0.021
RNFL T [µm, mean±SD]	62,10±14,94	50,69±15	[a] 0.044
RNFL S [µm, mean±SD]	108,53±32,77	90,38±18,66	[a] 0.060
RNFL N [µm, mean±SD]	71,85±19,41	61,25±8	[a] 0.010
RNFL I [µm, mean±SD]	109,7±31,92	94,94±19,55	[a] 0.062
GCL AVG [µm, mean±SD]	54,12±14,10	55,70±6,57	[a] 0.859
GCL SN [µm, mean±SD]	55,48±15,59	56,31±7,39	[a] 0.634
GCL S [µm, mean±SD]	53,83±14,47	55.12±6,77	[a] 0.771
GCL ST [µm, mean±SD]	54,40±14,60	55,80±6,91	[a] 0.843
GCL IT [µm, mean±SD]	55,23±14,10	56,19±6,57	[a] 0.696
GCL I [µm, mean±SD]	51,35±14,34	54,25±5,5	[a] 0.757
GCL IN [µm, mean±SD]	54,43±15,21	56±7,16	[a] 0.750

Table 4. Neuro-ophthalmological results of MELAS and MERRF patients.

Continuous variables are presented as mean ± standard deviation, while categorical variables as absolute and relative frequencies.

[a] p-value referred Clustered Wilcoxon rank sum test.

[b] p-value referred to Chi-squared test.

Abbreviations: N: number, SD: standard deviation, VA: visual acuity, VF: visual fields, MD: mean deviation, OCT: optic coherence tomography, ONH: optic nerve head, RNFL: retinal nerve fiber layer, GCL: ganglion cell layer, AVG: average, T: temporal, S: superior, N: nasal, I: inferior, SN: supero-nasal, ST: supero-temporal, IT: inferotemporal, IN: inferonasal

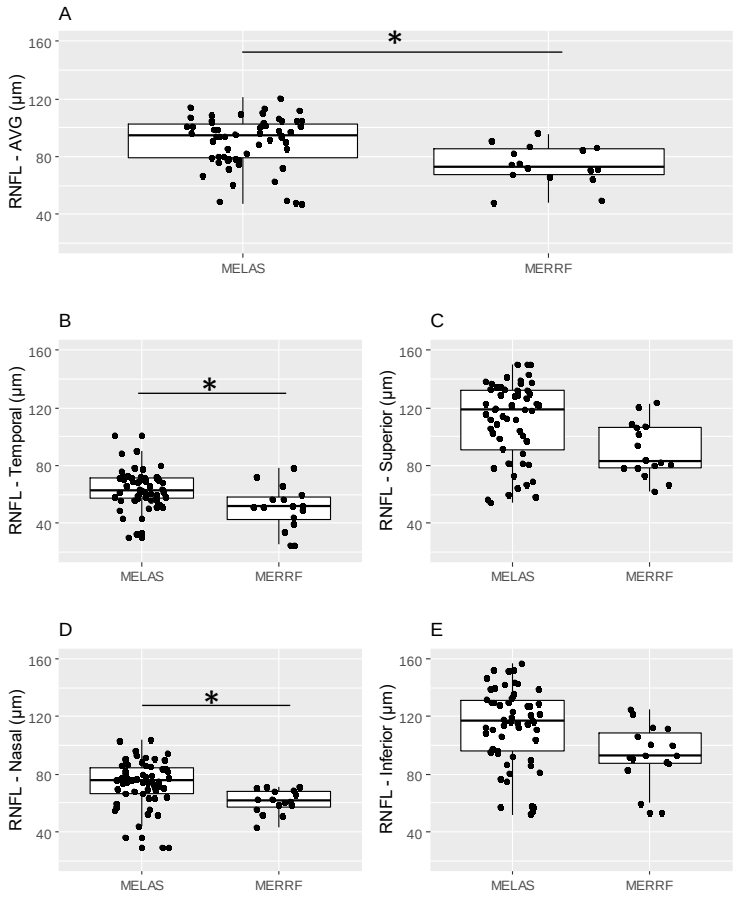

Figure 12. Average and sectorial RNFL thickness in MELAS and MERRF groups.
*p<0.05

We then stratified the neuro-ophthalmological results according to the type of mutation (classic or rarer) within the MELAS group in order to find possible specific genotype-phenotype correlations. We compared 26 patients with classic m.3243A>G mutation (MELAS-c) with 7 patients harboring a rarer mutation (MELAS-r). Mean age at onset was 34,34± 12,36 years in classic MELAS and 28,85 ±14,17 years in MELAS-r. Notably none among rare mutation carriers had diabetes mellitus. Neuro-ophthalmological results are shown in table 5.

MELAS-r showed reduced BCVA, colors, MD and fovea compared to MELAS-c, without reaching the significance threshold. While at OCT analysis, MELAS-r patients showed significantly lower values of RNFL thickness in average (p=0.015), temporal (p=0.005), superior (p=0.008) and inferior (p=0.015) sectors (Fig 13). Moreover, also GCL thickness resulted significantly lower in MELAS-r compared to MELAS-c in average (p=0.038), superotemporal (p=0.031), inferotemporal (p=0.017) and inferior (p=0.026) sectors, with superonasal (p=0.052) and superior sectors (p=0.053) close to being significant (Fig 14).

	MELAS-c	MELAS-r	P
Eyes [N]	51	13	
BCVA [LogMAR, mean±SD]	-0,15±0,64	0,37±0,65	0.074
Colors [mean±SD]	9,15±4,36	6,23±6,03	0.346
VF [eyes, N]	13	10	
MD [dB, mean±SD]	-10,63±5,15	-20,53±11,64	0.168
Fovea [dB mean±SD]	31,23±6,37	20,53±4,14	0.39
OCT [eyes, N]	51	13	
RNFL AVG [µm, mean±SD]	94±14,39	65±30,68	0.015
RNFL T [µm, mean±SD]	66,26±10,63	47,08±18,78	0.005
RNFL S [µm, mean±SD]	117,43±25,44	76,38±37,01	0.008
RNFL N [µm, mean±SD]	75,79±12,94	57,62±30,49	0.154
RNFL I [µm, mean±SD]	118,26±23,15	78,77±40,38	0.015
GCL AVG [µm, mean±SD]	56,35±14,03	46,08±11,58	0.038
GCL SN [µm, mean±SD]	57,28±16,18	49±11,51	0.052
GCL S [µm, mean±SD]	55,89±14,07	46,38±13,91	0.053
GCL ST [µm, mean±SD]	56,89±13,69	45,38±14,72	0.031
GCL IT [µm, mean±SD]	58,15±13,45	44,69±13,96	0.017
GCL I [µm, mean±SD]	53,62±14,5	43,15±10,6	0.026
GCL IN [µm, mean±SD]	56,26±15,91	47,85±10,33	0.062

Table 5. Neuro-ophthalmological results in patients with classic m.3243A>G/MT-TL1 mutation (MELAS-c) and patients harbouring a rarer mutation (MELAS-r).

P-values refer to Clustered Wilcoxon rank sum test.

Abbreviations: N: number, SD: standard deviation, VA: visual acuity, VF: visual fields, MD: mean deviation, OCT: optic coherence tomography, ONH: optic nerve head, RNFL: retinal nerve fiber layer, GCL: ganglion cell layer, AVG: average, T: temporal, S: superior, N: nasal, I: inferior, SN: supero-nasal, ST: supero-temporal, IT: inferotemporal, IN: inferonasal

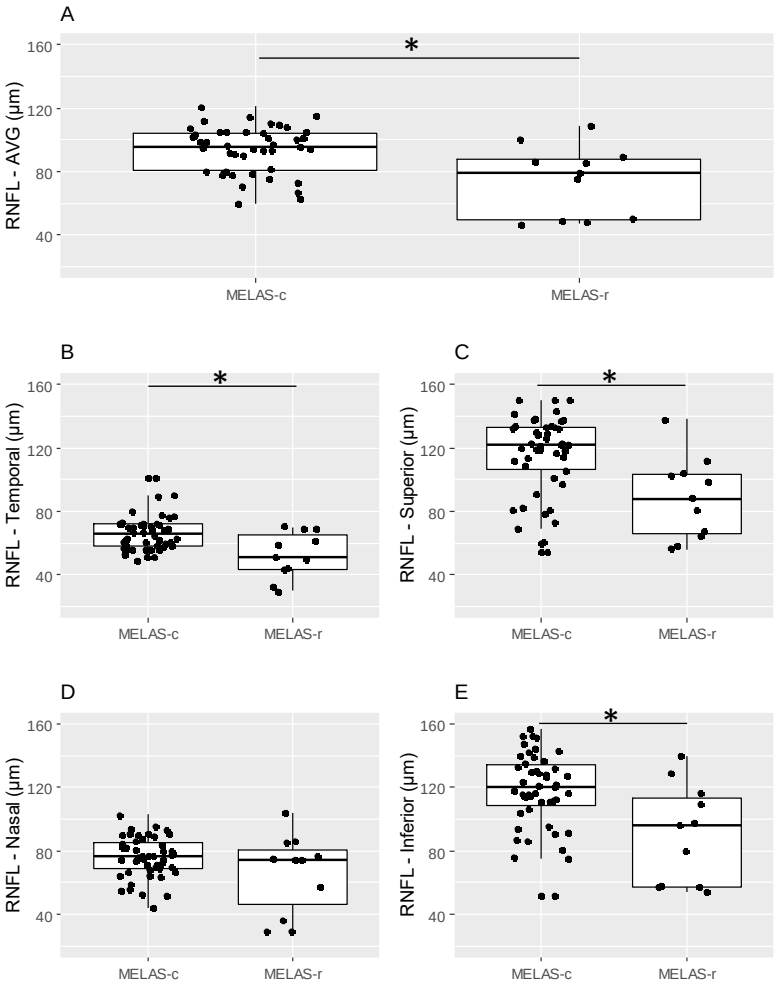

Fig 13. Average and sectorial RNFL thickness in patients with classic m.3243A>G/MT-TL1 mutation (MELAS-c) and patients harbouring a rarer mutation (MELAS-r).

*p<0.05

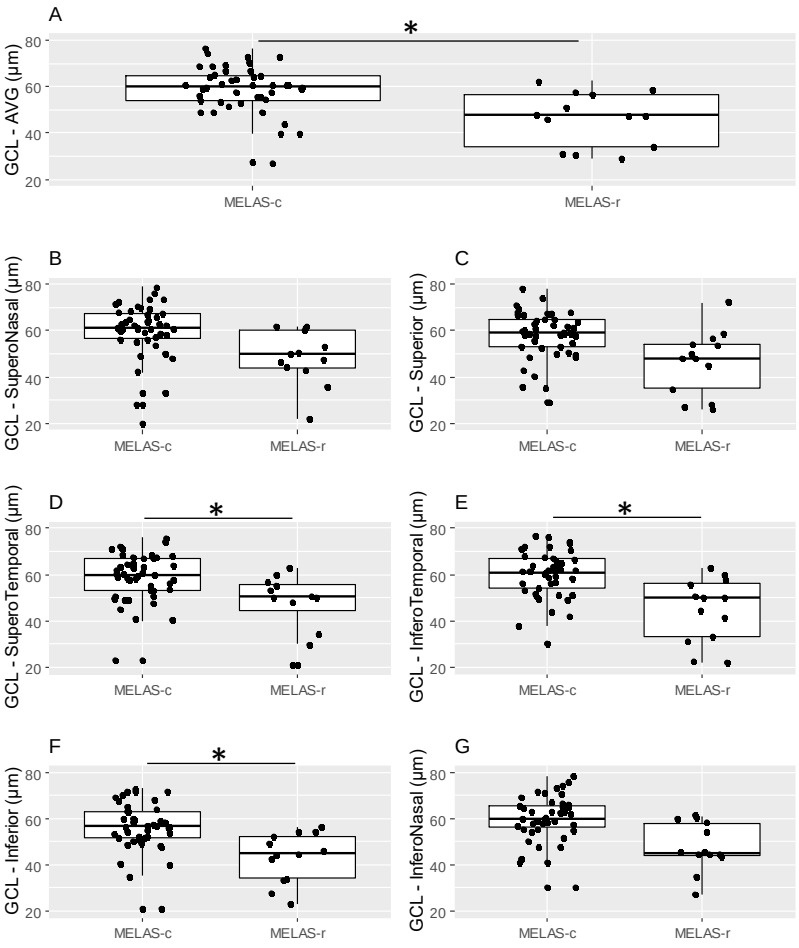

Figure 14. Average and sectorial GCL thickness in patients with classic m.3243A>G/MT-TL1 mutation (MELAS-c) and patients harbouring a rarer mutation (MELAS-r).

*p<0.05

We were able to collect electrophysiological data in a small subgroup of patients: 10 MELAS (7 females and 3 males) and 1 male MERRF (Table 6). Mean age in MELAS patients was 49,71±12,79 years and they all carried the classic m.3243A>G/MT-TL1 mutation, except one patient harboring the m.7896G>A/MT-CO2 mutation. We disclosed a high variability within MELAS patients: P-ERG were abolished in 2/10 patients, reduced in 2/10 and normal in 6/10, VEP were frankly abnormal in 3/10, mildly reduced in 1/10, normal in 6/10. ff-ERG were almost isoelectric in the patient carrying the m.7896G>A/MT-CO2 mutation, variably reduced in 4/10 patients, normal ERG were found in 4/10 patients. PhNR could not be performed/evaluated in 2 patients and was reduced in one patient, the remaining presented normal PhNR response. To note, mild abnormalities at electrophysiological tests were present in 2 patients, respectively at P-ERG-ERG in patient n° 2 and VEP in patient n°3, without clinical evidence of optic atrophy or retinopathy.

The only MERRF patient tested had only OCT signs of mild temporal optic atrophy with normal vision, electrophysiological testing resulted all normal.

Patient n°	Gender	Phenotype	Mutation	P-ERG	VEP	ff-ERG	PhNR	Optic atrophy	Retinopathy
1	F	MELAS	m.3243A>G/ MT-TL1	Reduced N95	Reduced	Normal	Normal	Yes	No
2	F	MELAS	m.3243A>G/ MT-TL1	Reduced P50-N95	Normal	Mildly reduced	Normal	No	No
3	F	MELAS	m.3243A>G/ MT-TL1	Normal	Mildy reduced	Normal	Normal	No	No
4	F	MELAS	m.3243A>G/ MT-TL1	Severely reduced	Reduced	Mildly reduced	/	No	Yes
5	F	MELAS	m.3243A>G/ MT-TL1	Normal	Normal	Normal	Normal	No	No
6	M	MELAS	m.3243A>G/ MT-TL1	Normal	Normal	Normal	Normal	No	No
7	F	MELAS	m.3243A>G/ MT-TL1	Normal	Normal	Normal	Normal	No	No
8	F	MELAS	m.3243A>G/ MT-TL1	Normal	Normal	Mild rod reduction	Normal	No	Yes
9	M	MELAS	m.3243A>G/ MT-TL1	Normal	Normal	Reduced	Reduced	No	Yes
10	M	MELAS	m.7896G>A/ MT-CO2	Severely reduced	Severely reduced	Severely reduced	/	No	Yes
11	M	MERRF	m.8344A>G/ MT-TK	Normal	Normal	Normal	Normal	Yes	No

Table 6. Electrophysiological results in MELAS and MERRF.

Abbreviations: P-ERG: pattern electroretinogram, VEP visual evoked potentials, ff-ERG: full-field electroretinogram, PhNR: photopic negative response

Correlation with heteroplasmy

We first evaluated the mtDNA heteroplasmy levels in different tissues in relation to age in MELAS and MERRF patients. In MELAS patients, as already described in literature (Grady et al., 2018), we found that levels of heteroplasmy in the blood cells decreased as the age of the patients increased, displaying a significant negative correlation (pearson -0.484, sig 0.011). The same correlation analysis between heteroplasmy levels and age was performed using available samples of DNA extracted from urinary sediment flaking cells and skeletal muscle biopsies. A significant negative correlation was confirmed also in urine samples (pearson -0.541, sig 0.006) but not in muscle specimens (pearson -0.388, sig 0.061) (Fig 15)

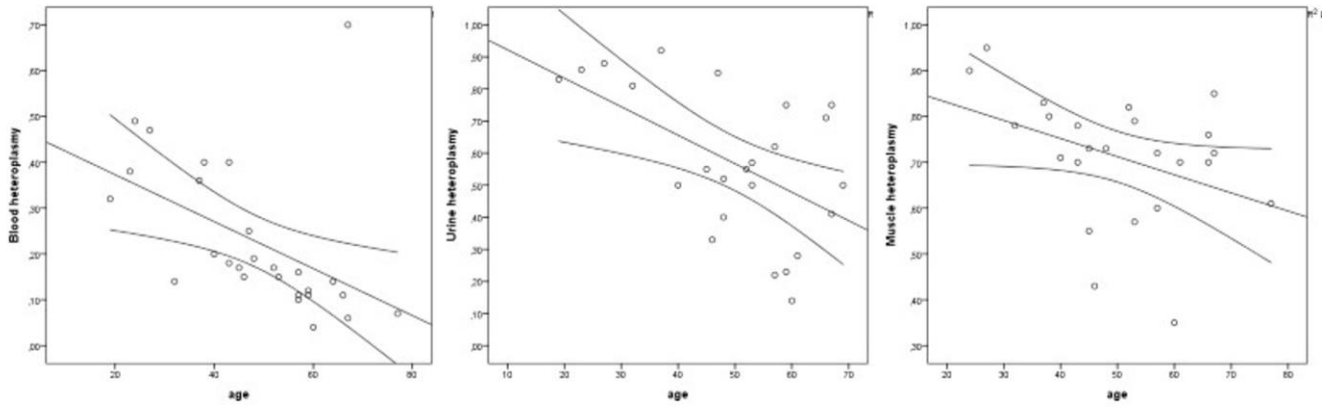

Figure 15. Correlation of mutant mtDNA heteroplasmy levels with aging in MELAS patients in the three available tissues (from left to right: blood, urine and muscle).

In contrast to the previous MELAS findings, in MERRF patients, blood heteroplasmy did not show any significant correlation with age (pearson -0.327, sig 0.430). Given the small number of urinary and muscular samples, we analyzed the levels of heteroplasmy in these two tissues combined and we found a mild negative correlation with age (pearson -0.765, sig 0.045) (Fig 16).

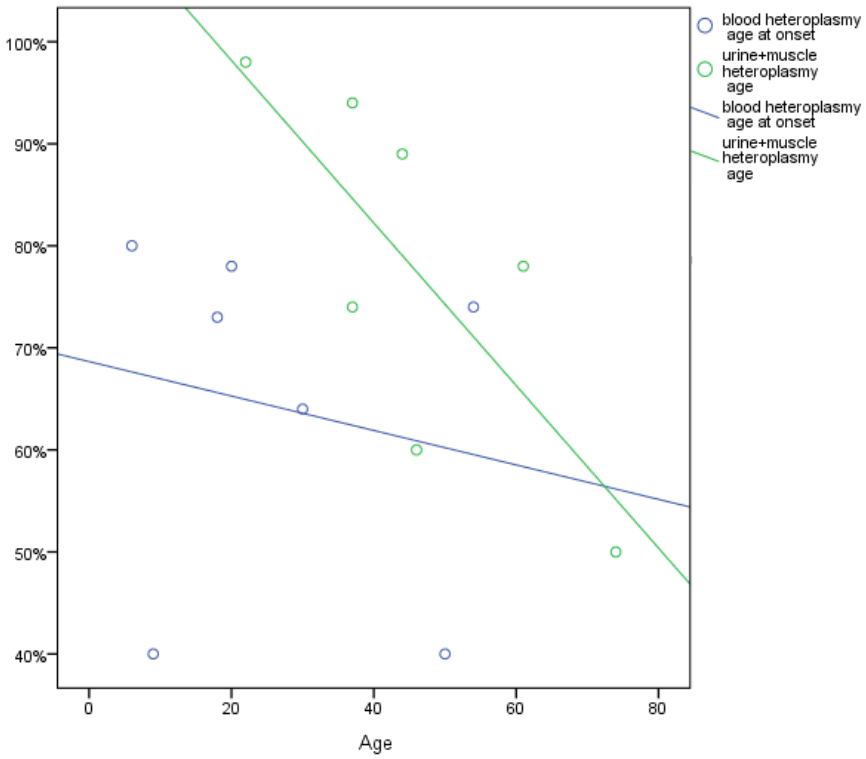

Figure 16. Correlation of heteroplasmy levels with aging in MERRF patients in blood (blue dots and line) and urine combined with muscle (green dots and line).

Given the high correlation of blood heteroplasmy with age in MELAS patients, for classic m.3243A>G/MT-TL1 mutation we normalized the values using the published formula from Grady and colleagues (Grady et al,. 2018). We then correlated heteroplasmy levels in these three tissues with lactic acid values (at rest, after exercise and after recovery). In MELAS patients, we did not find any significant correlation between heteroplasmy and lactic acid levels. While in MERRF patients, we found a mild positive correlation only between blood heteroplasmy and lactic acid levels after recovery (pearson 0.818, sig 0.047). We also correlated heteroplasmy levels with modified NMDAS score, failing to find any significance both in MELAS and MERRF patients.
We then correlated heteroplasmy levels with neuro-ophthalmological results in MELAS and MERRF patients. Right and left eyes were analysed first separately. In MELAS patients, blood heteroplasmy correlated negatively with average and sectorial RNFL thickness in both eyes, nevertheless using normalized blood heteroplasmy values, we lost the significant correlation with RNFL. Urine and muscle heteroplasmy did not correlate with any neuro-ophthalmological parameter in MELAS. In MERRF patients, we found a negative correlation between blood heteroplasmy and average RNFL (pearson -0.754, sig 0.031) in the right eye and temporal RNFL in the left eye (pearson -0.730, sig 0.040). Combined urine and muscle heteroplasmy correlated negatively with average RNFL in both eyes (right eye pearson -0.867, sig 0.012; left eye pearson -0.789, sig 0.035), and also with superior (pearson -0.768, sig 0.044), nasal (pearson -0.860, sig 0.013) and inferior RNFL sectors (pearson -0.795, sig 0.033) and inferotemporal CGL sector (pearson -0.785, sig 0.036) in the right eye.

Considering all eyes together, in MELAS patients, normalized blood heteroplasmy and urine heteroplasmy did not correlate with any OCT parameter while muscle heteroplasmy correlated negatively only with inferior RNFL thickness (pearson -0.321, sig 0.036).
In MERRF patients, blood heteroplasmy negatively correlated with average RNFL and all but nasal RNFL sectors, and with average GCL and all but inferior GCL sectors. Combined urine and muscle heteroplasmy negatively correlated with average and sectorial RNFL and with all but inferior GCL sectors (Table 7, Figure 17).

		blood heteroplasmy	urine+muscle heteroplasmy
RNFL avg	N	16	14
	Pearson's correlation	-,711**	-,827**
	Sig.	,002	,000
RNFL T	Pearson's correlation	-,641**	-,717**
	Sig.	,007	,004
RNFL S	Pearson's correlation	-,653**	-,728**
	Sig.	,006	,003
RNFL N	Pearson's correlation	-,410	-,648*
	Sig.	,115	,012
RNFL I	Pearson's correlation	-,604*	-,771**
	Sig.	,013	,001
GCL avg	Pearson's correlation	-,541*	-,638*
	Sig.	,030	,014
GCL S	Pearson's correlation	-,558*	-,647*
	Sig.	,025	,012
GCL SN	Pearson's correlation	-,611*	-,690**
	Sig.	,012	,006
GCL IN	Pearson's correlation	-,540*	-,631*
	Sig.	,031	,016
GCL I	Pearson's correlation	-,330	-,445
	Sig.	,213	,110
GCL IT	Pearson's correlation	-,536*	-,692**
	Sig.	,032	,006
GCL ST	Pearson's correlation	-,619*	-,709**
	Sig.	,011	,004

Table 7. Pearson's correlation between heteroplasmy and OCT parameters (RNFL and GCL) in MERRF patients all eyes considered.

** sig. <0.01 *sig. <0.05

Abbreviations: AVG: average, T: temporal, S: superior, N: nasal, I: inferior, SN: supero-nasal, ST: supero-temporal, IT: inferotemporal, IN: inferonasal

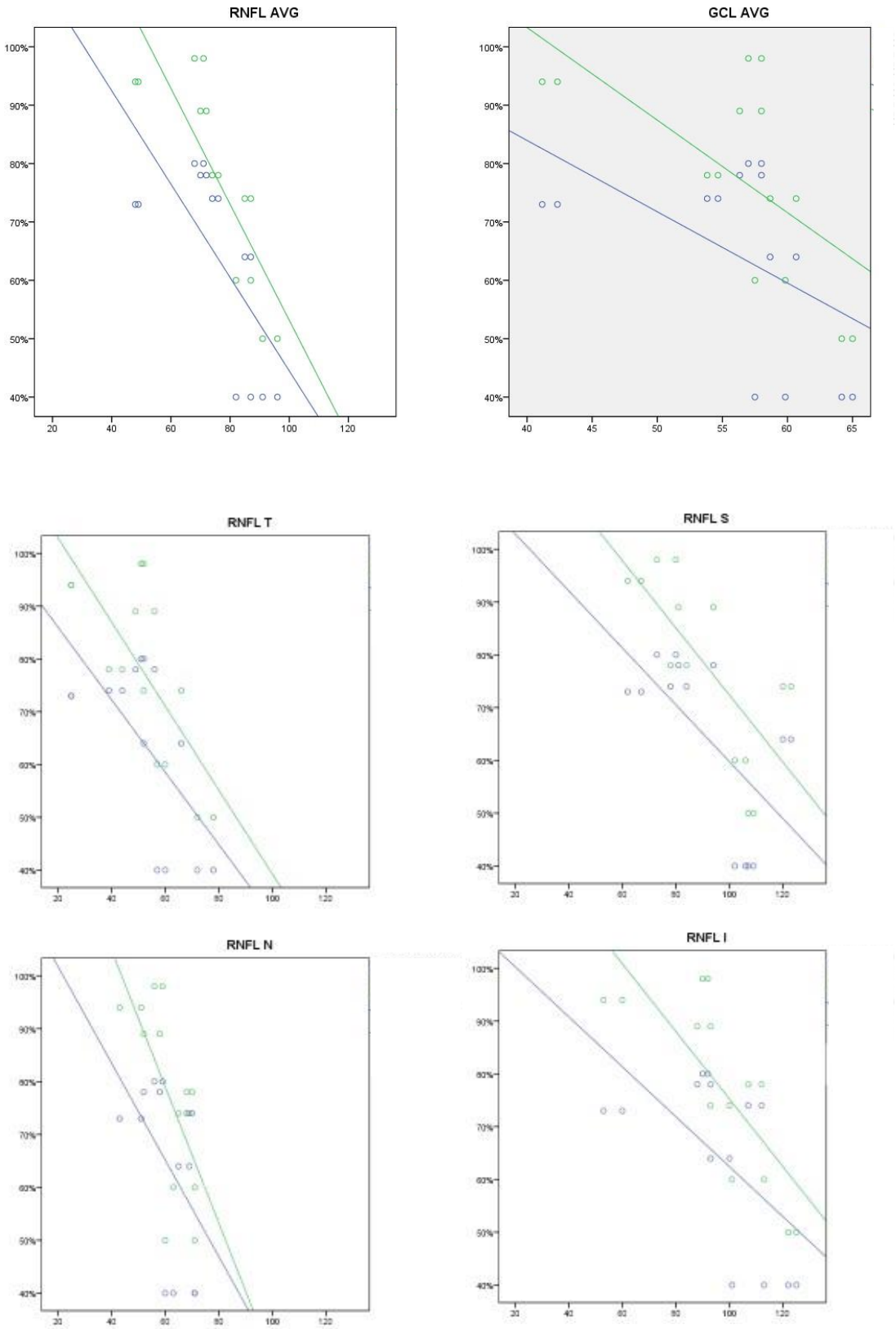

Figure 17. Correlation between blood (blue dots and line) and urine combined with muscle (green dots and line) heteroplasmy with average and sectorial RNFL and average CGL in MERRF patients.

Abbreviations: AVG: average, T: temporal, S: superior, N: nasal, I: inferior.

4.6 Discussion

We compared the neuro-ophthalmological phenotype of patients carrying mtDNA mutations associated respectively with MELAS and MERRF syndromes. In our cohort, possibly biased due to the recruitment in a Neuro-ophthalmology Clinic, we found an overall prevalence of neuro-ophthalmological involvement in 69% of MELAS patients and 87% of MERRF. A first result, which confirms previous reports, is that retinopathy is the most common neuro-ophthalmological symptom in MELAS followed by optic atrophy, as opposed to MERRF in which optic atrophy was present in all cases with neuro-ophthalmological involvement.

Overall, our study showed a prevalence of retinopathy, considering all 33 MELAS patients, of 51%, which is higher than the one reported in literature in m.3243A>G/MT-TL1 mutation carriers ranging from 15% to 38% (Chinnery et al., 1997; Latlava et al., 2002). Optic atrophy was present in 33% of our MELAS patients, as opposed to the reported prevalence ranging from 1% to 9% in literature (Chinnery et al., 1997; Zhu et al., 2017). Again, it must be considered that we recruited patients referred to our Neuro-ophthalmology Clinic, hence these figures are possibly overestimated if we consider the overall group of patients carrying these mutations, which includes also cases without any ocular involvement.

In MERRF, the previously reported prevalence of optic atrophy is variable, ranging from 13% to 36% (Chinnery et al., 1997). Interestingly, optic nerve involvement has been described also in completely visually asymptomatic patients (Gronlund et al., 2008; Najjar et al., 2019) and thus its real prevalence could have been previously underestimated. In our limited cohort, remarkably, we found an overall prevalence of optic atrophy of 87%, confirming also that the majority of patients were visually asymptomatic. In fact, only 1/7 patient presented a clear reduction in visual acuity, interestingly developed in a subacute LHON-like course.

Noticeably, the prevalence of CPEO/ptosis was similar in both groups (39% in MELAS vs 37% in MERRF), and close to the values reported in literature: 28% in MELAS (Chinnery et al., 1997) and 29% in MERRF (Mancuso et al., 2013). As expected, none of the MERRF patients presented retrochiasmal visual loss, which instead was present in 12% of our MELAS patients and intimately correlated with stroke-like events.

If the myopathic involvement of extraocular muscles is common in several and genetically heterogeneous mitochondrial diseases, because of the higher density of mitochondria and thus augmented susceptibility to metabolic defects compared to the other skeletal muscle districts, the reason for the striking distinct ocular involvement (retinopathy vs optic atrophy) in these two diseases is yet to be fully understood. Despite both associated with mutations occurring in

mitochondrial tRNA genes, which impair by definition mitochondrial translation and thus leading to a generalized impairment of the mitochondrial respiratory chain, other molecular mechanisms must be responsible for the selective susceptibility of different retinal cell types, namely photoreceptors/RPE in MELAS and RGCs in MERRF. These cell types are all particularly susceptible to OXPHOS impairment and ROS accumulation: photoreceptors have a high consumption of mitochondrial-generated ATP, particularly for regeneration of the outer segment which is constantly exposed to photo-related oxidative stress, while RCGs are highly depend on mitochondrial energy production for transmitting the action potential along their unmyelinated axons running in the RNFL and the optic disc until passing the lamina cribrosa, where they finally acquire the oligodendrocyte-dependent myelin sheet (Zeviani and Carelli, 2021).

The distinct ocular involvement may be a consequence of different segregation or proliferation of mutant mtDNA in different cell types (Macmillan et al., 1993) or it is possible that, given a specific mutant load, the two mutations impair mitochondrial function to different degrees in the two retinal cell types (Chinnery et al., 1997). An old paradigm, discussed in the past, was based on the assumption that RGCs might be more susceptible to ROS overload, whereas photoreceptors and RPE may be more energy-dependent, thus sensitive to decreased ATP production. This clearly occurs in the case of NARP syndrome characterized by point mutation in the ATPase6 subunit gene of complex V (Zeviani and Carelli, 2021). Conversely, a prevalent contribution from ROS overproduction seems to characterize selective defects of complex I, as recently shown in a mouse model of LHON (Lin et al., 2012). However, this oversimplified paradigm was recently broken by the discovery of dominant forms of optic atrophy co-existing with foveopathy and retinal dystrophy associated with mutations in the *SSBP1* gene, leading to partial mtDNA depletion affecting the eye, but also kidney (frequently evolving into end-stage renal failure) and other tissues (Del Dotto et al., 2020). In this latter case, we have an example for which a global OXPHOS impairment is assumed as pathogenic mechanism, similar to tRNA mutations or single deletions, but leading to simultaneous affection of RGCs, photoreceptors and RPE.

In MELAS, the OXPHOS defect causes photoreceptors and RPE dysfunction, which manifests in accumulation of toxic lipofuscin in the RPE (visible at autofluorescence) and decreased photoreceptor outer segment phagocytosis, leading ultimately to photoreceptors death and retinal atrophy (de Laat et al., 2013). Whether the primary degeneration occurs at the level of the RPE or photoreceptors, remains unclear. Moreover, it is known that the energy deficiency caused by the mitochondrial mutation promotes mitochondrial proliferation leading to angiopathy and a relative deficiency of nitric oxide, a potent vasodilator (Kisilevsky et al., 2019). This mechanism is thought to contribute mainly to acute ischemia during stroke-like episodes, nevertheless one could expect

some chronic angiopathy/vascular change in the choriocapillaris that could affect more the external layers of the retina. With this in mind, the evaluation with angio-OCT would be useful in the future to explore this hypothesis.

In MERRF, the defective incorporation of lysine within the 13 mtDNA-encoded proteins results in premature termination of translation and truncated proteins with increased degradation rate. The final outcome is a disturbed assembly of respiratory chain complexes, most prominently affecting the cytochrome-c-oxidase (COX) complex (complex IV) (Altmann et al., 2016; Capristo et al., 2022). This biochemical defect probably affects more selectively RGCs than RPE but, contrarywise to the classical paradigm of optic neuropathies due to mtDNA point mutations affecting complex I subunits, such as in LHON, in which an impairment of central vision is sudden and always evident, in MERRF the optic atrophy probably evolves more insidiously and presents a relevant functional-anatomical discrepancy. This probably reflects a different underlying pathogenetic mechanism in MERRF as compared to LHON. Only occasionally, a LHON-like phenotype may occur, as in a single case of our series, and in previous publications. This somehow mirrors, even if the pattern of RGC loss is profoundly different, what has been observed in Friedreich Ataxia, for which an indolent course of the RGC degeneration is the standard, with some exceptions in patients harbouring a compound heterozygosis (for one allele carrying the classical expansion and the other carrying a point mutation) for whom a subacute LHON-like course is also described (Fortuna et al., 2009).

It can also be hypothesized that the respiratory chain shows slightly different defects depending on the type of mutated tRNA. Complex I is the respiratory chain enzyme with the most mitochondrial DNA-encoded subunits and most impaired in mitochondrial hereditary optic neuropathy (Yu-Wai-Man et al., 2016); analysis of the amino acid composition of the mitochondrial-encoding subunits of complex I (UniProt database; ProtParam ExPASy analysis) showed high percentage of leucine (ranging from 10 ,9 % in ND4 to 24,3% in ND3), agreeing with the fact that leucine is an hydrophobic amino acid highly represented in membrane proteins. However, the percentage of lysine is not negligible and interestingly, its highest percentages are present in the subunits forming the proton channels (ND2 3,5%; ND4 2,6%; ND5 3,5%), which are essential to generate the proton gradient underlying the energy conservation of complex I and the respiratory chain in general (Fiedorczuk et al., 2016). Since it is known that complex I is one of the major sites of ROS production along the respiratory chain, it could be hypothesized that the m.3243A>G/MT-TL1 MELAS mutation results in a general decrease in the enzymatic activity of complex I and, downstream, of all the respiratory chain energy production. The global and deeper energy deficit could be responsible in MELAS for an early and prevalent dysfunction of the retinal photoreceptor

component, explaining also the greater selective pressure on blood cells that we will discuss later. On the other hand, the m.8344A > G/MT-TK MERRF mutation could alter more specifically the proton channel activity of complex I, possibly increasing ROS production and thus causing oxidative damage affecting more selectively RGCs and favouring the occurrence of optic neuropathy in MERRF.

Comparing neuro-ophthalmological results, the higher prevalence of optic atrophy in MERRF reflected as expected in significant lower values of average, temporal and nasal RNFL thickness assessed by OCT compared to MELAS patients. Interestingly, no difference was found in terms of functional visual parameters, such as VF measures and BCVA. Visual acuity, in particular, resulted overall within the range of normal vision in both groups, possibly explained by the high variability among patients, ranging from severely affected to almost asymptomatic even within the same family. The same high variability was observed also at electrophysiological testing in MELAS. We failed to find any difference in macular GCL thickness. This result should probably not come as a surprise since a reduced GCL thickness has been observed, albeit in a low number of patients, both in MERRF and MELAS. Najjar and colleagues described 3 asymptomatic MERRF patients showing RNFL and GCL reduced thickness at OCT (Najjar et al., 2019). Shinkai and colleagues showed in 5 MELAS patients that GCL thickness was significantly thinner than controls but thicker compared to LHON, and also that GCL thickness negatively correlated with disease duration (Shinkai et al., 2020). No information was given regarding the mutations nor the heteroplasmy levels.

Within the MELAS group, we further compared patients harboring the classic m.3243A>G/MT-TL1 mutation with patients presenting rarer mutations, in the same or a different mitochondrial gene. Overall, patients with rare mutations displayed a more severe ophthalmological phenotype, both in terms of VA and VF, despite not reaching significance, and anatomical measures assessed by OCT, which instead were clearly significant. The same observation was evident at electrophysiological testing. Moreover, within the group with rare mutations, 3/7 patients displayed a combination of retinopathy and optic atrophy, while only 1 patient with classic m.3243A>G/MT-TL1 mutation presented both. This result can be explained by the presence of mutations in subunits of Complex I (m.13094 T>C/MT-ND5, m.10191 T>C/MT-ND3), more prone to lead to severe optic atrophy as in LHON, and Complex IV (m.7896G>A/MT-CO2), possibly leading to a severe respiratory defect.

As MELAS and MERRF mutations are heteroplasmic, we also assessed if the mutation load correlated with the neuro-ophthalmology phenotype in our cohort. Both in carriers of the MELAS-associated m.3243A > G/MT-TL1 mutation and MERRF-associated m.8344A > G/MT-TK mutation it has been highlighted that a critical threshold is necessary to manifest symptoms and that heteroplasmic mutational load correlates with disease severity (Grady et al., 2018, Capristo et al., 2022). Nevertheless, the grade of mitochondrial retinal dystrophy in MELAS, despite correlating significantly with both age and visual acuity, did not correlate with heteroplasmy (de Laat et al., 2013). To our knowledge, there are no studies correlating the heteroplasmy load with optic atrophy in MERRF.

We first evaluated the effect of age on heteroplasmy levels in our cohort, confirming the already established negative correlation of blood heteroplasmy with age in MELAS due to high selective pressure in cells undergoing rapid turn-over, and thus needing a mathematical correction (Grady et al., 2018). We also observed a less significant negative correlation with urinary heteroplasmy, while no correlation was found in muscle. Contrarywise, in MERRF patients we found no correlation between blood heteroplasmy and age, as expected from previous reports (Altmann et al., 2016), while a mild negative correlation was observed in urinary and muscular heteroplasmy levels combined. This supports the hypothesis that the lysine tRNA mutation is exposed to less stringent selective pressure in blood cells than leucine tRNA mutation, suggesting also that the MERRF mutation might be considered globally less severe than the MELAS mutation.

Correlation with neuro-ophthalmological parameters failed to show any significance in MELAS patients, considering age-normalized blood heteroplasmy, as well as urine and muscle mutant load. On the contrary, in MERRF, both blood and combined urine and muscle heteroplasmy negatively correlated with both RNFL and GCL thickness, reaching the highest significance on the temporal RNFL sector, which is the most sensitive to respiratory chain dysfunction.

In conclusion, we demonstrated a high prevalence of neuro-ophthalmological involvement in our cohort of MELAS and MERRF patients, confirming also a distinct ocular phenotype, respectively retinopathy in MELAS and optic atrophy in MERRF. This striking difference possibly reflects a selective susceptibility of different retinal cell types, namely photoreceptors/RPE in MELAS and RGCs in MERRF, respectively prevalently sensitive to OXPHOS impairment or ROS accumulation. The higher prevalence of optic atrophy in MERRF reflected in significant lower values of RNFL thickness compared to MELAS patients, despite visual acuity, visual fields measures and GCL thickness resulted comparable. Correlation with heteroplasmy, apart from the already known effect of age on the leucine tRNA mutation causing a selective negative pressure in

blood cells, and less significantly in urinary cells, failed to disclose any significant correlation with neuro-ophthalmological parameter in MELAS patients.

Contrarywise, lysine tRNA mutational load, albeit not correlating with age, negatively correlated with both RNFL and GCL thickness in MERRF patients, with the highest significance on the temporal RNFL sector. This, provides the opportunity to better elaborate on disease prognosis for MERRF, whereas for MELAS it seems less predictable which natural history a specific patients may undergo in the future follow up.

5. PART 3: LONGITUDINAL NEURO-OPHTHALMOLOGICAL AND ELECTROPHYSIOLOGICAL ASSESSMENT FOLLOWING GENE THERAPY IN ACUTE LHON PATIENTS.

5.1 Introduction

Leber's Hereditary Optic Neuropathy (LHON) is a maternally inherited disease, associated with mitochondrial DNA (mtDNA) point mutations in genes encoding subunits of complex I of the respiratory chain. The three most common mtDNA mutations, accounting for about 90% of cases, are: 11778/ND4 (69%), 14484/ND6 (14%), and 3460/ND1 (13%) (Carelli et al., 2004). The classical presentation of LHON is a rapid, painless loss of vision in one eye, followed by the fellow eye within days to months; males are more affected than females with a 4:1 ratio (Newman, 2005). The loss of vision is due to selective vulnerability of retinal ganglion cells (RGCs) in the papillomacular bundle that causes a typical central scotoma and a subsequent optic atrophy (Carelli et al., 2009). The prognosis is usually severe, with most patients progressing to very poor visual acuities. Fundus findings in the acute stages, and possibly in the asymptomatic mutation carriers, include circumpapillary telangiectatic microangiopathy and swelling of the retinal nerve fiber layer (RNFL) without leakage (pseudoedema). As the disease progresses a rapid axonal loss in the papillomacular bundle leads to temporal and eventually diffuse atrophy of the optic nerve head. The selective involvement of RGCs in LHON has been confirmed by optical coherence tomography (OCT) and histopathological studies (Barboni et al., 2010; Barboni et al., 2012; Pan et al., 2012). OCT allows quantifying the characteristic RNFL and RGC changes over time and can help identifying the conversion from the presymptomatic to the affected stage in LHON (Carbonelli et al., 2022). Electrophysiological studies in LHON variably demonstrated a retinal dysfunction at pattern electroretinogram (P-ERG), multifocal ERG and impaired neural conduction at Visual Evoked Potentials (VEP) (Salomao et al., 2004; Kurtenbach et al., 2004; Ziccardi et al., 2013; Guy et al., 2014; Jarc-Vidmar et al., 2016). Nevertheless, limitations of these techniques include the fact that they do not represent a direct measure of RGC function, moreover they need a precise refractive correction and foveal fixation, which is often very challenging for LHON patients, especially in the acute stage. Recently, it was discovered that RGCs generate a slow negative wave response following the b-wave of the cone response on photopic electroretinogram (ERG) and is referred to as the photopic negative response (PhNR) (Viswanathan et al., 1999). Studies on LHON families, reported that PhNR amplitudes were severely reduced in patients affected by LHON compared to carriers and mildly reduced in carriers, suggesting a potential subclinical RGC dysfunction also in asymptomatic patients (Karanjia et al., 2017; Majander et al., 2017). Moreover,

PhNR amplitude has been shown to negatively correlate with total macular ganglion cell thickness (Botelho et al., 2021).

Therapeutic options in LHON include idebenone, a synthetic analogue of CoQ10 acting as an antioxidant, whose efficacy was assessed in a randomised, double-blinded, placebo-controlled study (RHODOS) leading to its approval by European Medicines Agency (EMA) in 2015 (Amore et al., 2021). In more recent years, several phase 3 trials have been conducted on gene therapy targeting the m.11778G>A/MTND4 mutation and showed a promising alternative for the treatment of LHON. In details, RESCUE and REVERSE trials evaluated the effects of the rAAV2/2-ND4 (GS010 LUMEVOQ) delivered by unilateral intravitreal injections, reporting a bilateral improvement of visual acuity at 96 weeks, sustained also 3 years after treatment. The most recent REFLECT trial, comparing bilateral with unilateral intravitreal injections, confirmed a significant improvement of vision in the bilateral group (Davila-Siliezar et al., 2022). LUMEVOQ is currently under review by the EMA for approval. In the meantime, as the only Italian recruiting center for gene therapy in LHON, over the last year we had the opportunity to offer gene therapy as compassionate use in a number of acute LHON patients harbouring the m.11778G>A/MTND4 mutation.

The purpose of this study was to prospectively investigate modifications in visual acuity, OCT parameters, Flash VEP (FVEP) and PhNR responses in this group of acute/subacute LHON patients treated with rAAV2/2-ND4 gene therapy in co-administration with idebenone.

5.2 Methods

Gene therapy was administered after approval by the internal ethical committee for compassionate use and signing of the informed consent. We included m.11778/MTND4 LHON patients with onset of disease within one year from the last affected eye and already on treatment with idebenone 900mg/die. Each subject received an intravitreal injection in each eye containing 9×10^{10} viral genomes in 90 ml (REFLECT www.clinicaltrials.gov NCT03293524). The procedure was carried out in an aseptic surgical room at Bellaria Hospital. Treatment with prophylactic oral steroids was provided.

Demographic features such as age, sex, onset of vision loss for the first and second eye and idebenone therapy were recorded. Patients were tested at time 1 (T1) one to three days before injection, 6 months after injection (T2) and 1 year after injection (T3). Best corrected visual acuity (BCVA) was measured using a retro-illuminated Early Treatment Diabetic Retinopathy Study (ETDRS) chart positioned at 4 m and expressed as LogMAR. Counting fingers and hand movement were respectively converted to 2.0 and 2.3 LogMAR.

OCT images (DRI Triton, Topcon, Tokyo, Japan) were obtained using a 3-dimensional wide scan protocol with a size of 12×9 mm consisting of 256 B-scans, each comprising 512 A-scans. Peripapillary RNFL thickness were measured using a 360° 3.4-mm diameter circle scan with thicknesses measured across the superior, nasal, inferior, and temporal sectors and segmentation analysis of the macula measured across six sectors of the 6-mm diameter circular annulus centered on the foveal included GCL.

FVEP were presented by the ColorDome ganzfeld (Diagnosys LLC). Gold cup skin electrodes were placed in Oz for active, Cz for reference and Fz for ground. The resulting first and the second positive deflections were named P1 and P2, their preceding negative deflections, N1 and N2. Amplitudes (μV) were measured for N2 and P2. Peak times (ms) were measured for N2 and P2.

The PhNR stimulus conditions were produced also by the ColorDome. Both pupils were dilated (pupil diameter >7 mm) with one drop each of tropicamide 1% and phenylephrine 10% and then light-adapted for 10 min. The corneal surface was anesthetized with two drops of tetracaine 1% to apply Dawson-Trick-Litzkow (DTL-Plus™) micro conductors (Diagnosys LLC, Lowell, MA, USA) on the lower conjunctival fornix. Gold cup electrodes were used in the temple for reference and Fz for ground. Electrode impedance was checked and set at 5 kilo Ohms (kΩ) or less. Red (640 nm) stimulus flashes of 4 ms duration were presented at a 4-Hz rate on a blue (470 nm) rod saturating background. Red flash stimulation was presented at 1, 3 and 7 cd·s/m^2, while the blue background remained at 10 cd/m^2. An Espion E3 was used to record PhNR waveforms. A total of six sets of 25 sweeps of 150-ms duration per eye were recorded with bandpass filtering between 0.3 and 300 Hz. Each of the six repetitions was manually filtered to remove eye blink and other motion artifacts, and an average of the remained responses was generated for each eye. Recordings were obtained from both right and left eyes. PhNR waveforms were visually inspected, and the a-wave, b-wave, and PhNR components were determined. Peak time (ms) and amplitude of PhNR (μV) from peak to trough (amplitude between the peak of the b-wave and the trough of the PhNR) were recorded.

The following visual parameters were analyzed: BCVA, RNFL thickness (average, temporal, superior, nasal, and inferior quadrants), GCL thickness (average, superotemporal, superior, superonasal, inferonasal, inferior, and inferotemporal), N2 and P2 amplitudes and peak times, PhNR amplitude and peak time. Statistical analysis included a descriptive analysis of the cohort and of neuro-ophthalmological and electrophysiological parameters for each patient at T1, T2 and T3. We compared the results from T1 to T2, and from T1 to T3 using Mann-Whitney U test. We then correlated the results with time from onset using Pearson's correlation. IBM SPSS Statistics for Windows, version 20.0 (IBM Corp., Armonk, N.Y., USA) software was used for statistical analysis.

5.3 Results

We included a total of 9 LHON patients, 8 males and 1 female. Mean age at onset was 30 ±15,59 years (median 27, min-max 14-53). Four patients had a positive family history for LHON. Six male patients had a classic onset within their thirties (LHON type I), the remaining two males and the female patient had a delayed onset of disease after 40 years of age (LHON type II) (Carelli et al., 2016). Six patients had an asynchronous onset of disease, while three had a bilateral onset.
A short description of each patient history and risk factors is provided. Demographic and onset characteristics with times from therapies are summarized in table 8.

Patient 1

Woman with onset of vision loss at 53 years in the right eye followed by left eye in 4 months. Negative family history for LHON. Former smoker (10 cigarettes/die from 20 to 50 years of age). Personal history of recent menopause after prolonged estroprogestinic therapy for ovariectomy and treatment with tamoxifen for breast cancer suspended 4 months after onset for possible toxicity. She was treated 9,5 months after onset and started contextually idebenone 900mg/die.

Patient 2

Man with onset of vision loss at 48 years in the left eye followed by right eye in 1 month. Negative family history for LHON. Personal history of hypertension, heavy smoker since 30 years of age (20 cigarettes/die) and moderate alcohol intake reduced after onset of disease. He started idebenone 900 mg/die 3,5 months after onset and was treated 15,5 months from onset.

Patient 3

Young man with onset of vision loss at 15 years in the left eye followed by right eye in 4 months. Positive family history for LHON. No apparent risk factors. He started idebenone 900mg/die 3 months after onset and was treated 13 months after onset.

Patient 4

Young man with onset of vision loss at 27 years in the left eye followed by right eye in 3 months. Negative family history for LHON. Smoker from 20 years of age (20 cigarettes/die) and occasional alcohol consumption, discontinued after onset of disease. Personal history of clinical depression from 7 years of age, treated with olanzapine, venlafaxine, delorazepam and valproate, this last suspended 10 months after onset for possible toxicity. He started idebenone 900mg/die 4 months after onset and was treated 7 months after onset.

Patient 5

Young man with onset of vision loss at 17 years in the right eye followed by left eye in 7,5 months. Negative family history for LHON. No apparent risk factors. He started idebenone 900mg/die 8 months after onset and was treated 14,5 months after onset.

Patient 6

Young man with onset of vision loss at 33 years in the left eye followed by right eye in 7 months. Positive family history for LHON. Smoker from 16 years of age (20 cigarettes/die) and moderate alcohol consumption, stopped after onset of disease. Personal history of viral meningitis at 17 years of age. Evidence of reduced levels of folates at blood exams at onset. He started idebenone 900mg/die 9 months after onset and was treated 19,5 months after onset.

Patient 7

Man with bilateral onset of vision loss at 46 years. Negative family history for LHON. Smoker from 18 years of age (20 cigarettes/die) and moderate alcohol consumption, stopped after onset of disease. He started idebenone 900 mg/die 11 months after onset and was treated 14,5 months after onset.

Patient 8

Young man with bilateral onset of vision loss at 17 years. Positive family history for LHON. No apparent risk factors. He started idebenone 900mg/die 4 months after onset and was treated 15 months after onset.

Patient 9

Young man with bilateral onset of vision loss at 14 years. Positive family history for LHON. Evidence of vitamin B12 and folates deficiency at blood exams at onset. He started idebenone 900 mg/die 2,5 months after onset and was treated 5,5 months after onset.

Patient n°	Gender	Family history	Risk factors	Age at onset (years)	Eye onset	Second eye involvement (months)	Idebenone therapy (months from onset)	Gene Therapy (months from onset)
1	F	-	+	53	OD	4	9,5	9,5
2	M	-	+	48	OS	1	3,5	15,5
3	M	+	-	15	OS	4	3	13
4	M	-	+	27	OS	3	4	7
5	M	-	-	17	OD	7,5	8	14,5
6	M	+	+	33	OS	7	9	19,5
7	M	-	+	46	Bilateral	/	11	14,5
8	M	+	-	17	Bilateral	/	4	15
9	M	+	-	14	Bilateral	/	2,5	5,5

Table 8. Demographic and onset characteristics with times from therapies. M=male F= female. OD=right eye. OS= left eye.

All 9 patients were tested at T1, 8 were also tested at T2 and 8 at T3. Mean age at T1 was 31,22 ±15,31 years. Mean time from onset of vision loss at T1 (both eyes included) was 11,22 ±4,55 months (median 12,74, min-max 4-19). Mean time from onset in the first eye (including bilateral cases) was 12,42±4,47 months (median 14,4, min-max 5,5-19,5), time from onset in the second eye was 8,83±4 months (median 8,25, min-max 4-14,5). Mean time from onset of vision loss at T2 was 17,92 ±4,48 months (median 19,5, min-max 10-25), while at T3 mean time from onset of vision loss was 24,14 ±4,58 months (median 24,25, min-max 17,5-31,5).

All patients were also treated with idebenone 900 mg/die, started variably from 3 to 11 months after onset of disease (mean 6,11±3,34 months). At T1 mean duration of idebenone therapy was 6,61 ±4,26 months, at T2 12,5±4,59 months and at T3 20,21±5,84 months.

The trend over time of changes in BCVA, RNFL and GCL average thickness, N2, P2 and PhNR amplitudes at T1, T2 and T3 is shown for patient 1 (Fig 18), patient 2 (Fig 19), patient 4 (Fig 20), patient 5 (Fig 21), patient 6 (Fig 22), patient 7 (Fig 23), patient 8 (Fig 24) and patient 9 (fig 25). Patient 8 was only tested at T1 and T2. Patient 9 was only tested at T1 and T3. Results from patient 3 at T2 and T3 were excluded because of poor technical quality (variable fixation, excessive blinking). Flash VEP at T1 and T3 of patient 4 and at T1 for patient 9 were excluded of poor quality (physiological noise).

Overall, we observed a tendency in improving BCVA in all patients at last evaluation, except for patient 8 who remained stable. As expected, RNFL average thickness decreased over time in all patients. GCL average thickness tended more to a stabilization, interestingly some patients (patient 1,2 and 3) presented a temporary increase in GCL thickness at T2 probably linked to mild vitreous inflammation and protein deposits. N2 and P2 amplitudes showed more variability among patients, overall a tendency to reduction or stabilization overtime was observed, except in patient 1 who showed increasing P2 amplitude. PhNR amplitudes showed a clear reduction overtime in all patients.

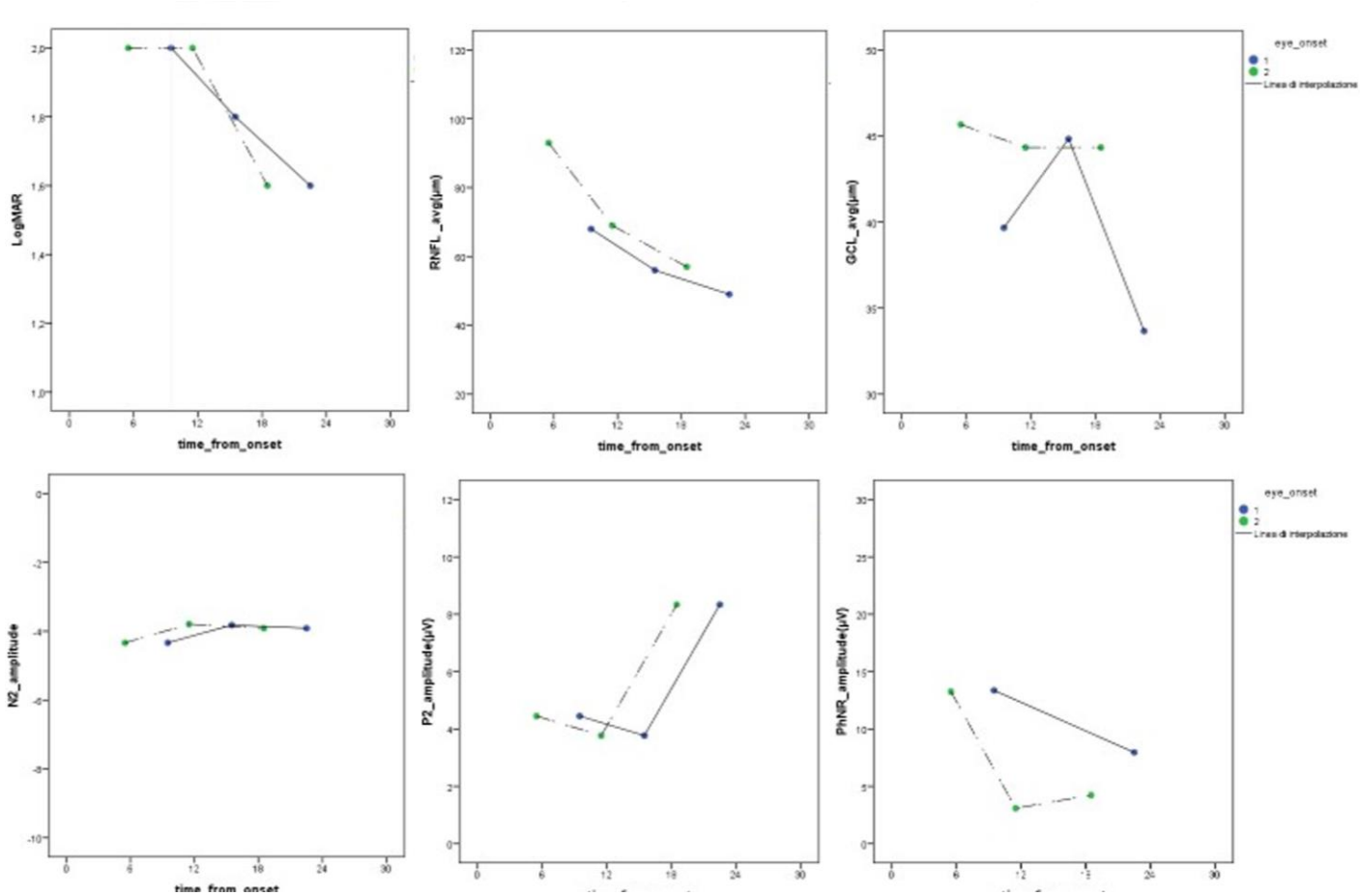

Figure 18. Patient 1. Longitudinal analysis of BCVA, RNFL and GCL average thickness (upper panels from left to right), N2, P2 and PhNR amplitudes (lower panels from left to right) at T1, T2 and T3 evaluation. First affected eye in blue, second affected eye in green.

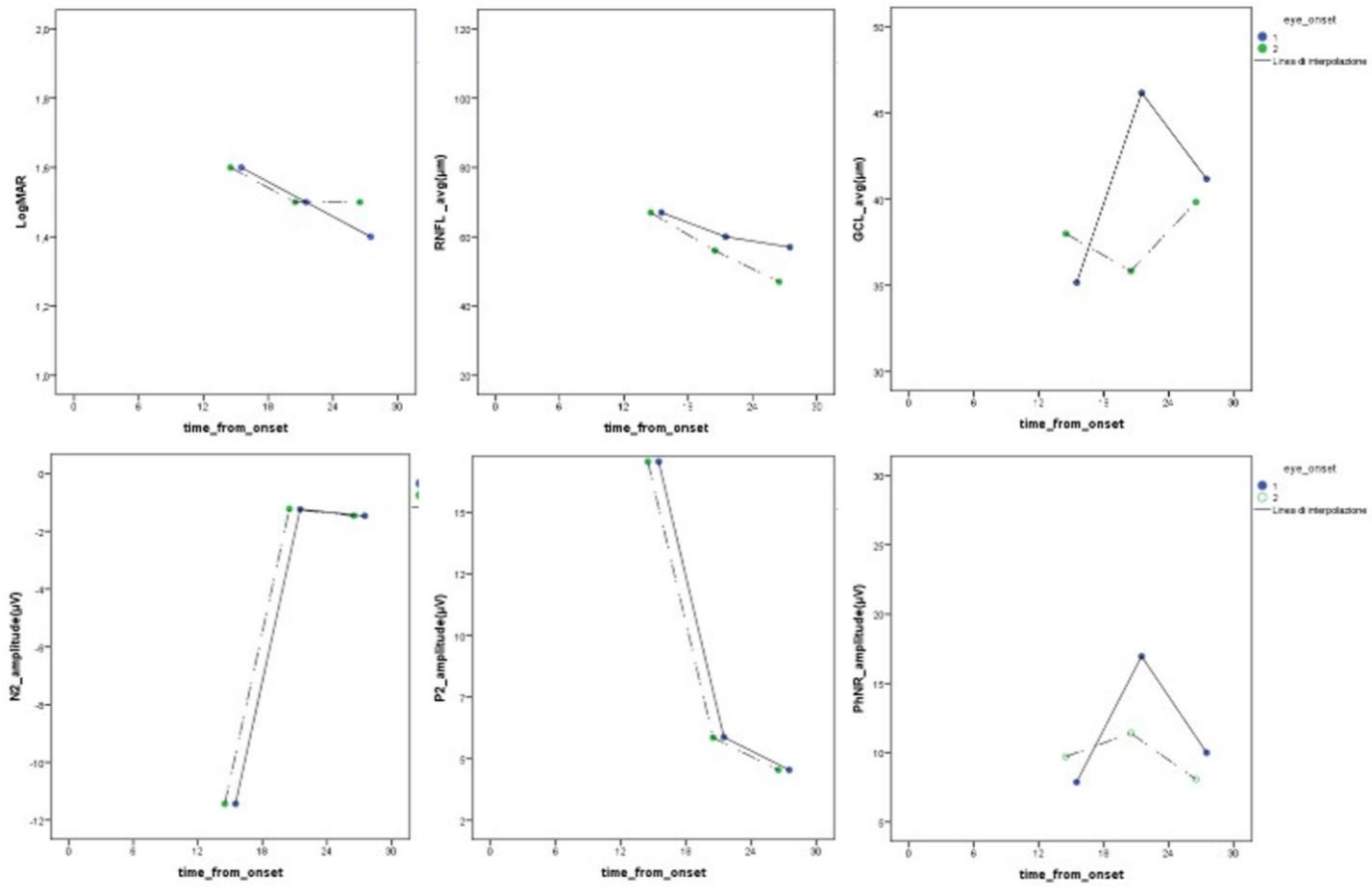

Figure 19. Patient 2. Longitudinal analysis of BCVA, RNFL and GCL average thickness (upper panels from left to right), N2, P2 and PhNR amplitudes (lower panels from left to right) at T1, T2 and T3 evaluation. First affected eye in blue, second affected eye in green.

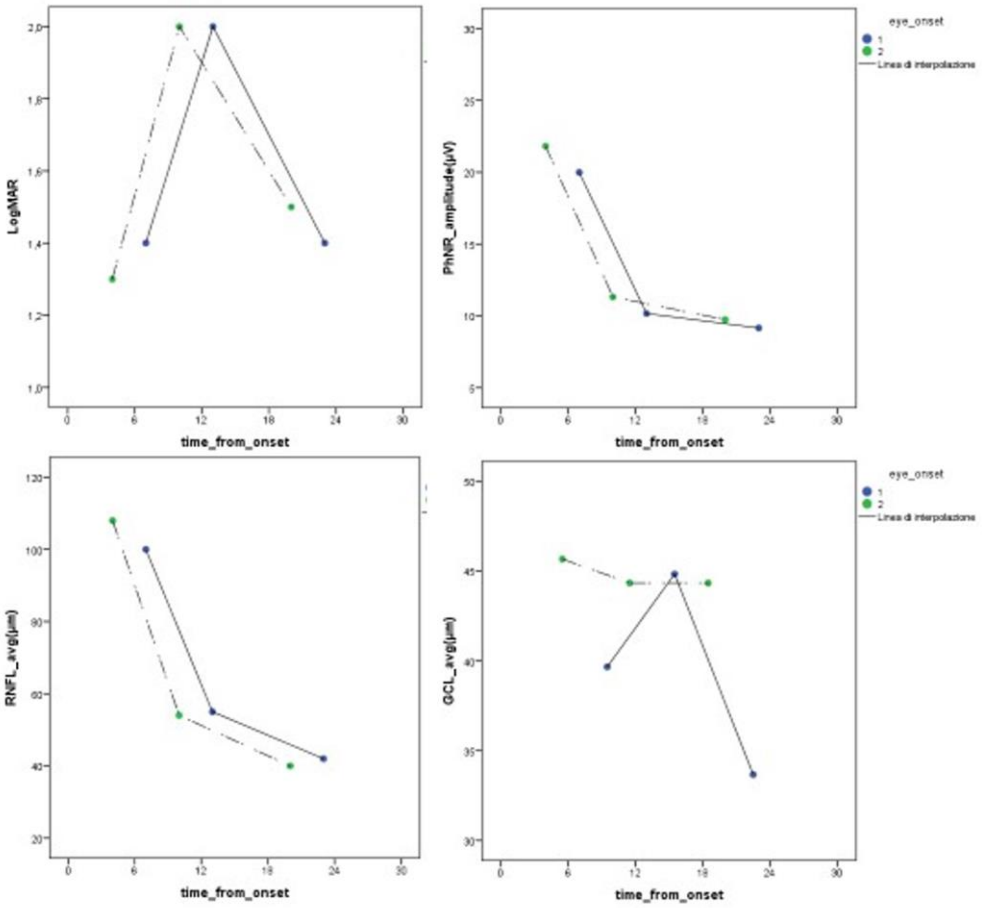

Figure 20. Patient 4. Longitudinal analysis of BCVA and PhNR amplitudes (upper panels from left to right), RNFL and GCL average thickness (lower panels from left to right) at T1, T2 and T3 evaluation. First affected eye in blue, second affected eye in green.

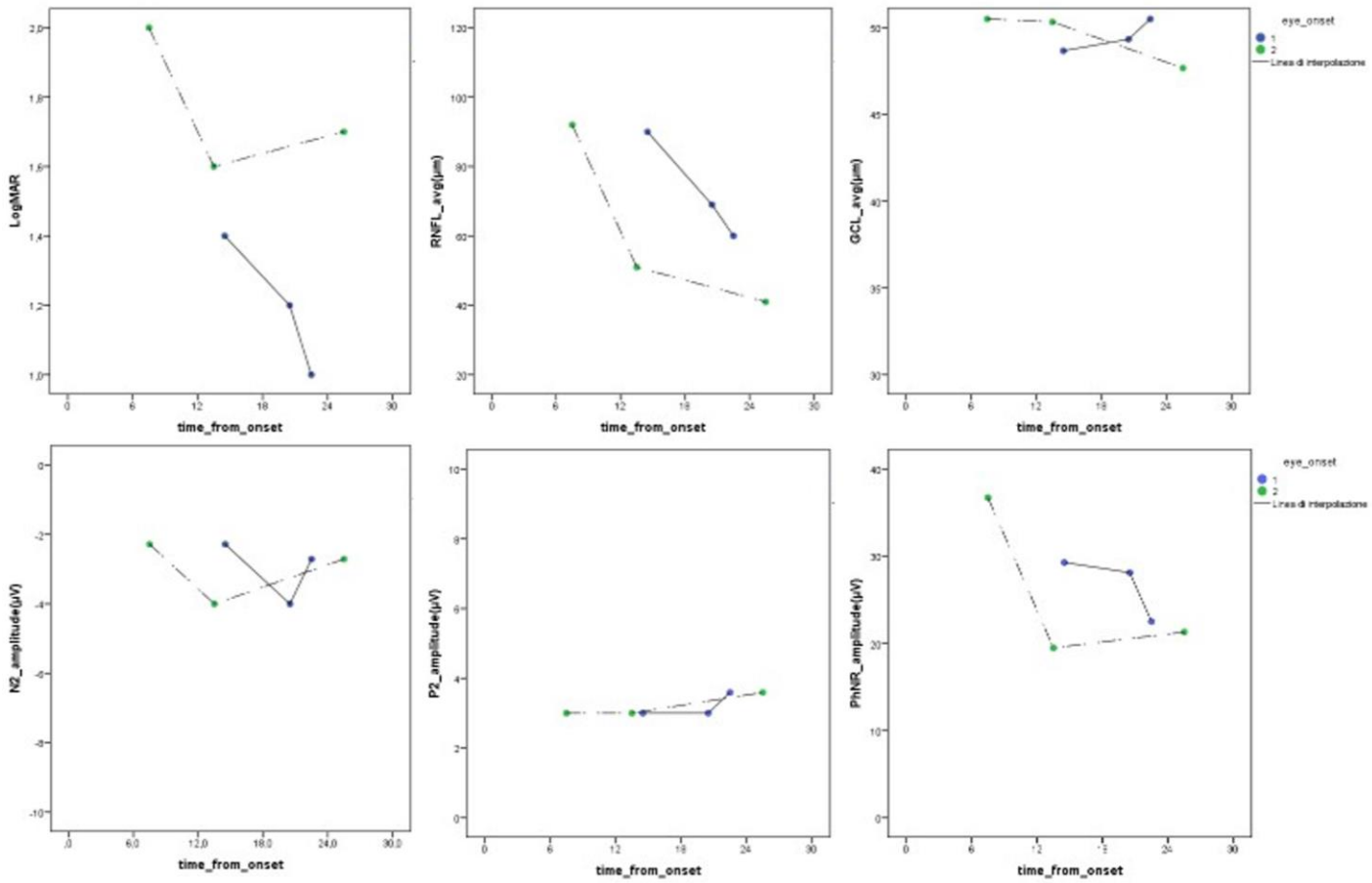

Figure 21. Patient 5. Longitudinal analysis of BCVA, RNFL and GCL average thickness (upper panels from left to right), N2, P2 and PhNR amplitudes (lower panels from left to right) at T1, T2 and T3 evaluation. First affected eye in blue, second affected eye in green.

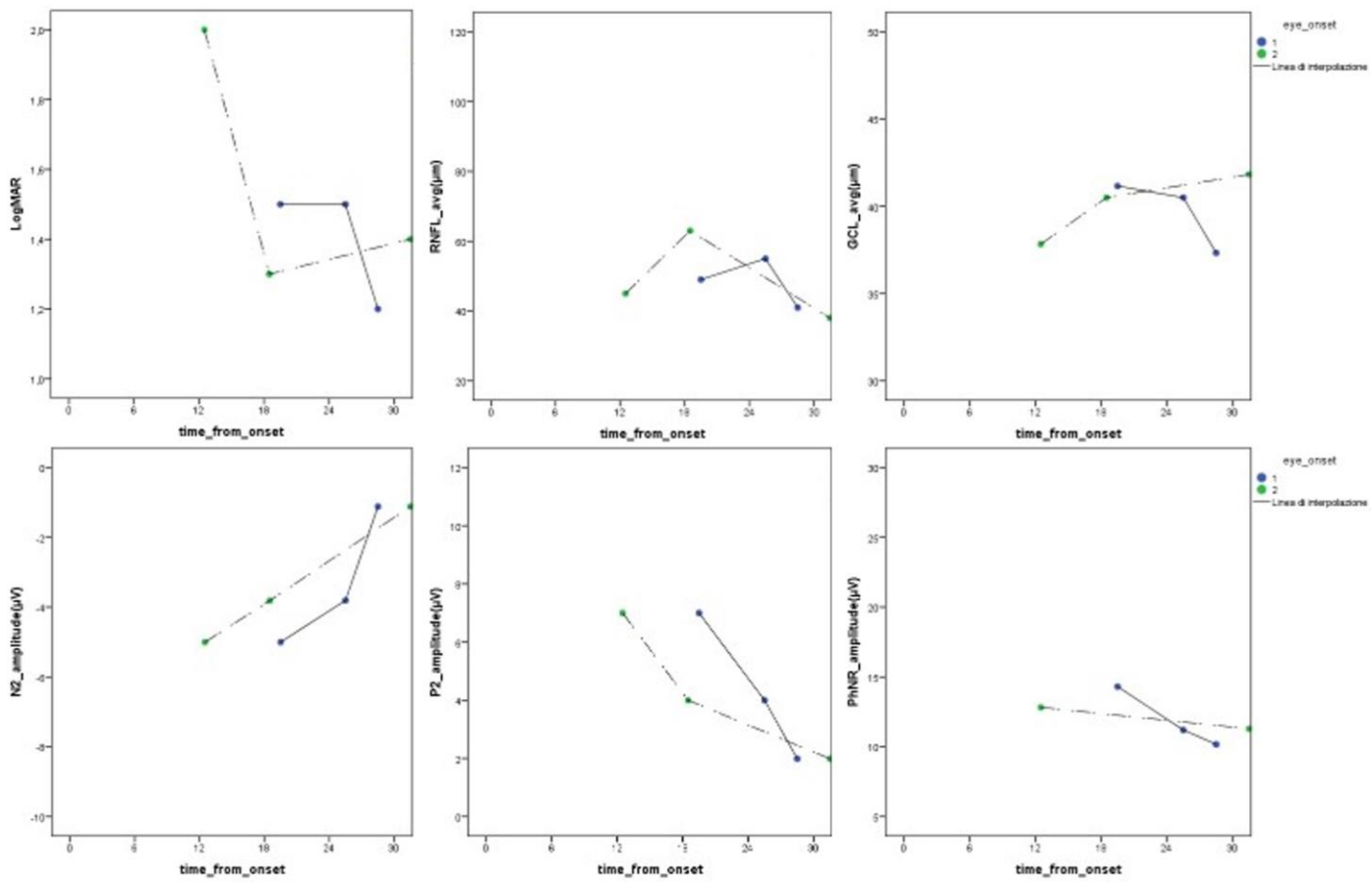

Figure 22. Patient 6. Longitudinal analysis of BCVA, RNFL and GCL average thickness (upper panels from left to right), N2, P2 and PhNR amplitudes (lower panels from left to right) at T1, T2 and T3 evaluation. First affected eye in blue, second affected eye in green.

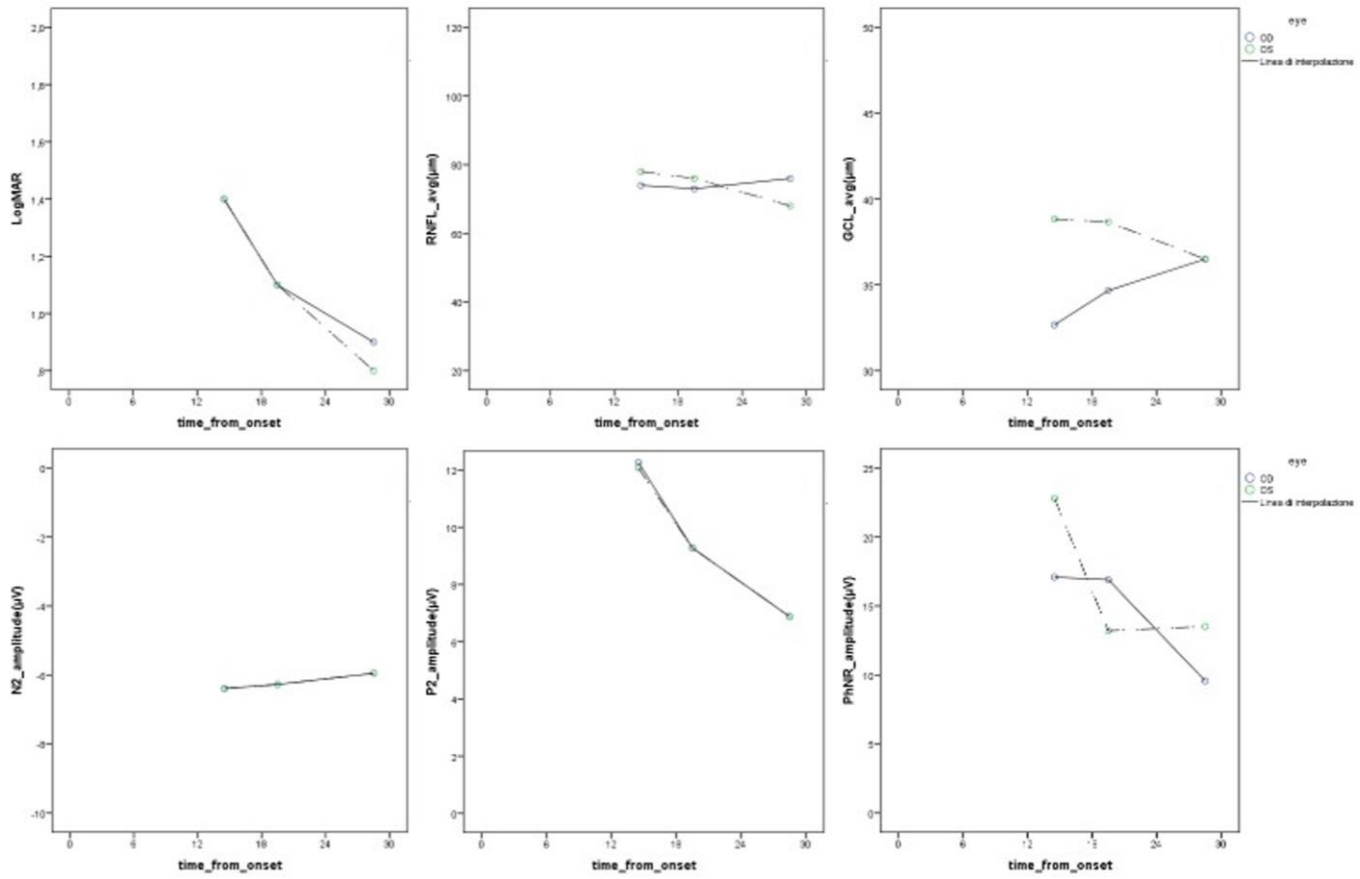

Figure 23. Patient 7. Longitudinal analysis of BCVA, RNFL and GCL average thickness (upper panels from left to right), N2, P2 and PhNR amplitudes (lower panels from left to right) at T1, T2 and T3 evaluation. Right eye in blue, left eye in green.

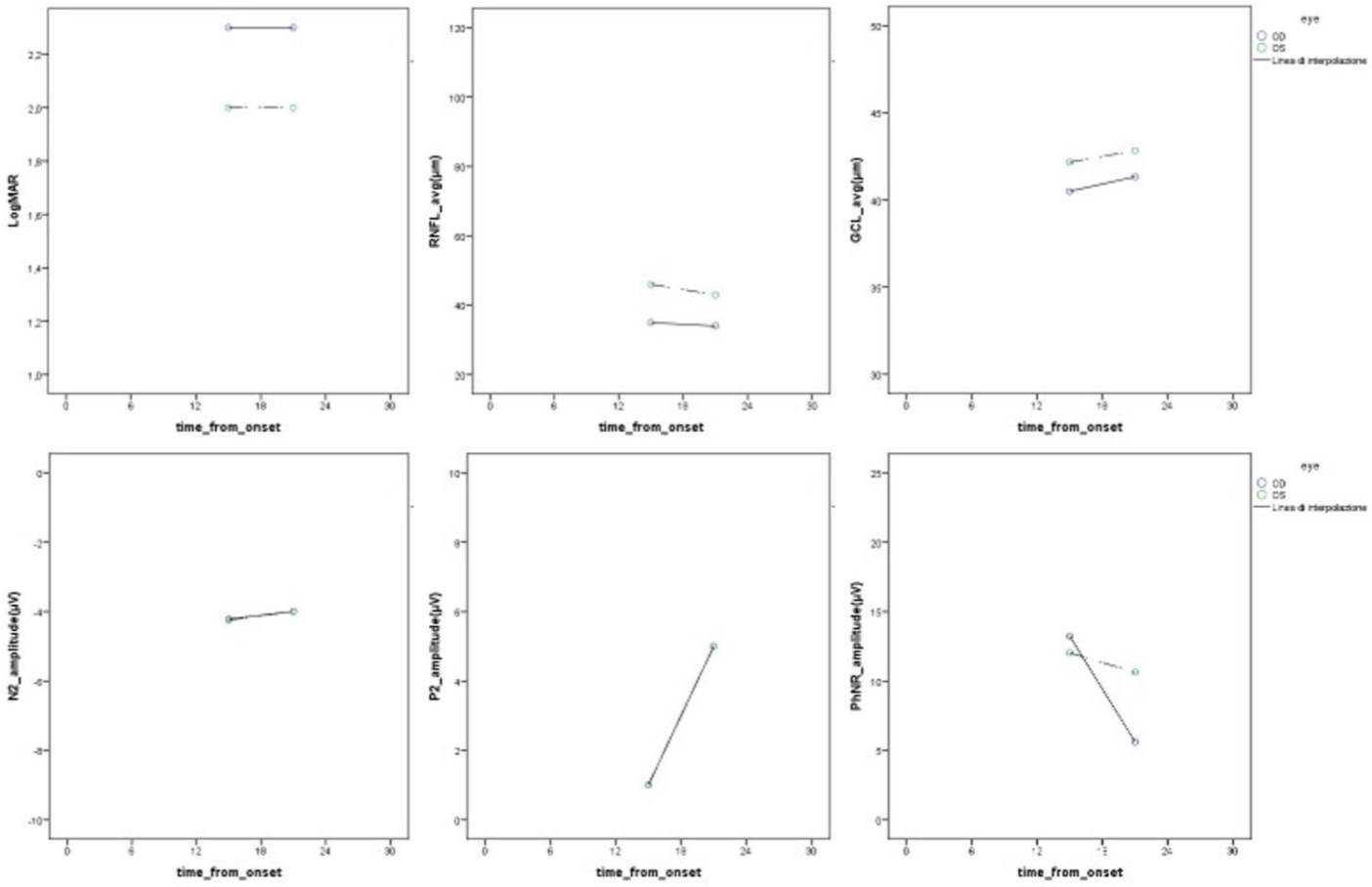

Figure 24. Patient 8. Longitudinal analysis of BCVA, RNFL and GCL average thickness (upper panels from left to right), N2, P2 and PhNR amplitudes (lower panels from left to right) at T1 and T2 evaluation. Right eye in blue, left eye in green.

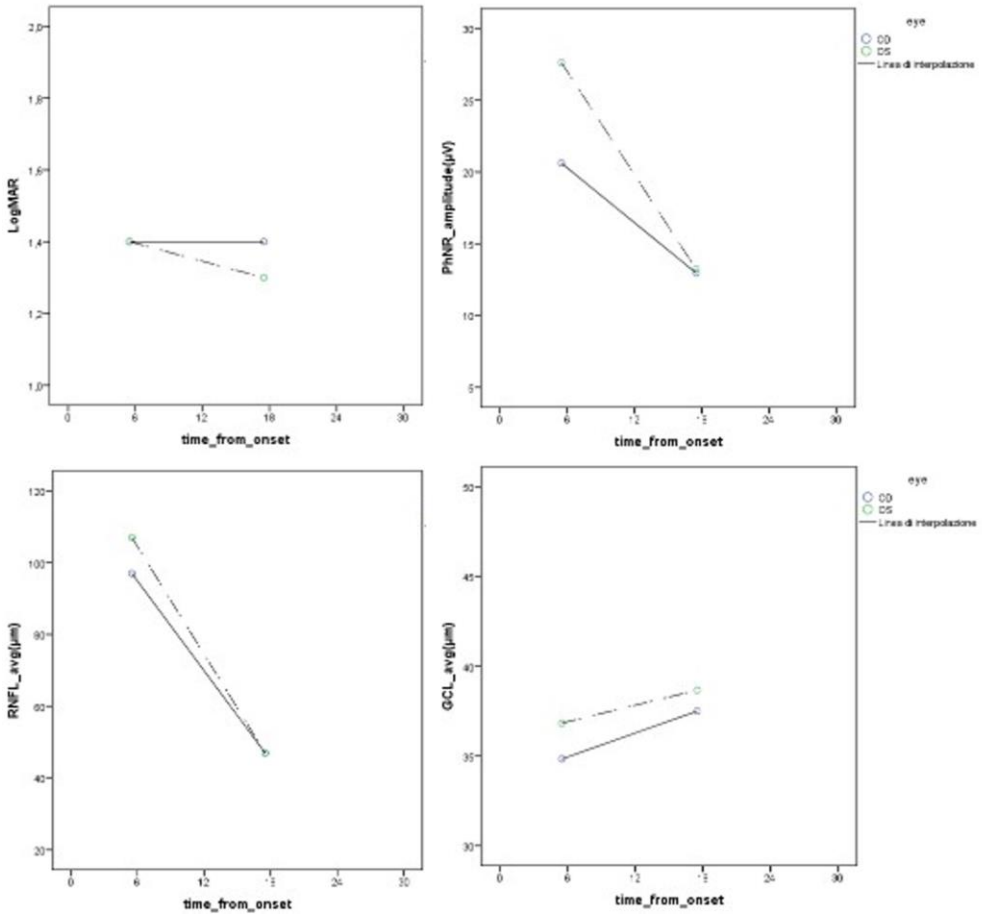

Figure 25. Patient 9. Longitudinal analysis of BCVA and PhNR amplitudes (upper panels from left to right), RNFL and GCL average thickness (lower panels from left to right) at T1 and T3 evaluation. Right eye in blue, left eye in green.

We tried to look globally at the results obtained in the 3 timepoints, comparing results from T1 with T2 and from T1 to T3. Neuro-ophthalmological and electrophysiological parameters at T1, T2 and T3 are shown in table 9.

	T1	T2	T3
Eyes [N]	18	14	14
Time from onset [months, mean±SD]	11,22 ±4,55	17,92 ±4,48	24,14 ±4,58
Duration of idebenone therapy [months, mean±SD]	6,61 ±4,26	12,5±4,59	20,21±5,84
BCVA [LogMAR, mean±SD]	1,7±0,36	1,63±0,38	1,33±0,27
RNFL AVG [µm, mean±SD]	73,11±23,57	58,14±11,47	50,71±11,39
RNFL T [µm, mean±SD]	32,06±6,64	32,28±6,26	27,05±3,18
RNFL S [µm, mean±SD]	94,78±34,97	70,29±17,63	64,29±19,98
RNFL N [µm, mean±SD]	68,99±23,71	61,7±15,26	50,25±14,43
RNFL I [µm, mean±SD]	96,76±36,76	71,92±14,82	61,64±12,65
GCL AVG [µm, mean±SD]	41,13±5,25	42,2±4,52	40,42±4,56
GCL SN [µm, mean±SD]	41,94±4,33	43,07±4,32	41,93±3,81
GCL S [µm, mean±SD]	41,11±6,72	43,14±5,64	41,50±4,89
GCL ST [µm, mean±SD]	41,06±5,78	40,79±3,74	38,14±6,50
GCL IT [µm, mean±SD]	40,56±7,34	41,21±5,86	38,29±7,58
GCL I [µm, mean±SD]	42,33±4,85	42,64±5,91	42,64±7,46
GCL IN [µm, mean±SD]	39,83±5,5	42,29±5,04	40,07±4,92
	12	12	12
N2 amplitude [µV, mean±SD]	-5,61±3	-4±1,55	-2,94±1,69
N2 peak time [ms, mean±SD]	76,58±21,4	70,17±16,80	65,17±14,18
P2 amplitude [µV, mean±SD]	7,33±5,8	5,67±2,22	5,13±2,23
P2 peak time [ms, mean±SD]	107,83±16,31	119,08±6,43	112,38±11,71
PhNR amplitude [µV, mean±SD]	-16,83±8,56	-13,17±6,57	-11,69±4,95
PhNR peak time [ms, mean±SD]	66,74±3,52	70,59±4,80	70,91±3,76

Table 9. Neuro-ophthalmological and electrophysiological parameters at T1, T2 and T3.

Abbreviations: N: number, SD: standard deviation, BCVA: best corrected visual acuity, VF: visual fields, MD: mean deviation, OCT: optic coherence tomography, ONH: optic nerve head, RNFL: retinal nerve fiber layer, GCL: ganglion cell layer, AVG: average, T: temporal, S: superior, N: nasal, I: inferior, SN: supero-nasal, ST: supero-temporal, IT: inferotemporal, IN: inferonasal

We first compared results at T1 and T2, no significant difference was evident in BCVA and OCT parameters, while we found reduced N2 (p=0.041) and PhNR (p= 0.034) amplitudes with increased PhNR latency (p=0.024) at T2 compared to T1. Comparing T1 and T3, we found, as expected by the disease progression, a significant reduction in average (p=0.005), superior (p=0.009), temporal (p=0.013), inferior (p=0.003) and nasal (p=0.020) sectors of RNFL thickness (Fig 26). N2 and PhNR amplitudes were also reduced (respectively p=0.010 and p=0,005) with increased PhNR

latency (p=0,005) at T3 compared to T1 (Fig 27 and Fig 28). Interestingly, BCVA significantly improved overall from T1 to T3 of about -0.37 LogMAR (1,7±0,36 to 1,33±0,27, p=0.010).

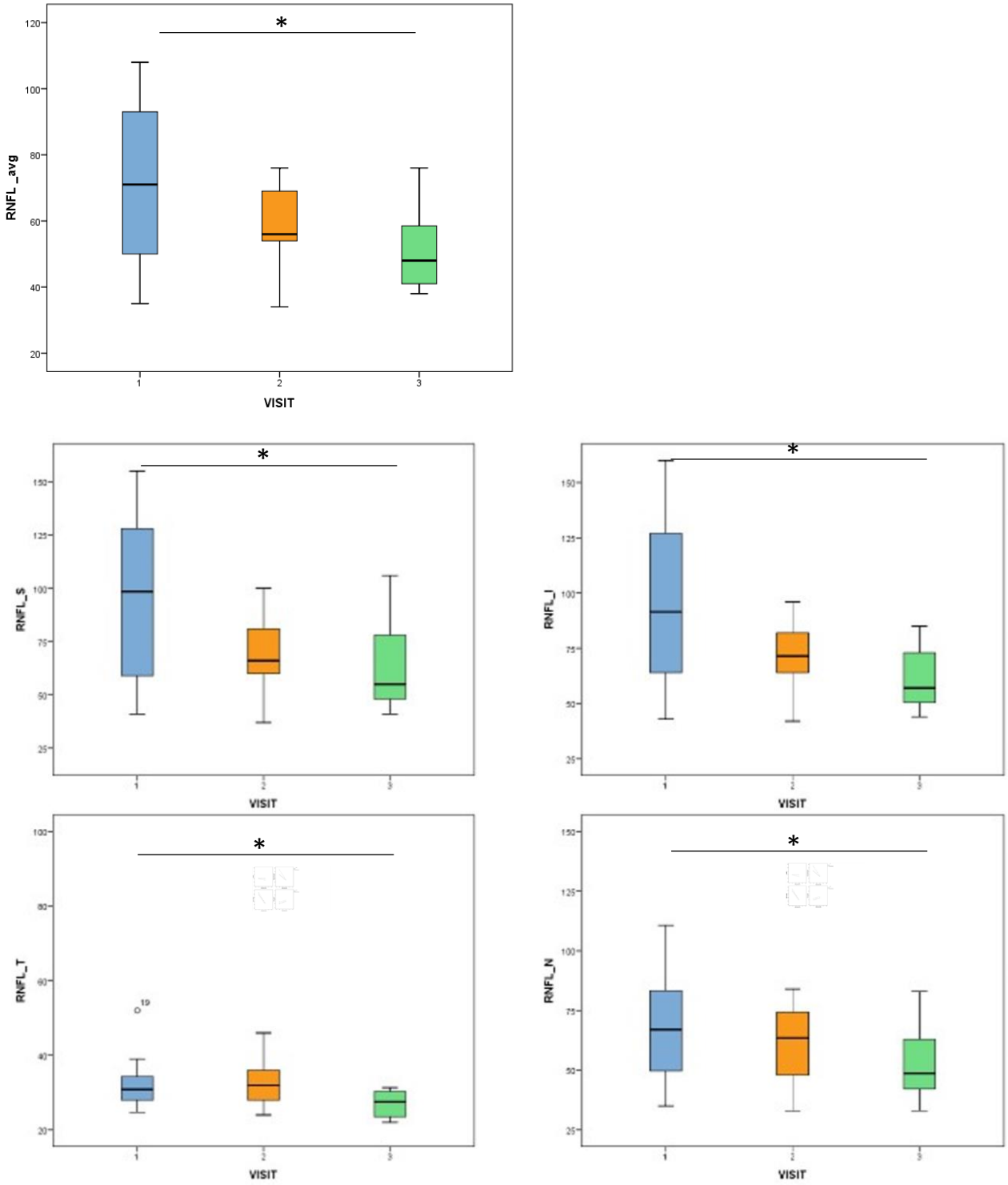

Figure 26. Average and sectorial RNFL and GCL thickness (µm) at T1, T2 and T3.

*p<0.05 at comparison between T1 and T3

Abbreviations: AVG=average, S=superior, I = inferior, T=temporal, N=nasal.

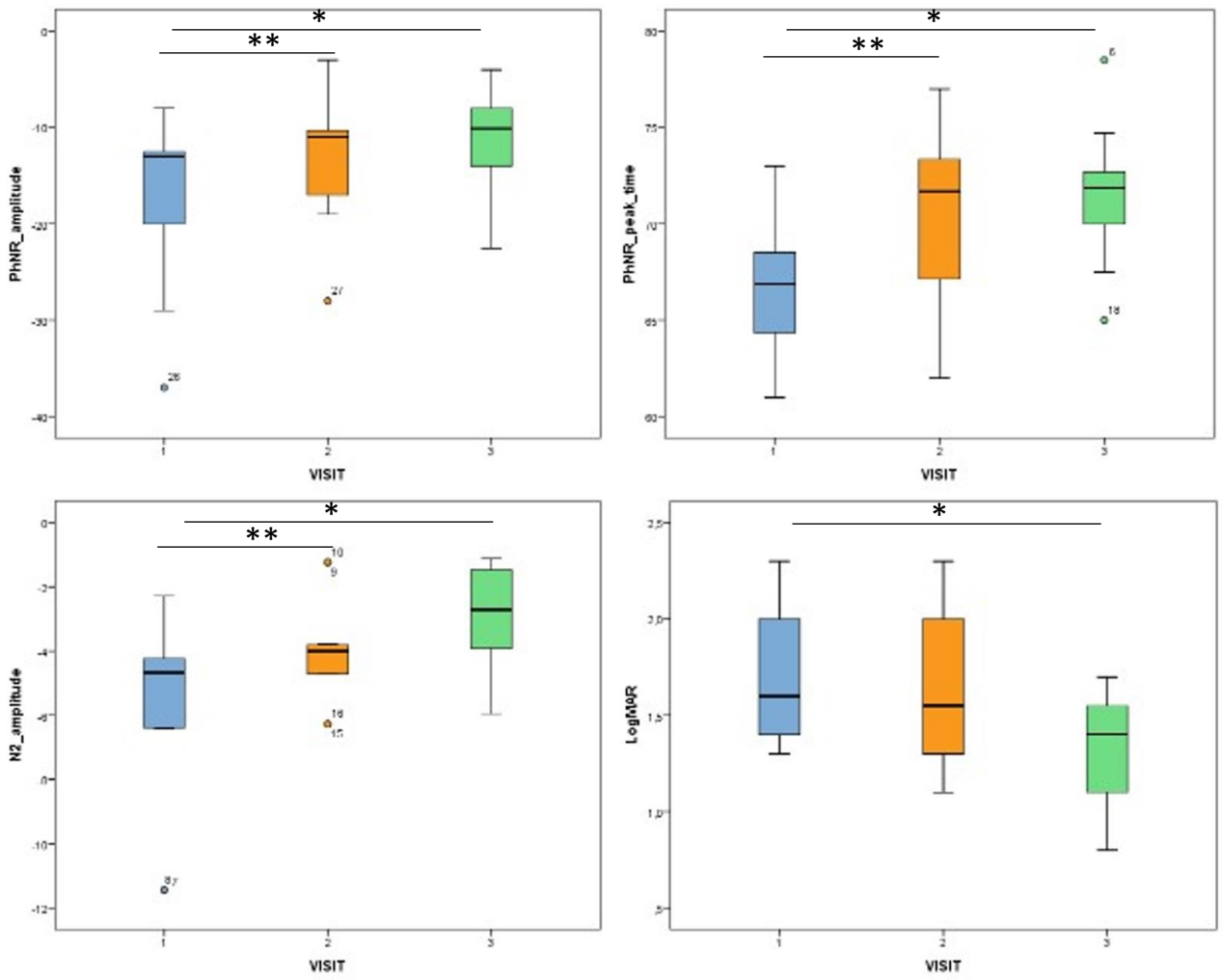

Figure 27. PhNR amplitudes (µV) and peak latency (ms) (upper panels), N2 amplitude (µV) and BCVA in logMAR (lower panels) at T1, T2 and T3.

*p<0.05 at comparison between T1 and T3

**p<0.05 at comparison between T1 and T2

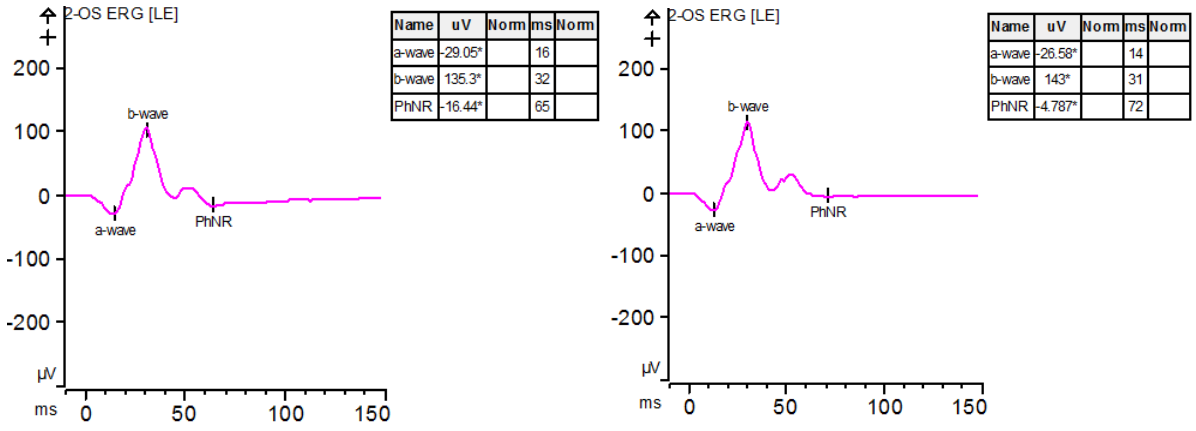

Figure 28. Reduction in PhNR amplitude from T1 (left panel) to T3 (right panel) in patient 1.

We then evaluated separately the first and the second affected eye (when bilateral onset occurred we considered both eyes as first eye). We found no difference in visual parameters between first and secondly affected eyes at T1 and T2, while at T3 first eyes compared to second eyes showed a significant better BCVA in LogMAR (1,22±0,26 vs 1,54±0,11, p=0.019) despite a significantly reduced GCL thickness in superior (39,78±5,04 vs 44,6±2,88 μm, p=0.019) and supero-temporal quadrants (35,89±7,02 vs 42,2±2,58 μm, p=0.019)

Both first and second eyes separately did not present any difference at T2 compared to T1. While, comparing T3 with T1 results, first eyes showed a significant improvement of BCVA of about -0,39 LogMAR (1,61±0,32 vs 1,22±0,26, p=0.006) and a significant reduction in PhNR amplitude (18,01±6,71 vs 12,11±4,36 μm, p=0.031). Considering the second eyes, we observed a significant reduction in RNFL thickness in average (75,83±25,63 vs 44,6±7,7 μm, p=0.030) and all sectors, more pronounced in the temporal (35,83±8,8 vs 25,86±3,67 μm, p=0.017) with increased PhNR latency (67,32±3,43 vs 73,70±2,71 ms, p=0.030) at T3 compared to T1. The change in BCVA of the second affected eye, despite showing some improvement from T1 to T3 of about -0,32 LogMAR, did not reach the significance level (1,86±0,35 to 1,54±0,11, p=0.126).

We then correlated visual parameters with time from onset. Considering all eyes, time from onset correlated negatively as expected with average and sectorial RNFL thickness (average pearson -0.584 p=0.000, superior pearson –0.509 p=0.000, temporal pearson -0.448 p=0.002, inferior pearson -0.624 p=0.000, nasal pearson -0.451 p=0.002), with PhNR amplitude (pearson -0.407 p=0.007), and counterintuitively with BCVA in LogMAR (pearson -0.438 p=0.002) (Fig 29). All those correlations were confirmed considering the eyes separately, significance was lost for temporal and nasal RNFL sectors in the first eye and for PhNR amplitude in the second eye.

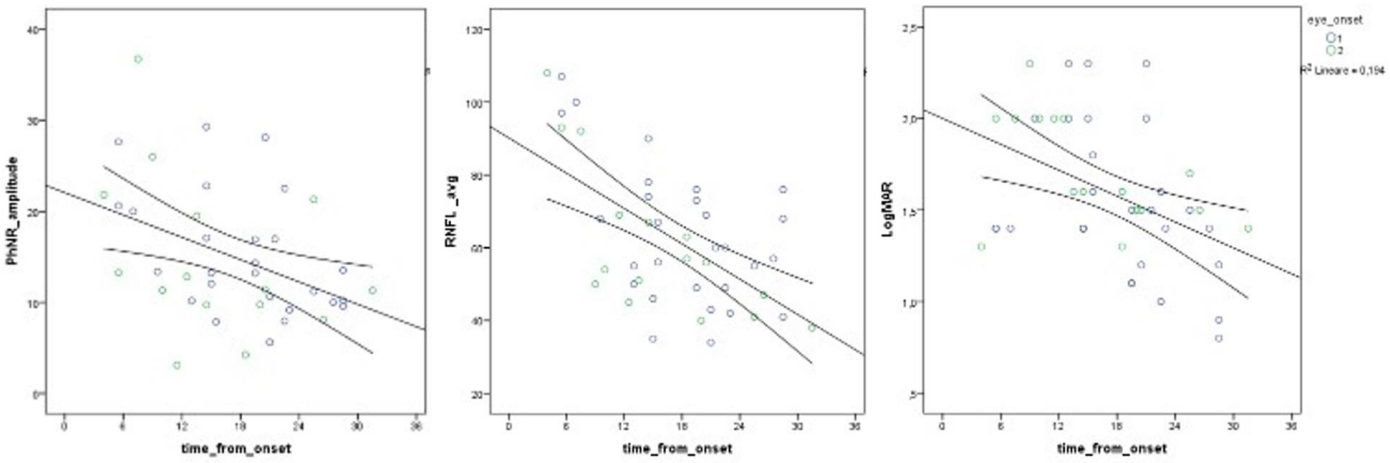

Figure 29. Correlation of PhNR amplitude, average RNFL thickness and BCVA in LogMAR with time from onset.

Despite some spontaneous improvement is described in natural history of LHON (Yu-Wai-Man et al., 2022), to explain the significant improvement of BCVA at last evaluation and its negative correlation with time from onset, we tried to assess if this improvement in visual acuity was better correlated with idebenone therapy or gene therapy. Correlation of BCVA with duration of idebenone therapy failed to find any significance (pearson -0.280 p=0.059), while it correlated significantly with time from injection (pearson -0.434 p=0.003) (Figure 30). Interestingly, the negative correlation of time from injection with BCVA was confirmed for the first affected eye (pearson -0.475 p=0.008) but not for the second eye (pearson -0.447 p=0.083).

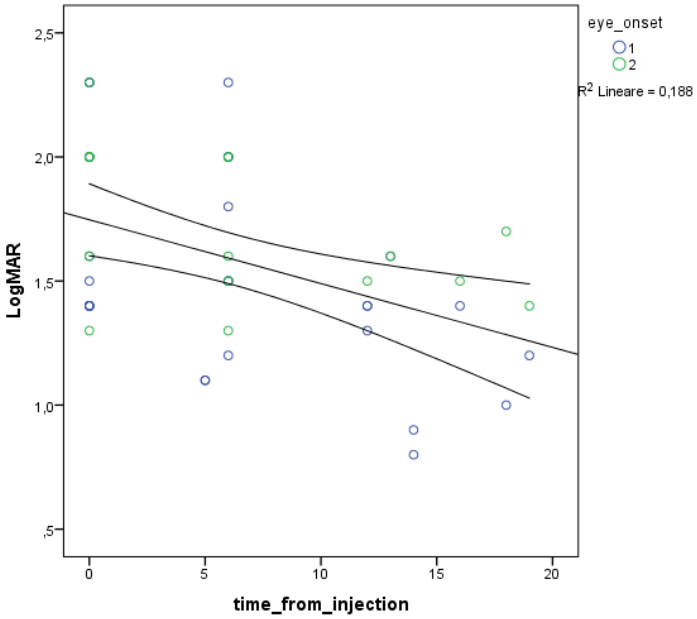

Figure 30. Correlation of BCVA with time from injection.

5.3 Discussion

We comprehensively described the longitudinal changes in neuro-ophthalmological and electrophysiological parameters in a group of subacute LHON harbouring the m.11778G>A/MTND4 mutation treated with rAAV2/2-ND4 gene therapy (LUMEVOQ) as compassionate use in our Neuro-ophthalmology Clinic in Bologna.

As expected by the disease progression (Barboni et al., 2010), overtime we observed a reduction in OCT parameters that was clearly evident for RNFL thickness, both average and sectorial even if less pronounced in the nasal sector, while GCL thickness values tended to stabilize.

Electrophysiological results showed concordantly a tendency to reduction over time in FVEP components (N2 more than P2), while PhNR amplitude showed significant reduction coupled with

an increased in peak time. To this regard, despite PhNR amplitude reduction in LHON patients has been extensively demonstrated in different studies (Karanjia et al., 2017, Majander et al., 2017, Botelho et al., 2021), to our knowledge this is the first study documenting its progressive decline in the acute/dynamic phase of the disease. This general decrease of structural and functional readouts, as expected by natural history, confirms that neither idebenone or gene therapy are able to stop or significantly diverge the disease evolution, as already known from literature (ref Amore). However, counterintuitively to what expected by disease progression, we observed a significant improvement in BCVA from first to last evaluation of overall -0.37 LogMAR, that was more clearly pronounced in first affected eyes (-0,39 LogMAR including bilateral cases), as compared to second affected eyes (-0,32 LogMAR). The improvement in visual acuity observed in our cohort is remarkably similar to the values obtained in the REVERSE trial, in which a mean improvement in BCVA of -0.308 LogMAR was observed in treated eyes at 96 weeks from injection (Yu-Wai Man et al., 2020), and in the REFLECT trial, in which a clinically meaningful improvement from the nadir of at least -0.3 LogMAR was reported in 73% of bilaterally treated subjects and 66% of unilaterally treated subjects (Yu-Wai-Man et al., 2022). A recent systematic review indirectly compared data from natural history with the results of the gene therapy trials RESCUE and REVERSE showing a meaningful improvement BCVA of -0.33 LogMAR in treated eyes compared to untreated ones (Newman et al., 2021). Notwithstanding all these evidences point to a major effect of the gene therapy on visual improvement, our patients presented a relevant confounding factor that was the idebenone therapy, that was started in almost all cases before the injection and continued through after. Therefore, we cannot exclude a superimposed or combining effect of the idebenone therapy in the observed improvement of visual acuity in our patients, nevertheless correlation analysis failed to find a significance with duration of idebenone therapy. It must be considered, that full idebenone effect is observed better on the long run, as it has been shown that improvements of idebenone treated patients may be observed up to 3 years of drug administration (vedi dati expanded access program e ref.). Thus, the real impact of the double administration idebenone-gene therapy might not be emerging until later stages in these patients, as we continue to follow them.

In conclusion, we confirmed the reduction in RNFL thickness expected by disease progression and described for the first time the progressive deterioration in electrophysiological parameters, in particular of PhNR. We also observed an improvement in visual acuity similar to those described in the recent clinical trials with rAAV2/2-*ND4* gene therapy, nevertheless the effect of idebenone therapy in our cohort cannot be completely evaluated at this time.

6. GENERAL CONCLUSIONS AND FUTURE DIRECTIONS

In the first part of the project, we described a cohort of patients presenting with a DOA phenotype harbouring a rare mutation respectively in the ACO2 or AFG3L2 nuclear genes, comparing them with the classic OPA1-associated DOA. In conclusion, DOA remains clinically a fairly homogeneous entity despite the growing genetic heterogeneity underlying the disease. However, while AFG3L2-DOA resulted virtually indistinguishable from OPA1-DOA, ACO2 mutations seem to cause an overall milder phenotype, in terms of better preservation of RGCs, which was confirmed also in visually asymptomatic patients. This subtle difference possibly depends on a different pathogenic mechanism involving mtDNA maintenance in ACO2, as opposed to AFG3L2, which obeys the OPA1 dysfunction paradigm affecting mitochondrial dynamics, being involved in OPA1 processing.

In the second part of the project, we demonstrated a high prevalence of neuro-ophthalmological involvement in our cohort of MELAS and MERRF patients, confirming also a distinct ocular phenotype, respectively retinopathy in MELAS and optic atrophy in MERRF. This striking difference possibly reflects a selective susceptibility of different retinal cell types, namely photoreceptors/RPE in MELAS and RGCs in MERRF, which may relate to prevalent OXPHOS impairment or ROS accumulation respectively. The higher prevalence of optic atrophy in MERRF reflected in significant lower values of RNFL thickness compared to MELAS patients, despite visual acuity, visual fields measures and GCL thickness resulted comparable. Correlation with heteroplasmy, apart from the already known effect of age on the leucine tRNA mutation causing a negative selective pressure in blood cells, and less significantly in urinary cells, failed to disclose any significant correlation with neuro-ophthalmological parameter in MELAS patients. Contrarywise, lysine tRNA mutational load, albeit not correlating with age, negatively correlated with both RNFL and GCL thickness in MERRF patients, with the highest significance on the temporal RNFL sector. In addition to the interacting pathogenic mechanisms involving OXPHOS deficiency and ROS overproduction, this difference between the two entities might be also related to a different pattern of segregation in specific cell types that the two mutant mtDNAs may present.

Lastly, in a group of subacute LHON treated with gene therapy and followed longitudinally with neuro-ophthalmic and electrophysiological examinations, we confirmed the reduction in RNFL thickness expected by disease progression and described for the first time the progressive deterioration in electrophysiological parameters, in particular of PhNR amplitude. We also observed a progressive improvement in visual acuity at last evaluation of about -0,37 LogMAR, which is remarkably similar to the figures obtained in the recent clinical trials with rAAV2/2-*ND4* gene therapy, nevertheless the effect of idebenone therapy in our cohort, despite not clearly correlating with visual acuity, may emerge later, on a longer time of observation.

Currently, multiple research programs are ongoing in the biological labs of the IRCCS ISNB, taking advantage of reprogramming from patient-derived somatic cells of induced pluripotent stem cells (iPSCs). The iPSCs are instrumental to differentiate neuronal cells, and more specifically RGCs, as well as retinal organoids, or even eye-thalamus assembloids. This cutting-edge approach should further clarify on the preclinical ground many of the open questions raised in this thesis. Single cell multi-omic analysis will provide some of the answers, for example how heteroplasmic mtDNA tRNA mutations associated with MELAS or MERRF may differentially segregate in organoid development, or how the metabolic profiles may characterise the different genes involved in DOA. Ultimately, the mechanistic understanding of mitochondrial diseases is instrumental to define therapeutic targets, a rapidly expanding field returning possible cures for these patients.

7. REFERENCES

Åkebrand R, Andersson S, Seyedi Honarvar AK, Sofou K, Darin N, Tulinius M, Grönlund MA. Ophthalmological characteristics in children with Leigh syndrome - A long-term follow-up. Acta Ophthalmol. 2016 Sep;94(6):609-17. doi: 10.1111/aos.12983. Epub 2016 Feb 19. PMID: 26893257.

Alexander C, Votruba M, Pesch UE, Thiselton DL, Mayer S, Moore A, Rodriguez M, Kellner U, Leo-Kottler B, Auburger G, Bhattacharya SS, Wissinger B. OPA1, encoding a dynamin-related GTPase, is mutated in autosomal dominant optic atrophy linked to chromosome 3q28. Nat Genet. 2000 Oct;26(2):211-5. doi: 10.1038/79944. PMID: 11017080.

Altmann J, Büchner B, Nadaj-Pakleza A, Schäfer J, Jackson S, Lehmann D, Deschauer M, Kopajtich R, Lautenschläger R, Kuhn KA, Karle K, Schöls L, Schulz JB, Weis J, Prokisch H, Kornblum C, Claeys KG, Klopstock T. Expanded phenotypic spectrum of the m.8344A>G "MERRF" mutation: data from the German mitoNET registry. J Neurol. 2016 May;263(5):961-972. doi: 10.1007/s00415-016-8086-3. Epub 2016 Mar 19. PMID: 26995359.

Ambrosio G, De Marco R, Loffredo L, Magli A. Visual dysfunction in patients with mitochondrial myopathies. I. Electrophysiologic impairments. Doc Ophthalmol. 1995;89(3):211-8. doi: 10.1007/BF01203374. PMID: 7555588.

Amore G, Romagnoli M, Carbonelli M, Barboni P, Carelli V, La Morgia C. Therapeutic Options in Hereditary Optic Neuropathies. Drugs. 2021 Jan;81(1):57-86. doi: 10.1007/s40265-020-01428-3. PMID: 33159657; PMCID: PMC7843467.

Arena IG, Pugliese A, Volta S, Toscano A, Musumeci O. Molecular Genetics Overview of Primary Mitochondrial Myopathies. J Clin Med. 2022 Jan 26;11(3):632. doi: 10.3390/jcm11030632. PMID: 35160083; PMCID: PMC8836969.

Asanad S, Tian JJ, Frousiakis S, Jiang JP, Kogachi K, Felix CM, Fatemeh D, Irvine AG, Ter-Zakarian A, Falavarjani KG, Barboni P, Karanjia R, Sadun AA. Optical Coherence Tomography of the Retinal Ganglion Cell Complex in Leber's Hereditary Optic Neuropathy and Dominant Optic Atrophy. Curr Eye Res. 2019 Jun;44(6):638-644. doi: 10.1080/02713683.2019.1567792. Epub 2019 Feb 4. PMID: 30649972.

Baderna V, Schultz J, Kearns LS, Fahey M, Thompson BA, Ruddle JB, Huq A, Maltecca F. A novel AFG3L2 mutation close to AAA domain leads to aberrant OMA1 and OPA1 processing in a family with optic atrophy. Acta Neuropathol Commun. 2020 Jun 29;8(1):93. doi: 10.1186/s40478-020-00975-w. PMID: 32600459; PMCID: PMC7325028.

Balducci N, Savini G, Cascavilla ML, La Morgia C, Triolo G, Giglio R, Carbonelli M, Parisi V, Sadun AA, Bandello F, Carelli V, Barboni P. Macular nerve fibre and ganglion cell layer changes in acute Leber's hereditary optic neuropathy. Br J Ophthalmol. 2016 Sep;100(9):1232-7. doi: 10.1136/bjophthalmol-2015-307326. Epub 2015 Nov 27. PMID: 26614631.

Barboni P, Savini G, Valentino ML, Montagna P, Cortelli P, De Negri AM, Sadun F, Bianchi S, Longanesi L, Zanini M, de Vivo A, Carelli V. Retinal nerve fiber layer evaluation by optical coherence tomography in Leber's hereditary optic neuropathy. Ophthalmology. 2005 Jan;112(1):120-6. doi: 10.1016/j.ophtha.2004.06.034. PMID: 15629831.

Barboni P, Carbonelli M, Savini G, Ramos Cdo V, Carta A, Berezovsky A, Salomao SR, Carelli V, Sadun AA. Natural history of Leber's hereditary optic neuropathy: longitudinal analysis of the retinal nerve fiber layer by optical coherence tomography. Ophthalmology. 2010 Mar;117(3):623-7. doi: 10.1016/j.ophtha.2009.07.026. Epub 2010 Jan 19. PMID: 20031228.

Barboni P, Savini G, Feuer WJ, Budenz DL, Carbonelli M, Chicani F, Ramos Cdo V, Salomao SR, Negri AD, Parisi V, Carelli V, Sadun AA. Retinal nerve fiber layer thickness variability in Leber hereditary optic neuropathy carriers. Eur J Ophthalmol. 2012 Nov-Dec;22(6):985-91. doi: 10.5301/ejo.5000154. Epub 2012 May 4. PMID: 22562299.

Barboni P, Savini G, Cascavilla ML, Caporali L, Milesi J, Borrelli E, La Morgia C, Valentino ML, Triolo G, Lembo A, Carta A, De Negri A, Sadun F, Rizzo G, Parisi V, Pierro L, Bianchi Marzoli S, Zeviani M, Sadun AA, Bandello F, Carelli V. Early macular retinal ganglion cell loss in dominant optic atrophy: genotype-phenotype correlation. Am J Ophthalmol. 2014 Sep;158(3):628-36.e3. doi: 10.1016/j.ajo.2014.05.034. Epub 2014 Jun 5. PMID: 24907432.

Berdjis H, Heider W, Demisch K. ERG and VECP in chronic progressive external ophthalmoplegia (CPEO). Doc Ophthalmol. 1985 Oct 15;60(4):427-34. doi: 10.1007/BF00158934. PMID: 4064883.

Berezovsky A, Karanjia R, Fernandes AG, Botelho GIS, Bueno TLN, Ferraz NN, Sacai PY, Coupland SG, Sadun AA, Salomão SR. Photopic negative response using a handheld mini-ganzfeld stimulator in healthy adults: normative values, intra- and inter-session variability. Doc Ophthalmol. 2021 Apr;142(2):153-163. doi: 10.1007/s10633-020-09784-x. Epub 2020 Jul 17. PMID: 32681419

Birtel J, von Landenberg C, Gliem M, Gliem C, Reimann J, Kunz WS, Herrmann P, Betz C, Caswell R, Nesbitt V, Kornblum C, Charbel Issa P. Mitochondrial Retinopathy. Ophthalmol Retina. 2022 Jan;6(1):65-79. doi: 10.1016/j.oret.2021.02.017. Epub 2021 Jul 10. PMID: 34257060.

Botelho GIS, Salomão SR, Tengan CH, Karanjia R, Moura FV, Rocha DM, da Silva PBE, Fernandes AG, Watanabe SES, Sacai PY, Belfort R Jr, Carelli V, Sadun AA, Berezovsky A. Impaired Ganglion Cell Function Objectively Assessed by the Photopic Negative Response in Affected and Asymptomatic Members From Brazilian Families With Leber's Hereditary Optic Neuropathy. Front Neurol. 2021 Jan 18;11:628014. doi: 10.3389/fneur.2020.628014. PMID: 33584522; PMCID: PMC7874135.

Caporali L, Magri S, Legati A, Del Dotto V, Tagliavini F, Balistreri F, Nasca A, La Morgia C, Carbonelli M, Valentino ML, Lamantea E, Baratta S, Schöls L, Schüle R, Barboni P, Cascavilla ML, Maresca A, Capristo M, Ardissone A, Pareyson D, Cammarata G, Melzi L, Zeviani M, Peverelli L, Lamperti C, Marzoli SB, Fang M, Synofzik M, Ghezzi D, Carelli V, Taroni F. ATPase Domain AFG3L2 Mutations Alter OPA1 Processing and Cause Optic Neuropathy. Ann Neurol. 2020 Jul;88(1):18-32. doi: 10.1002/ana.25723. Epub 2020 Apr 21. PMID: 32219868.

Capristo M, Del Dotto V, Tropeano CV, Fiorini C, Caporali L, La Morgia C, Valentino ML, Montopoli M, Carelli V, Maresca A. Rapamycin rescues mitochondrial dysfunction in cells carrying the m.8344A > G mutation in the mitochondrial $tRNA^{Lys}$. Mol Med. 2022 Aug 3;28(1):90. doi: 10.1186/s10020-022-00519-z. PMID: 35922766; PMCID: PMC9347137.

Carbonelli M, La Morgia C, Romagnoli M, Amore G, D'Agati P, Valentino ML, Caporali L, Cascavilla ML, Battista M, Borrelli E, Di Renzo A, Parisi V, Balducci N, Carelli V, Barboni P. Capturing the Pattern of Transition From Carrier to Affected in Leber Hereditary Optic Neuropathy. Am J Ophthalmol. 2022 Sep;241:71-79. doi: 10.1016/j.ajo.2022.04.016. Epub 2022 May 2. PMID: 35513027.

Carelli V, Ross-Cisneros FN, Sadun AA. Mitochondrial dysfunction as a cause of optic neuropathies. Prog Retin Eye Res. 2004 Jan;23(1):53-89. doi: 10.1016/j.preteyeres.2003.10.003. PMID: 14766317.

Carelli V, La Morgia C, Valentino ML, Barboni P, Ross-Cisneros FN, Sadun AA. Retinal ganglion cell neurodegeneration in mitochondrial inherited disorders. Biochim Biophys Acta. 2009 May;1787(5):518-28. Doi: 10.1016/j.bbabio.2009.02.024. Epub 2009 Mar 5. PMID: 19268652.

Carelli V, Chan DC. Mitochondrial DNA: impacting central and peripheral nervous systems. Neuron. 2014 Dec 17;84(6):1126-42. doi: 10.1016/j.neuron.2014.11.022. PMID: 25521375; PMCID: PMC4271190.

Carelli V, Musumeci O, Caporali L, Zanna C, La Morgia C, Del Dotto V, Porcelli AM, Rugolo M, Valentino ML, Iommarini L, Maresca A, Barboni P, Carbonelli M, Trombetta C, Valente EM, Patergnani S, Giorgi C, Pinton P, Rizzo G, Tonon C, Lodi R, Avoni P, Liguori R, Baruzzi A, Toscano A, Zeviani M. Syndromic parkinsonism and dementia associated with OPA1 missense mutations. Ann Neurol. 2015 Jul;78(1):21-38. doi: 10.1002/ana.24410. Epub 2015 Jun 10. PMID: 25820230; PMCID: PMC5008165.

Carelli V, d'Adamo P, Valentino ML, La Morgia C, Ross-Cisneros FN, Caporali L, Maresca A, Loguercio Polosa P, Barboni P, De Negri A, Sadun F, Karanjia R, Salomao SR, Berezovsky A, Chicani F, Moraes M, Moraes Filho M, Belfort R Jr, Sadun AA. Parsing the differences in affected with LHON: genetic versus environmental triggers of disease conversion. Brain. 2016 Mar;139(Pt 3):e17. doi: 10.1093/brain/awv339. Epub 2015 Dec 10. PMID: 26657166; PMCID: PMC6080496.

Carelli V, La Morgia C, Ross-Cisneros FN, Sadun AA. Optic neuropathies: the tip of the neurodegeneration iceberg. Hum Mol Genet. 2017 Oct 1;26(R2):R139-R150. doi: 10.1093/hmg/ddx273. PMID: 28977448; PMCID: PMC5886475.

Carelli V, La Morgia C. Clinical syndromes associated with mtDNA mutations: where we stand after 30 years. Essays Biochem. 2018 Jul 20;62(3):235-254. Doi: 10.1042/EBC20170097. PMID: 30030360.

Casari G, De Fusco M, Ciarmatori S, Zeviani M, Mora M, Fernandez P, De Michele G, Filla A, Cocozza S, Marconi R, Dürr A, Fontaine B, Ballabio A. Spastic paraplegia and OXPHOS impairment caused by mutations in paraplegin, a nuclear-encoded mitochondrial metalloprotease. Cell. 1998 Jun 12;93(6):973-83. doi: 10.1016/s0092-8674(00)81203-9. PMID: 9635427.

Charif M, Roubertie A, Salime S, Mamouni S, Goizet C, Hamel CP, Lenaers G. A novel mutation of AFG3L2 might cause dominant optic atrophy in patients with mild intellectual disability. Front Genet. 2015 Oct 19;6:311. doi: 10.3389/fgene.2015.00311. PMID: 26539208; PMCID: PMC4609881.

Charif M, Chevrollier A, Gueguen N, Bris C, Goudenège D, Desquiret-Dumas V, Leruez S, Colin E, Meunier A, Vignal C, Smirnov V, Defoort-Dhellemmes S, Drumare Bouvet I, Goizet C, Votruba M, Jurkute N, Yu-Wai-Man P, Tagliavini F, Caporali L, La Morgia C, Carelli V, Procaccio V, Zanlonghi X, Meunier I, Reynier P, Bonneau D, Amati-Bonneau P, Lenaers G. Mutations in the m-AAA proteases AFG3L2 and SPG7 are causing isolated dominant optic atrophy. Neurol Genet. 2020 May 20;6(3):e428. doi: 10.1212/NXG.0000000000000428. PMID: 32548275; PMCID: PMC7251510.

Charif M, Gueguen N, Ferré M, Elkarhat Z, Khiati S, LeMao M, Chevrollier A, Desquiret-Dumas V, Goudenège D, Bris C, Kane S, Alban J, Chupin S, Wetterwald C, Caporali L, Tagliavini F, LaMorgia C, Carbonelli M, Jurkute N, Barakat A, Gohier P, Verny C, Barth M, Procaccio V, Bonneau D, Zanlonghi X, Meunier I, Weisschuh N, Schimpf-Linzenbold S, Tonagel F, Kellner U, Yu-Wai-Man P, Carelli V, Wissinger B, Amati-Bonneau P, Reynier P; European ION Group, Lenaers G. Dominant *ACO2* mutations are a frequent cause of isolated optic atrophy. Brain Commun. 2021 Apr 7;3(2):fcab063. doi: 10.1093/braincomms/fcab063. PMID: 34056600; PMCID: PMC8152918.

Chinnery PF, Howell N, Lightowlers RN, Turnbull DM. Molecular pathology of MELAS and MERRF. The relationship between mutation load and clinical phenotypes. Brain. 1997 Oct;120 (Pt 10):1713-21. doi: 10.1093/brain/120.10.1713. PMID: 9365365.

Colavito D, Maritan V, Suppiej A, Del Giudice E, Mazzarolo M, Miotto S, Farina S, Dalle Carbonare M, Piermarocchi S, Leon A. Non-syndromic isolated dominant optic atrophy caused by the p.R468C mutation in the AFG3 like matrix AAA peptidase subunit 2 gene. Biomed Rep. 2017

Nov;7(5):451-454. doi: 10.3892/br.2017.987. Epub 2017 Sep 22. PMID: 29181157; PMCID: PMC5700392.

Courage C, Jackson CB, Hahn D, Euro L, Nuoffer JM, Gallati S, Schaller A. SDHA mutation with dominant transmission results in complex II deficiency with ocular, cardiac, and neurologic involvement. Am J Med Genet A. 2017 Jan;173(1):225-230. doi: 10.1002/ajmg.a.37986. Epub 2016 Sep 28. PMID: 27683074.

Davila-Siliezar P, Carter M, Milea D, Lee AG. Leber hereditary optic neuropathy: new and emerging therapies. Curr Opin Ophthalmol. 2022 Aug 25. doi: 10.1097/ICU.0000000000000891. Epub ahead of print. PMID: 36066375.

De Laat P, Smeitink JAM, Janssen MCH, Keunen JEE, Boon CJF. Mitochondrial retinal dystrophy associated with the m.3243A>G mutation. Ophthalmology. 2013 Dec;120(12):2684-2696. doi: 10.1016/j.ophtha.2013.05.013. Epub 2013 Jun 24. PMID: 23806424.

Del Dotto V, Fogazza M, Carelli V, Rugolo M, Zanna C. Eight human OPA1 isoforms, long and short: What are they for? Biochim Biophys Acta Bioenerg. 2018 Apr;1859(4):263-269. doi: 10.1016/j.bbabio.2018.01.005. Epub 2018 Jan 31. PMID: 29382469.

Del Dotto V, Ullah F, Di Meo I, Magini P, Gusic M, Maresca A, Caporali L, Palombo F, Tagliavini F, Baugh EH, Macao B, Szilagyi Z, Peron C, Gustafson MA, Khan K, La Morgia C, Barboni P, Carbonelli M, Valentino ML, Liguori R, Shashi V, Sullivan J, Nagaraj S, El-Dairi M, Iannaccone A, Cutcutache I, Bertini E, Carrozzo R, Emma F, Diomedi-Camassei F, Zanna C, Armstrong M, Page M, Stong N, Boesch S, Kopajtich R, Wortmann S, Sperl W, Davis EE, Copeland WC, Seri M, Falkenberg M, Prokisch H, Katsanis N, Tiranti V, Pippucci T, Carelli V. SSBP1 mutations cause mtDNA depletion underlying a complex optic atrophy disorder. J Clin Invest. 2020 Jan 2;130(1):108-125. doi: 10.1172/JCI128514. PMID: 31550240; PMCID: PMC6934201.

Delettre C, Lenaers G, Griffoin JM, Gigarel N, Lorenzo C, Belenguer P, Pelloquin L, Grosgeorge J, Turc-Carel C, Perret E, Astarie-Dequeker C, Lasquellec L, Arnaud B, Ducommun B, Kaplan J, Hamel CP. Nuclear gene OPA1, encoding a mitochondrial dynamin-related protein, is mutated in dominant optic atrophy. Nat Genet. 2000 Oct;26(2):207-10. doi: 10.1038/79936. PMID: 11017079.

Di Bella D, Lazzaro F, Brusco A, Plumari M, Battaglia G, Pastore A, Finardi A, Cagnoli C, Tempia F, Frontali M, Veneziano L, Sacco T, Boda E, Brussino A, Bonn F, Castellotti B, Baratta S, Mariotti C, Gellera C, Fracasso V, Magri S, Langer T, Plevani P, Di Donato S, Muzi-Falconi M, Taroni F. Mutations in the mitochondrial protease gene AFG3L2 cause dominant hereditary ataxia SCA28. Nat Genet. 2010 Apr;42(4):313-21. doi: 10.1038/ng.544. Epub 2010 Mar 7. PMID: 20208537.

DiMauro S, Hirano M, Kaufmann P, Tanji K, Sano M, Shungu DC, Bonilla E, DeVivo DC. Clinical features and genetics of myoclonic epilepsy with ragged red fibers. Adv Neurol. 2002;89:217-29. PMID: 11968448.

DiMauro S, Schon EA, Carelli V, Hirano M. The clinical maze of mitochondrial neurology. Nat Rev Neurol. 2013 Aug;9(8):429-44. doi: 10.1038/nrneurol.2013.126. Epub 2013 Jul 9. PMID: 23835535; PMCID: PMC3959773.

Fiedorczuk K, Letts JA, Degliesposti G, Kaszuba K, Skehel M, Sazanov LA. Atomic structure of the entire mammalian mitochondrial complex I. Nature. 2016 Oct 20;538(7625):406-410. doi: 10.1038/nature19794. Epub 2016 Sep 5. PMID: 27595392; PMCID: PMC5164932.

Fortuna F, Barboni P, Liguori R, Valentino ML, Savini G, Gellera C, Mariotti C, Rizzo G, Tonon C, Manners D, Lodi R, Sadun AA, Carelli V. Visual system involvement in patients with Friedreich's ataxia. Brain. 2009 Jan;132(Pt 1):116-23. doi: 10.1093/brain/awn269. Epub 2008 Oct 18. PMID: 18931386.

Fraser JA, Biousse V, Newman NJ. The neuro-ophthalmology of mitochondrial disease. Surv Ophthalmol. 2010 Jul-Aug;55(4):299-334. doi: 10.1016/j.survophthal.2009.10.002. Epub 2010 May 14. PMID: 20471050; PMCID: PMC2989385.

Frederiksen AL, Andersen PH, Kyvik KO, Jeppesen TD, Vissing J, Schwartz M. Tissue specific distribution of the 3243A->G mtDNA mutation. J Med Genet. 2006 Aug;43(8):671-7. Doi: 10.1136/jmg.2005.039339. Epub 2006 Feb 20. PMID: 16490799; PMCID: PMC2564591.

Gerber S, Charif M, Chevrollier A, Chaumette T, Angebault C, Kane MS, Paris A, Alban J, Quiles M, Delettre C, Bonneau D, Procaccio V, Amati-Bonneau P, Reynier P, Leruez S, Calmon R,

Boddaert N, Funalot B, Rio M, Bouccara D, Meunier I, Sesaki H, Kaplan J, Hamel CP, Rozet JM, Lenaers G. Mutations in DNM1L, as in OPA1, result in dominant optic atrophy despite opposite effects on mitochondrial fusion and fission. Brain. 2017 Oct 1;140(10):2586-2596. doi: 10.1093/brain/awx219. PMID: 28969390.

Gerdes F, Tatsuta T, Langer T. Mitochondrial AAA proteases--towards a molecular understanding of membrane-bound proteolytic machines. Biochim Biophys Acta. 2012 Jan;1823(1):49-55. doi: 10.1016/j.bbamcr.2011.09.015. Epub 2011 Oct 6. PMID: 22001671.

Gorman GS, Chinnery PF, DiMauro S, Hirano M, Koga Y, McFarland R, Suomalainen A, Thorburn DR, Zeviani M, Turnbull DM. Mitochondrial diseases. Nat Rev Dis Primers. 2016 Oct 20;2:16080. doi: 10.1038/nrdp.2016.80. PMID: 27775730.

Goto Y, Nonaka I, Horai S. A mutation in the tRNA(Leu)(UUR) gene associated with the MELAS subgroup of mitochondrial encephalomyopathies. Nature. 1990 Dec 13;348(6302):651-3. Doi: 10.1038/348651a0. PMID: 2102678.

Grady JP, Pickett SJ, Ng YS, Alston CL, Blakely EL, Hardy SA, Feeney CL, Bright AA, Schaefer AM, Gorman GS, McNally RJ, Taylor RW, Turnbull DM, McFarland R. mtDNA heteroplasmy level and copy number indicate disease burden in m.3243A>G mitochondrial disease. EMBO Mol Med. 2018 Jun;10(6):e8262. doi: 10.15252/emmm.201708262. PMID: 29735722; PMCID: PMC5991564.

Gränse L, Bergstrand I, Thiselton D, Ponjavic V, Heijl A, Votruba M, Andréasson S. Electrophysiology and ocular blood flow in a family with dominant optic nerve atrophy and a mutation in the OPA1 gene. Ophthalmic Genet. 2003 Dec;24(4):233-45. doi: 10.1076/opge.24.4.233.17230. PMID: 14566653.

Grönlund MA, Honarvar AK, Andersson S, Moslemi AR, Oldfors A, Holme E, Tulinius M, Darin N. Ophthalmological findings in children and young adults with genetically verified mitochondrial disease. Br J Ophthalmol. 2010 Jan;94(1):121-7. doi: 10.1136/bjo.2008.154187. PMID: 20385529.

Guy J, Qi X, Pallotti F, Schon EA, Manfredi G, Carelli V, Martinuzzi A, Hauswirth WW, Lewin AS. Rescue of a mitochondrial deficiency causing Leber Hereditary Optic Neuropathy. Ann Neurol. 2002 Nov;52(5):534-42. doi: 10.1002/ana.10354. PMID: 12402249.

Guy J, Feuer WJ, Porciatti V, Schiffman J, Abukhalil F, Vandenbroucke R, Rosa PR, Lam BL. Retinal ganglion cell dysfunction in asymptomatic G11778A: Leber hereditary optic neuropathy. Invest Ophthalmol Vis Sci. 2014 Feb 10;55(2):841-8. doi: 10.1167/iovs.13-13365. PMID: 24398093; PMCID: PMC3920864.

Han J, Lee YM, Kim SM, Han SY, Lee JB, Han SH. Ophthalmological manifestations in patients with Leigh syndrome. Br J Ophthalmol. 2015 Apr;99(4):528-35. doi: 10.1136/bjophthalmol-2014-305704. Epub 2014 Oct 28. PMID: 25351680.

Hirano M, Ricci E, Koenigsberger MR, Defendini R, Pavlakis SG, DeVivo DC, DiMauro S, Rowland LP. Melas: an original case and clinical criteria for diagnosis. Neuromuscul Disord. 1992;2(2):125-35. doi: 10.1016/0960-8966(92)90045-8. PMID: 1422200.

Holder GE, Votruba M, Carter AC, Bhattacharya SS, Fitzke FW, Moore AT. Electrophysiological findings in dominant optic atrophy (DOA) linking to the OPA1 locus on chromosome 3q 28-qter. Doc Ophthalmol. 1998-1999;95(3-4):217-28. doi: 10.1023/a:1001844021014. PMID: 10532406.

Hwang JM, Park HW, Kim SJ. Optic neuropathy associated with mitochondrial tRNA[Leu(UUR)] A3243G mutation. Ophthalmic Genet. 1997 Jun;18(2):101-5. doi: 10.3109/13816819709057122. PMID: 9228247.

Jarc-Vidmar M, Tajnik M, Brecelj J, Fakin A, Sustar M, Naji M, Stirn-Kranjc B, Glavač D, Hawlina M. Clinical and electrophysiology findings in Slovene patients with Leber hereditary optic neuropathy. Doc Ophthalmol. 2015 Jun;130(3):179-87. doi: 10.1007/s10633-015-9489-7. Epub 2015 Feb 19. PMID: 25690485.

Jiang M, Xie X, Zhu X, Jiang S, Milenkovic D, Misic J, Shi Y, Tandukar N, Li X, Atanassov I, Jenninger L, Hoberg E, Albarran-Gutierrez S, Szilagyi Z, Macao B, Siira SJ, Carelli V, Griffith JD, Gustafsson CM, Nicholls TJ, Filipovska A, Larsson NG, Falkenberg M. The mitochondrial single-

stranded DNA binding protein is essential for initiation of mtDNA replication. Sci Adv. 2021 Jul 2;7(27):eabf8631. doi: 10.1126/sciadv.abf8631. PMID: 34215584.

Jurkute N, Leu C, Pogoda HM, Arno G, Robson AG, Nürnberg G, Altmüller J, Thiele H, Motameny S, Toliat MR, Powell K, Höhne W, Michaelides M, Webster AR, Moore AT, Hammerschmidt M, Nürnberg P, Yu-Wai-Man P, Votruba M. SSBP1 mutations in dominant optic atrophy with variable retinal degeneration. Ann Neurol. 2019 Sep;86(3):368-383. doi: 10.1002/ana.25550. Epub 2019 Jul 31. PMID: 31298765; PMCID: PMC8855788.

Jüschke C, Klopstock T, Catarino CB, Owczarek-Lipska M, Wissinger B, Neidhardt J. Autosomal dominant optic atrophy: A novel treatment for *OPA1* splice defects using U1 snRNA adaption. Mol Ther Nucleic Acids. 2021 Oct 21;26:1186-1197. doi: 10.1016/j.omtn.2021.10.019. PMID: 34853716; PMCID: PMC8604756.

Karanjia R, Berezovsky A, Sacai PY, Cavascan NN, Liu HY, Nazarali S, Moraes-Filho MN, Anderson K, Tran JS, Watanabe SE, Moraes MN, Sadun F, DeNegri AM, Barboni P, do Val Ferreira Ramos C, La Morgia C, Carelli V, Belfort R Jr, Coupland SG, Salomao SR, Sadun AA. The Photopic Negative Response: An Objective Measure of Retinal Ganglion Cell Function in Patients With Leber's Hereditary Optic Neuropathy. Invest Ophthalmol Vis Sci. 2017 May 1;58(6):BIO300-BIO306. doi: 10.1167/iovs.17-21773. PMID: 29049835.

Keilland E, Rupar CA, Prasad AN, Tay KY, Downie A, Prasad C. The expanding phenotype of MELAS caused by the m.3291T > C mutation in the MT-TL1 gene. Mol Genet Metab Rep. 2016 Feb 22;6:64-9. Doi: 10.1016/j.ymgmr.2016.02.003. PMID: 27014580; PMCID: PMC4789386.

Kisilevsky E, Freund P, Margolin E. Mitochondrial disorders and the eye. Surv Ophthalmol. 2020 May-Jun;65(3):294-311. doi: 10.1016/j.survophthal.2019.11.001. Epub 2019 Nov 27. PMID: 31783046.

Klebe S, Depienne C, Gerber S, Challe G, Anheim M, Charles P, Fedirko E, Lejeune E, Cottineau J, Brusco A, Dollfus H, Chinnery PF, Mancini C, Ferrer X, Sole G, Destée A, Mayer JM, Fontaine B, de Seze J, Clanet M, Ollagnon E, Busson P, Cazeneuve C, Stevanin G, Kaplan J, Rozet JM, Brice A, Durr A. Spastic paraplegia gene 7 in patients with spasticity and/or optic neuropathy.

Brain. 2012 Oct;135(Pt 10):2980-93. doi: 10.1093/brain/aws240. PMID: 23065789; PMCID: PMC3470714.

Klopstock T, Yu-Wai-Man P, Dimitriadis K, Rouleau J, Heck S, Bailie M, Atawan A, Chattopadhyay S, Schubert M, Garip A, Kernt M, Petraki D, Rummey C, Leinonen M, Metz G, Griffiths PG, Meier T, Chinnery PF. A randomized placebo-controlled trial of idebenone in Leber's hereditary optic neuropathy. Brain. 2011 Sep;134(Pt 9):2677-86. doi: 10.1093/brain/awr170. Epub 2011 Jul 25. PMID: 21788663; PMCID: PMC3170530.

Kobayashi Y, Momoi MY, Tominaga K, Momoi T, Nihei K, Yanagisawa M, Kagawa Y, Ohta S. A point mutation in the mitochondrial tRNA(Leu)(UUR) gene in MELAS (mitochondrial myopathy, encephalopathy, lactic acidosis and stroke-like episodes). Biochem Biophys Res Commun. 1990 Dec 31;173(3):816-22. Doi: 10.1016/s0006-291x(05)80860-5. PMID: 2268345.

Kurtenbach A, Leo-Kottler B, Zrenner E. Inner retinal contributions to the multifocal electroretinogram: patients with Leber's hereditary optic neuropathy (LHON). Multifocal ERG in patients with LHON. Doc Ophthalmol. 2004 May;108(3):231-40. doi: 10.1007/s10633-004-8676-8. PMID: 15573947.

La Morgia C, Ross-Cisneros FN, Sadun AA, Hannibal J, Munarini A, Mantovani V, Barboni P, Cantalupo G, Tozer KR, Sancisi E, Salomao SR, Moraes MN, Moraes-Filho MN, Heegaard S, Milea D, Kjer P, Montagna P, Carelli V. Melanopsin retinal ganglion cells are resistant to neurodegeneration in mitochondrial optic neuropathies. Brain. 2010 Aug;133(Pt 8):2426-38. doi: 10.1093/brain/awq155. Epub 2010 Jul 21. PMID: 20659957; PMCID: PMC3139936.

La Morgia C, Caporali L, Gandini F, Olivieri A, Toni F, Nassetti S, Brunetto D, Stipa C, Scaduto C, Parmeggiani A, Tonon C, Lodi R, Torroni A, Carelli V. Association of the mtDNA m.4171C>A/MT-ND1 mutation with both optic neuropathy and bilateral brainstem lesions. BMC Neurol. 2014 May 28;14:116. Doi: 10.1186/1471-2377-14-116. PMID: 24884847; PMCID: PMC4047257.

La Morgia C, Maresca A, Caporali L, Valentino ML, Carelli V. Mitochondrial diseases in adults. J Intern Med. 2020 Jun;287(6):592-608. Doi: 10.1111/joim.13064. PMID: 32463135.

Latvala T, Mustonen E, Uusitalo R, Majamaa K. Pigmentary retinopathy in patients with the MELAS mutation 3243A-->G in mitochondrial DNA. Graefes Arch Clin Exp Ophthalmol. 2002 Oct;240(10):795-801. doi: 10.1007/s00417-002-0555-y. Epub 2002 Sep 21. PMID: 12397426.

Lenaers G, Neutzner A, Le Dantec Y, Jüschke C, Xiao T, Decembrini S, Swirski S, Kieninger S, Agca C, Kim US, Reynier P, Yu-Wai-Man P, Neidhardt J, Wissinger B. Dominant optic atrophy: Culprit mitochondria in the optic nerve. Prog Retin Eye Res. 2020 Dec 17:100935. doi: 10.1016/j.preteyeres.2020.100935. Epub ahead of print. PMID: 33340656.

Lin CS, Sharpley MS, Fan W, Waymire KG, Sadun AA, Carelli V, Ross-Cisneros FN, Baciu P, Sung E, McManus MJ, Pan BX, Gil DW, Macgregor GR, Wallace DC. Mouse mtDNA mutant model of Leber hereditary optic neuropathy. Proc Natl Acad Sci U S A. 2012 Dec 4;109(49):20065-70. doi: 10.1073/pnas.1217113109. Epub 2012 Nov 5. PMID: 23129651; PMCID: PMC3523873.

Lin J, Zhao CB, Lu JH, Wang HJ, Zhu WH, Xi JY, Lu J, Luo SS, Ma D, Wang Y, Xiao BG, Lu CZ. Novel mutations m.3959G>A and m.3995A>G in mitochondrial gene MT-ND1 associated with MELAS. Mitochondrial DNA. 2014 Feb;25(1):56-62. Doi: 10.3109/19401736.2013.779259. Epub 2013 Jul 8. PMID: 23834081.

Macmillan C, Lach B, Shoubridge EA. Variable distribution of mutant mitochondrial DNAs (tRNA(Leu[3243])) in tissues of symptomatic relatives with MELAS: the role of mitotic segregation. Neurology. 1993 Aug;43(8):1586-90. doi: 10.1212/wnl.43.8.1586. PMID: 8351017.

Majander A, Robson AG, João C, Holder GE, Chinnery PF, Moore AT, Votruba M, Stockman A, Yu-Wai-Man P. The pattern of retinal ganglion cell dysfunction in Leber hereditary optic neuropathy. Mitochondrion. 2017 Sep;36:138-149. doi: 10.1016/j.mito.2017.07.006. Epub 2017 Jul 18. PMID: 28729193; PMCID: PMC5644721.

Mancuso M, Orsucci D, Angelini C, Bertini E, Carelli V, Comi GP, Minetti C, Moggio M, Mongini T, Servidei S, Tonin P, Toscano A, Uziel G, Bruno C, Caldarazzo Ienco E, Filosto M, Lamperti C, Martinelli D, Moroni I, Musumeci O, Pegoraro E, Ronchi D, Santorelli FM, Sauchelli D, Scarpelli M, Sciacco M, Spinazzi M, Valentino ML, Vercelli L, Zeviani M, Siciliano G. Phenotypic heterogeneity of the 8344A>G mtDNA "MERRF" mutation. Neurology. 2013 May 28;80(22):2049-54. doi: 10.1212/WNL.0b013e318294b44c. Epub 2013 May 1. PMID: 23635963.

Maresca A, Carelli V. Molecular Mechanisms behind Inherited Neurodegeneration of the Optic Nerve. Biomolecules. 2021 Mar 25;11(4):496. doi: 10.3390/biom11040496. PMID: 33806088; PMCID: PMC8064499.

McFarland R., Taylor R.W., Turnbull D.M. A neurological perspective on mitochondrial disease. Lancet Neurol. 2010;9:829–840. doi: 10.1016/S1474-4422(10)70116-2

Metodiev MD, Gerber S, Hubert L, Delahodde A, Chretien D, Gérard X, Amati-Bonneau P, Giacomotto MC, Boddaert N, Kaminska A, Desguerre I, Amiel J, Rio M, Kaplan J, Munnich A, Rötig A, Rozet JM, Besmond C. Mutations in the tricarboxylic acid cycle enzyme, aconitase 2, cause either isolated or syndromic optic neuropathy with encephalopathy and cerebellar atrophy. J Med Genet. 2014 Dec;51(12):834-8. doi: 10.1136/jmedgenet-2014-102532. Epub 2014 Oct 28. PMID: 25351951.

Miyaue N, Yamanishi Y, Tada S, Ando R, Nagai M, Nomoto M. Phenotypic Diversity of Myoclonus Epilepsy Associated with Ragged-red Fibers with an 8344A>G mtDNA Mutation. Intern Med. 2019 Sep 15;58(18):2753. doi: 10.2169/internalmedicine.2416-18. Epub 2019 Jun 7. PMID: 31178486; PMCID: PMC6794172.

Montagna P, Plazzi G, Cortelli P, Carelli V, Lugaresi E, Barboni P, Fiocchi M. Abnormal lactate after effort in healthy carriers of Leber's hereditary optic neuropathy. J Neurol Neurosurg Psychiatry. 1995 May;58(5):640-1. doi: 10.1136/jnnp.58.5.640. PMID: 7745422; PMCID: PMC1073505.

Morny EK, Margrain TH, Binns AM, Votruba M. Electrophysiological ON and OFF Responses in Autosomal Dominant Optic Atrophy. Invest Ophthalmol Vis Sci. 2015 Dec;56(13):7629-37. doi: 10.1167/iovs.15-17951. PMID: 26624494.

Moura AL, Nagy BV, La Morgia C, Barboni P, Oliveira AG, Salomão SR, Berezovsky A, de Moraes-Filho MN, Chicani CF, Belfort R Jr, Carelli V, Sadun AA, Hood DC, Ventura DF. The pupil light reflex in Leber's hereditary optic neuropathy: evidence for preservation of melanopsin-expressing retinal ganglion cells. Invest Ophthalmol Vis Sci. 2013 Jul 2;54(7):4471-7. doi: 10.1167/iovs.12-11137. PMID: 23737476; PMCID: PMC4322722.

Najjar RP, Reynier P, Caignard A, Procaccio V, Amati-Bonneau P, Mack H, Milea D. Retinal Neuronal Loss in Visually Asymptomatic Patients With Myoclonic Epilepsy With Ragged-Red Fibers. J Neuroophthalmol. 2019 Mar;39(1):18-22. doi: 10.1097/WNO.0000000000000690. PMID: 29979334.

Neumann MA, Grossmann D, Schimpf-Linzenbold S, Dayan D, Stingl K, Ben-Menachem R, Pines O, Massart F, Delcambre S, Ghelfi J, Bohler J, Strom T, Kessel A, Azem A, Schöls L, Grünewald A, Wissinger B, Krüger R. Haploinsufficiency due to a novel ACO2 deletion causes mitochondrial dysfunction in fibroblasts from a patient with dominant optic nerve atrophy. Sci Rep. 2020 Oct 7;10(1):16736. doi: 10.1038/s41598-020-73557-4. PMID: 33028849; PMCID: PMC7541502.

Newman NJ. Hereditary optic neuropathies. In: Miller NR, Biousse V, Newman NJ, Kerrison JB, eds. Walsh and Hoyt ' s Clinical Neuro-Ophthalmology. Philadelphia: Lippin- cott Williams & Wilkins; 2005:465–501.

Newman NJ, Yu-Wai-Man P, Carelli V, Biousse V, Moster ML, Vignal-Clermont C, Sergott RC, Klopstock T, Sadun AA, Girmens JF, La Morgia C, DeBusk AA, Jurkute N, Priglinger C, Karanjia R, Josse C, Salzmann J, Montestruc F, Roux M, Taiel M, Sahel JA. Intravitreal Gene Therapy vs. Natural History in Patients With Leber Hereditary Optic Neuropathy Carrying the m.11778G>A *ND4* Mutation: Systematic Review and Indirect Comparison. Front Neurol. 2021 May 24;12:662838. doi: 10.3389/fneur.2021.662838. PMID: 34108929; PMCID: PMC8181419.
Orsucci D, Caldarazzo Ienco E, Rossi A, Siciliano G, Mancuso M. Mitochondrial Syndromes Revisited. J Clin Med. 2021 Mar 17;10(6):1249. doi: 10.3390/jcm10061249. PMID: 33802970; PMCID: PMC8002645.

Newman NJ, Yu-Wai-Man P, Carelli V, Moster ML, Biousse V, Vignal-Clermont C, Sergott RC, Klopstock T, Sadun AA, Barboni P, DeBusk AA, Girmens JF, Rudolph G, Karanjia R, Taiel M, Blouin L, Smits G, Katz B, Sahel JA; LHON Study Group. Efficacy and Safety of Intravitreal Gene Therapy for Leber Hereditary Optic Neuropathy Treated within 6 Months of Disease Onset. Ophthalmology. 2021 May;128(5):649-660. doi: 10.1016/j.ophtha.2020.12.012. Epub 2021 Jan 12. PMID: 33451738.

Newman NJ, Yu-Wai-Man P, Biousse V, Carelli V. Understanding the molecular basis and pathogenesis of hereditary optic neuropathies: towards improved diagnosis and management. Lancet Neurol. 2023 Feb;22(2):172-188. doi: 10.1016/S1474-4422(22)00174-0. Epub 2022 Sep 22. PMID: 36155660.

Pan BX, Ross-Cisneros FN, Carelli V, Rue KS, Salomao SR, Moraes-Filho MN, Moraes MN, Berezovsky A, Belfort R Jr, Sadun AA. Mathematically modeling the involvement of axons in Leber's hereditary optic neuropathy. Invest Ophthalmol Vis Sci. 2012 Nov 9;53(12):7608-17. doi: 10.1167/iovs.12-10452. PMID: 23060142; PMCID: PMC3495603

Pavlakis SG, Phillips PC, DiMauro S, De Vivo DC, Rowland LP. Mitochondrial myopathy, encephalopathy, lactic acidosis, and strokelike episodes: a distinctive clinical syndrome. Ann Neurol. 1984 Oct;16(4):481-8. Doi: 10.1002/ana.410160409. PMID: 6093682.

Pierson TM, Adams D, Bonn F, Martinelli P, Cherukuri PF, Teer JK, Hansen NF, Cruz P, Mullikin For The Nisc Comparative Sequencing Program JC, Blakesley RW, Golas G, Kwan J, Sandler A, Fuentes Fajardo K, Markello T, Tifft C, Blackstone C, Rugarli EI, Langer T, Gahl WA, Toro C. Whole-exome sequencing identifies homozygous AFG3L2 mutations in a spastic ataxia-neuropathy syndrome linked to mitochondrial m-AAA proteases. PLoS Genet. 2011 Oct;7(10):e1002325. doi: 10.1371/journal.pgen.1002325. Epub 2011 Oct 13. PMID: 22022284; PMCID: PMC3192828.

Piro-Mégy C, Sarzi E, Tarrés-Solé A, Péquignot M, Hensen F, Quilès M, Manes G, Chakraborty A, Sénéchal A, Bocquet B, Cazevieille C, Roubertie A, Müller A, Charif M, Goudenège D, Lenaers G, Wilhelm H, Kellner U, Weisschuh N, Wissinger B, Zanlonghi X, Hamel C, Spelbrink JN, Sola M, Delettre C. Dominant mutations in mtDNA maintenance gene SSBP1 cause optic atrophy and foveopathy. J Clin Invest. 2020 Jan 2;130(1):143-156. doi: 10.1172/JCI128513. PMID: 31550237; PMCID: PMC6934222.

Rath PP, Jenkins S, Michaelides M, Smith A, Sweeney MG, Davis MB, Fitzke FW, Bird AC. Characterisation of the macular dystrophy in patients with the A3243G mitochondrial DNA point mutation with fundus autofluorescence. Br J Ophthalmol. 2008 May;92(5):623-9. doi: 10.1136/bjo.2007.131177. PMID: 18441172; PMCID: PMC2569141.

Reis A, Mateus C, Viegas T, Florijn R, Bergen A, Silva E, Castelo-Branco M. Physiological evidence for impairment in autosomal dominant optic atrophy at the pre-ganglion level. Graefes Arch Clin Exp Ophthalmol. 2013 Jan;251(1):221-34. doi: 10.1007/s00417-012-2112-7. Epub 2012 Aug 4. PMID: 22865259.

Rocatcher A, Desquiret-Dumas V, Charif M, Ferré M, Gohier P, Mirebeau-Prunier D, Verny C, Milea D, Lenaers G; HON Collaborators Group; Bonneau D, Reynier P, Amati-Bonneau P. The top 10 most frequently involved genes in hereditary optic neuropathies in 2186 probands. Brain. 2022 Nov 1:awac395. doi: 10.1093/brain/awac395. Epub ahead of print. PMID: 36317462.

Romagnoli M, La Morgia C, Carbonelli M, Di Vito L, Amore G, Zenesini C, Cascavilla ML, Barboni P, Carelli V. Idebenone increases chance of stabilization/recovery of visual acuity in OPA1-dominant optic atrophy. Ann Clin Transl Neurol. 2020 Apr;7(4):590-594. doi: 10.1002/acn3.51026. Epub 2020 Apr 3. PMID: 32243103; PMCID: PMC7187718.

Salomão SR, Berezovsky A, Andrade RE, Belfort R Jr, Carelli V, Sadun AA. Visual electrophysiologic findings in patients from an extensive Brazilian family with Leber's hereditary optic neuropathy. Doc Ophthalmol. 2004 Mar;108(2):147-55. doi: 10.1023/b:doop.0000036829.37053.31. PMID: 15455797.

Salsano E, Giovagnoli AR, Morandi L, Maccagnano C, Lamantea E, Marchesi C, Zeviani M, Pareyson D. Mitochondrial dementia: a sporadic case of progressive cognitive and behavioral decline with hearing loss due to the rare m.3291T>C MELAS mutation. J Neurol Sci. 2011 Jan 15;300(1-2):165-8. Doi: 10.1016/j.jns.2010.09.022. Epub 2010 Oct 12. PMID: 20943236.

Sanderson KG, Millar E, Tumber A, Klatt R, Sondheimer N, Vincent A. Rod bipolar cell dysfunction in POLG retinopathy. Doc Ophthalmol. 2021 Feb;142(1):111-118. doi: 10.1007/s10633-020-09777-w. Epub 2020 Jun 21. PMID: 32567010.

Sarzi E, Seveno M, Piro-Mégy C, Elzière L, Quilès M, Péquignot M, Müller A, Hamel CP, Lenaers G, Delettre C. OPA1 gene therapy prevents retinal ganglion cell loss in a Dominant Optic Atrophy mouse model. Sci Rep. 2018 Feb 6;8(1):2468. doi: 10.1038/s41598-018-20838-8. PMID: 29410463; PMCID: PMC5802757.

Shaukat AN, Kaliatsi EG, Stamatopoulou V, Stathopoulos C. Mitochondrial tRNA-Derived Fragments and Their Contribution to Gene Expression Regulation. Front Physiol. 2021 Sep 3;12:729452. Doi: 10.3389/fphys.2021.729452. PMID: 34539450; PMCID: PMC8446549.

Shinkai A, Shinmei Y, Hirooka K, Tagawa Y, Nakamura K, Chin S, Ishida S. Optical coherence tomography as a possible tool to monitor and predict disease progression in mitochondrial myopathy, encephalopathy, lactic acidosis and stroke-like episodes. Mitochondrion. 2021 Jan;56:47-51. doi: 10.1016/j.mito.2020.11.003. Epub 2020 Nov 19. PMID: 33220496.

Skladal D, Sudmeier C, Konstantopoulou V, Stöckler-Ipsiroglu S, Plecko-Startinig B, Bernert G, Zeman J, Sperl W. The clinical spectrum of mitochondrial disease in 75 pediatric patients. Clin Pediatr (Phila). 2003 Oct;42(8):703-10. doi: 10.1177/000992280304200806. PMID: 14601919.

Spiegel R, Pines O, Ta-Shma A, Burak E, Shaag A, Halvardson J, Edvardson S, Mahajna M, Zenvirt S, Saada A, Shalev S, Feuk L, Elpeleg O. Infantile cerebellar-retinal degeneration associated with a mutation in mitochondrial aconitase, ACO2. Am J Hum Genet. 2012 Mar 9;90(3):518-23. doi: 10.1016/j.ajhg.2012.01.009. PMID: 22405087; PMCID: PMC3309186.

Stewart JB, Chinnery PF. Extreme heterogeneity of human mitochondrial DNA from organelles to populations. Nat Rev Genet. 2021 Feb;22(2):106-118. doi: 10.1038/s41576-020-00284-x. Epub 2020 Sep 28. PMID: 32989265.

Tsairis P, Engel WK, Kark P. Familial myoclonic epilepsy syndrome associated with skeletal muscle mitochondrial abnormalities. Neurology 1973; 23:408

Vacchiano V, Caporali L, La Morgia C, Carbonelli M, Amore G, Bartolomei I, Cascavilla ML, Barboni P, Lamperti C, Catania A, Chan JW, Karanja R, Sadun AA, Liguori R, Bianchi A, Gavazzi G, Mascalchi M, Salvi F, Carelli V. The m.3890G>A/MT-ND1 mtDNA rare pathogenic variant: Expanding clinical and MRI phenotypes. Mitochondrion. 2021 Sep;60:142-149. Doi: 10.1016/j.mito.2021.08.007. Epub 2021 Aug 11. PMID: 34390870.

Viswanathan S, Frishman LJ, Robson JG, Harwerth RS, Smith EL 3rd. The photopic negative response of the macaque electroretinogram: reduction by experimental glaucoma. Invest Ophthalmol Vis Sci. 1999 May;40(6):1124-36. PMID: 10235545.

Yu-Wai-Man P, Griffiths PG, Gorman GS, Lourenco CM, Wright AF, Auer-Grumbach M, Toscano A, Musumeci O, Valentino ML, Caporali L, Lamperti C, Tallaksen CM, Duffey P, Miller J, Whittaker RG, Baker MR, Jackson MJ, Clarke MP, Dhillon B, Czermin B, Stewart JD, Hudson G, Reynier P, Bonneau D, Marques W Jr, Lenaers G, McFarland R, Taylor RW, Turnbull DM, Votruba M, Zeviani M, Carelli V, Bindoff LA, Horvath R, Amati-Bonneau P, Chinnery PF. Multi-system neurological disease is common in patients with OPA1 mutations. Brain. 2010 Mar;133(Pt 3):771-86. doi: 10.1093/brain/awq007. Epub 2010 Feb 15. PMID: 20157015; PMCID: PMC2842512.

Yu-Wai-Man P, Griffiths PG, Burke A, Sellar PW, Clarke MP, Gnanaraj L, Ah-Kine D, Hudson G, Czermin B, Taylor RW, Horvath R, Chinnery PF. The prevalence and natural history of dominant optic atrophy due to OPA1 mutations. Ophthalmology. 2010 Aug;117(8):1538-46, 1546.e1. doi: 10.1016/j.ophtha.2009.12.038. Epub 2010 Apr 24. PMID: 20417570; PMCID: PMC4040407.

Yu-Wai-Man P, Newman NJ, Carelli V, Moster ML, Biousse V, Sadun AA, Klopstock T, Vignal-Clermont C, Sergott RC, Rudolph G, La Morgia C, Karanjia R, Taiel M, Blouin L, Burguière P, Smits G, Chevalier C, Masonson H, Salermo Y, Katz B, Picaud S, Calkins DJ, Sahel JA. Bilateral visual improvement with unilateral gene therapy injection for Leber hereditary optic neuropathy. Sci Transl Med. 2020 Dec 9;12(573):eaaz7423. doi: 10.1126/scitranslmed.aaz7423. PMID: 33298565.

Yu-Wai-Man P, Newman NJ, Carelli V, La Morgia C, Biousse V, Bandello FM, Clermont CV, Campillo LC, Leruez S, Moster ML, Cestari DM, Foroozan R, Sadun A, Karanjia R, Jurkute N, Blouin L, Taiel M, Sahel JA; LHON REALITY Study Group. Natural history of patients with Leber hereditary optic neuropathy-results from the REALITY study. Eye (Lond). 2022 Apr;36(4):818-826. doi: 10.1038/s41433-021-01535-9. Epub 2021 Apr 28. PMID: 33911213; PMCID: PMC8956580.

Yu-Wai-Man P, Newman N, Subramanian PS, Moster M, Wang AG, Donahue S, Leroy B, Carelli V, Biousse V, Vignal-Clermont C, Sadun A, Fernandez G, Fortin E, Banik R, Taiel M, Sahel JA; The phase III REFLECT trial: efficacy of bilateral gene therapy for Leber hereditary optic

neuropathy (LHON) is maintained 2 years post administration. ARVO abstract. Invest. Ophthalmol. Vis. Sci. 2022;63(7):434.

Zeviani M, Carelli V. Mitochondrial Retinopathies. Int J Mol Sci. 2021 Dec 25;23(1):210. Doi: 10.3390/ijms23010210. PMID: 35008635; PMCID: PMC8745158

Zhu CC, Traboulsi EI, Parikh S. Ophthalmological findings in 74 patients with mitochondrial disease. Ophthalmic Genet. 2017 Jan-Feb;38(1):67-69. doi: 10.3109/13816810.2015.1130153. Epub 2016 Mar 30. PMID: 27029465.

Ziccardi L, Sadun F, De Negri AM, Barboni P, Savini G, Borrelli E, La Morgia C, Carelli V, Parisi V. Retinal function and neural conduction along the visual pathways in affected and unaffected carriers with Leber's hereditary optic neuropathy. Invest Ophthalmol Vis Sci. 2013 Oct 21;54(10):6893-901. doi: 10.1167/iovs.13-12894. PMID: 24071953.

8. APPENDIX 1

Electrophysiological protocols

Pattern ERG + VEP protocol

A combined pattern ERG and VEP protocol was used to reduce examination time and increase patients' compliance.

For VEP recording, skin electrodes were placed on cleaned skin. Active electrode was placed over the occipital scalp (Oz), reference electrode was placed in the forehead (Fz) and ground electrode at vertex (Cz).

For P-ERG recording, a single use disposable corneal electrode (DTL Plus Electrode™ Diagnosys LLC) was placed in both eyes.

The patient was be placed in front of a monitor and the stimulation was performed one eye at time. Dilatation and dark adaptation were not needed.

A *pattern reversal* stimulus following ISCEV standards was used, it consisted on high contrast, black and white checkboard. Check size was 1 degree with a reversal rate of 4.0 reversals per second and a constant mean photopic luminance (50 cd.m-2).

VEP typical waveform consisted in 3 peaks: an initial negative component (N75), a larger positive component (P100) and a second negative component (N135). P100 amplitude (µV) and peak time/latency (ms) were used in the analysis.

Three major components result from PERG stimulation: an initial small negative component (N35), a larger positive component (P50) and a large negative component (N95). P50 and N95 amplitudes (µV) and peak times/latencies (ms) were used in the analysis.

An example of normal PERG (on the left) and VEP (on the right) waveforms is provided.

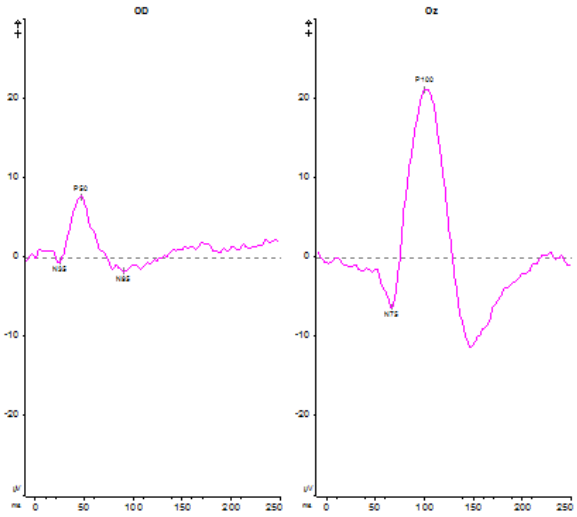

Flash VEP

FVEP are preferred in case of severe low vision even if are more variable than pattern VEP.

FVEP were presented by the ColorDome ganzfeld (Diagnosys LLC). Gold cup skin electrodes were placed in Oz for active, Cz for reference and Fz for ground. Stimulus consisted in a brief flash (5 ms) of 3 cd s m-2 presented at 1 Hz.

The typical FVEP consists of a series of negative and positive waves. The resulting first and the second positive deflections were named P1 and P2, their preceding negative deflections, N1 and N2. Amplitudes (µV) were measured N2 and P2. Peak times/latencies (ms) were measured for N2 and P2.

An example of normal FVEP waveform is provided.

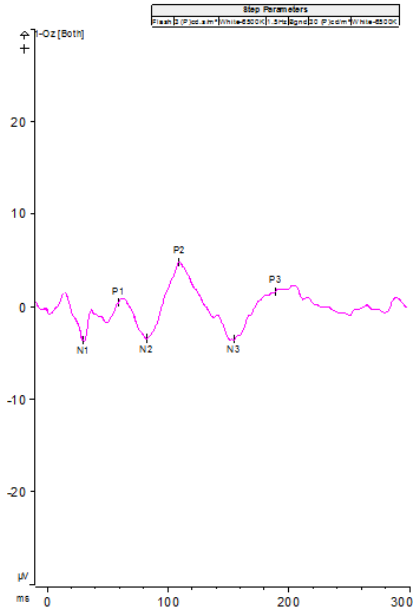

Full field-ERG protocol

Skin electrodes were placed on cleaned skin on temples (references) and vertex (ground). A single use disposable corneal electrode (DTL Plus Electrode™ Diagnosys LLC) was placed in both eyes under topical anesthesia with tetracaine 1%. Both pupils were dilated with one drop each of tropicamide 1% and then dark adapted for 20 minutes. Patients were placed in front of a Ganzfield stimulator (Color-Dome system, Espion E3, Diagnosys, UK, Ltd) and exposed to 3 different sequences of stimuli following ISCEV standard.

- Step 1 Dark adapted 0.01 ERG (rod-driven response from bipolar cells)
- Step 2 Dark adapted 3 ERG (rod-driven response from photoreceptor and bipolar cells). During this step, Oscillatory potentials were recorded using an high pass filter 75 Hz.
- Step 3 Dark adapted 10 ERG (combined response)

Then patients were light adapted for 10 minutes on blue background illumination and other 2 sequences of stimuli were given:

- Step 4 Light adapted 3 ERG (cone-driven response)
- Step 5 Light adapted 30Hz flicker ERG (cone driven response)

The following parameters were used in data analysis: a-wave amplitude, b-wave amplitude, peak times from the stimulus onset, oscillatory potentials (amplitude of the three main positive peaks), flicker ERG amplitude and peak time.

An example of normal ERG is provided.

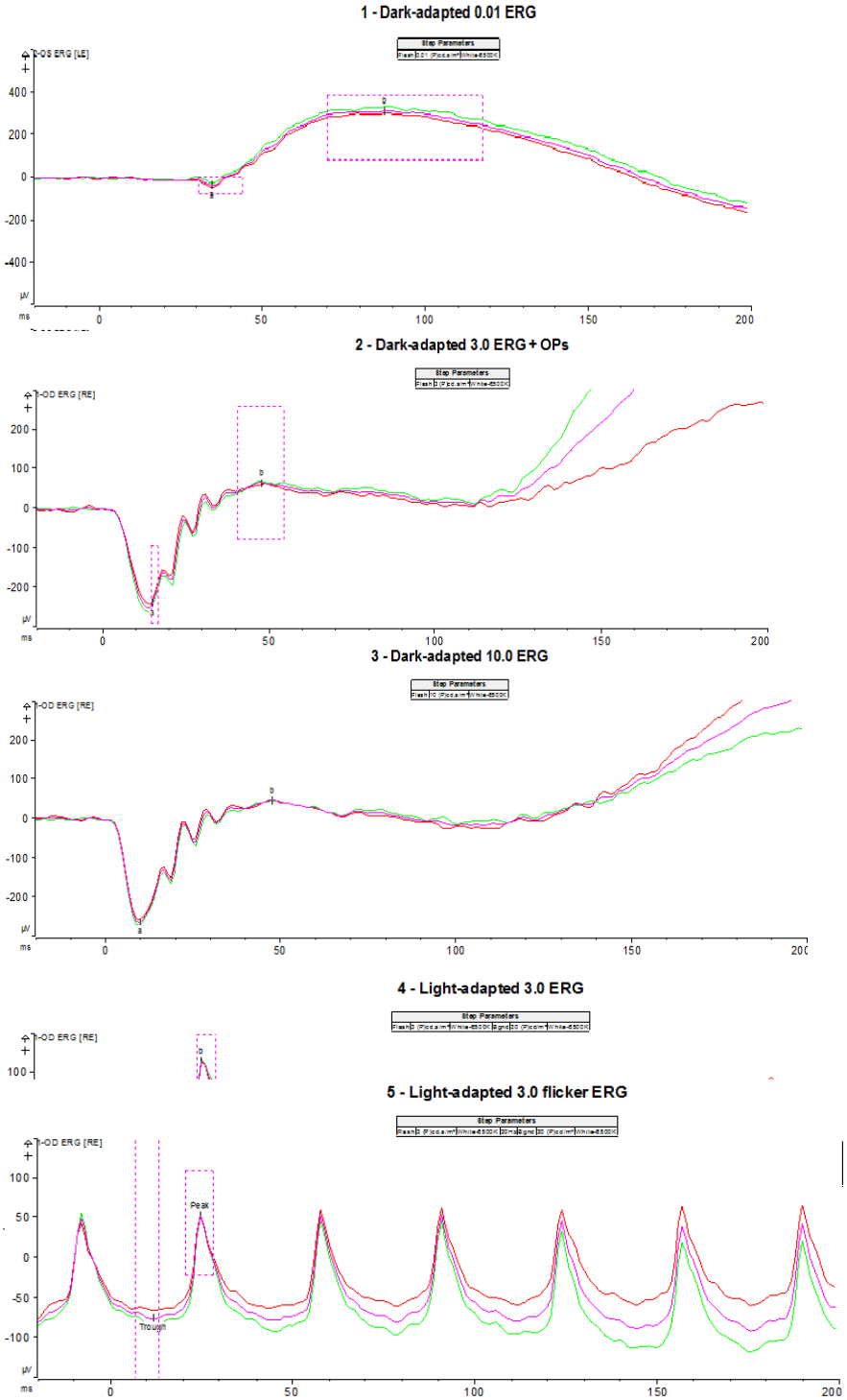

Photopic Negative Response protocol

PhNR is a slow negative component of a flash photopic ff-ERG following b-wave that has been shown to be specific for RGC activity. It was recorded at the end of the ff-ERG protocol. Red (640 nm) stimulus flashes at 1, 3 and 7 cd·s/m^2 of 4 ms duration were presented at a 4-Hz rate on a blue (470 nm) rod saturating background at 10 cd/m^2. PhNR amplitude(µV) and peak time/latency (ms) were used in the analysis.

An example of normal PhNR is provided.

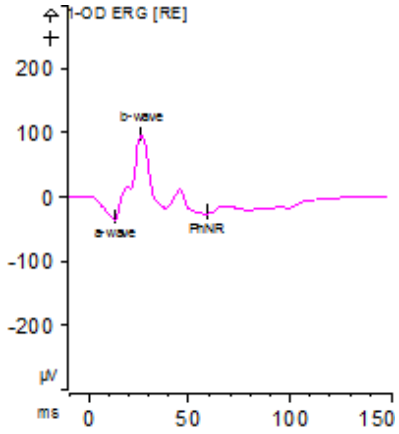

<u>ISCEV standards</u>

Robson AG, Nilsson J, Li S, Jalali S, Fulton AB, Tormene AP, Holder GE, Brodie SE. ISCEV guide to visual electrodiagnostic procedures. Doc Ophthalmol. 2018 Feb;136(1):1-26.

Bach M, Brigell MG, Hawlina M, Holder GE, Johnson MA, McCulloch DL, Meigen T, Viswanathan S. ISCEV standard for clinical pattern electroretinography (PERG): 2012 update. Doc Ophthalmol. 2013 Feb;126(1):1-7.

Odom JV, Bach M, Brigell M, Holder GE, McCulloch DL, Mizota A, Tormene AP; International Society for Clinical Electrophysiology of Vision. ISCEV standard for clinical visual evoked potentials: (2016 update). Doc Ophthalmol. 2016 Aug;133(1):1-9.

Frishman L, Sustar M, Kremers J, McAnany JJ, Sarossy M, Tzekov R, Viswanathan S. ISCEV extended protocol for the photopic negative response (PhNR) of the full-field electroretinogram. Doc Ophthalmol. 2018 Jun;136(3):207-211.

9. APPENDIX 2

List of mutations in *ACO2* (NM_001098.3), *AFG3L2* (NM_006796.3) and *OPA1* (NM_015560.3) genes.

Gene	Family	n° subjects	Mutation	Effect	Category
ACO2	1	1	c.2011C>T	p.Arg671Trp	missense
	2	3	c.1761+1G>A	Splice defect	Haploinsufficincy
	3	1	c.1370+1G>A	Splice defect	Haploinsufficincy
	4	1	c.2012G>A	p.Arg671Gln	missense
	5	1	c.2012G>A	p.Arg671Gln	missense
	6	1	c.2012G>A	p.Arg671Gln	missense
	7	3	c.1452_1459de	p.Glu485fs	Haploinsufficincy
	8	1	c.1300C>T	p.Gln434*	Haploinsufficincy
	9	1	c.1454A>G	p.Glu485Gly	missense
	10	1	c.1420A>G	p.Arg474Gly	missense
	11	2	c.935G>A	p.Arg312Gln	missense
	12	2	c.1949A>C	p.Tyr650Ser	missense
	13	2	c.1753_1755del	p.Leu585del	Other
	14	2	c.1438A>G	p.Asn480Asp	missense
	15	1	c.494T>C	p.Phe165Ser	missense
AFG3L2	1	4	c.1385C>T	p.Ala462Val	missense
	2	4	c.1385C>T	p.Ala462Val	missense
	3	2	c.1220A>G	p.Asp407Gly	missense
	4	1	c.1394G>A	p.Arg465Lys	missense
	5	1	c.1130T>C	p.Phe377Ser	missense
	6	1	c.1064C>T	p.Thr355Met	missense
OPA1	1	1	c.1212+1G>A	Splice defect	Haploinsufficiency
NM_015560.3	2	1	c.2197C>T	p.Arg733*	Haploinsufficiency
	3	1	c.2708_2711del	p.Val903Glyfs*3	Haploinsufficiency
	4	1	c.1463G>T	p.Gly488Ala	Missense
	5	1	c.1146A>G	p.Ile382Met	Missense
	6	1	c.1725_1726del	p.Glu575Aspfs*2	Haploinsufficiency
	7	1	c.320C>A	p.Ser107*	Haploinsufficiency
	8	1	c.751del	p.Asp251Metfs*14	Haploinsufficiency
	9	3	c.631_634del	p.Asp211Lysfs*16	Haploinsufficiency
	10	1	c.703C>T	p.Arg235*	Haploinsufficiency
	11	2	c.2825_2828del	p.Val942Glufs*25	Haploinsufficiency
	12	1	c.2482del	p.Val82*	Haploinsufficiency
	13	1	c.190_194del	p.Ser64Aspfs*7	Haploinsufficiency
	14	1	c.2819-2A>C	Splice defect	Haploinsufficiency
	15	1	c.2713C>T	p.Arg905*	Haploinsufficiency
	16	1	c.889C>T	p.Gln297*	Haploinsufficiency
	17	1	c.1444-1G>T	Splice defect	Haploinsufficiency
	18	3	c.794_797del	p.Ile265ThrfsTer42	Haploinsufficiency
	19	1	c.2708_2711del	p.Val903Glyfs*3	Haploinsufficiency
	20	1	c.1196T>A	p.Leu399*	Haploinsufficiency

21	1	c.2496+1G>A	Splice defect	Haploinsufficiency
22	2	c.1516+1G>T	Splice defect	Haploinsufficiency
23	1	c.2708_2711del	p.Val903Glyfs*3	Haploinsufficiency
24	1	c.751del; c.2341C>T	p.Asp251Metfs*14; p.Arg781Trp	Haploinsufficiency ; Missense
25	1	c.1212+3A>T	Splice defect	Haploinsufficiency
26	1	c.869G>A	p.Arg290Gln	Missense
27	1	c.112C>T	p.Arg38*	Haploinsufficiency
28	1	c.1847+1G>T	Splice defect	Haploinsufficiency
29	1	c.2708_2711del	p.Val903Glyfs*3	Haploinsufficiency
30	1	c.1589del	p.Lys530Argfs*5	Haploinsufficiency
31	1	c.869G>A	p.Arg290Gln	Missense
32	1	c.1516+3A>G	Splice defect	Haploinsufficiency
33	1	c.931G>C	p.Ala311Pro	Missense
34	2	Exon 5 deletion	p.?	Haploinsufficiency
35	1	c.889C>T	p.Gln297*	Haploinsufficiency
36	2	c.2825_2828del	p.Val942Glufs*25	Haploinsufficiency
37	1	c.1410_1433del	p.Leu471_Ser478del	Haploinsufficiency
38	1	c.984+3A>T	Splice defect	Haploinsufficiency
39	1	c.2708_2711del	p.Val903Glyfs*3	Haploinsufficiency
40	1	c.1771-1G>C	Splice defect	Haploinsufficiency
41	1	c.784-1G>C	Splice defect	Haploinsufficiency
42	1	c.1334G>A	p.Arg445His	Missense
43	1	c.869G>A	p.Arg290Gln	Missense
44	1	c.869G>A	p.Arg290Gln	Missense
45	1	c.320C>A	p.Ser107*	Haploinsufficiency
46	1	c.2331C>A	p.Tyr777*	Haploinsufficiency
47	1	c.889C>T	p.Gln297*	Haploinsufficiency
48	4	c.2846T>C	p.Leu949Pro	Missense
49	2	c.889C>T	p.Gln297*	Haploinsufficiency
50	3	c.2331C>A	p.Tyr777*	Haploinsufficiency
51	1	Exons 2-11 deletion	p.?	Haploinsufficiency
52	1	c.703C>T	p.Arg235*	Haploinsufficiency
53	2	c.784-21_784-22InsAluYb8	-	Haploinsufficiency
54	1	c.1316G>T	p.Gly439Val	Missense
55	1	Exons 1-28 deletion	p.0	Haploinsufficiency
56	2	c.2815del	p.Leu939Serfs*29	Haploinsufficiency